



OTTO VON GUERICKE
UNIVERSITÄT
MAGDEBURG

VST

FAKULTÄT FÜR VERFAHRENS-
UND SYSTEMTECHNIK

Development of a glucose-oxygen enzymatic fuel cell

Dissertation

zur Erlangung des akademischen Grades

Doktoringenieur (Dr.-Ing.)

von M.Sc. Ivan Ivanov

geb. am 30 März 1983 in Pirdop

genehmigt durch die Fakultät für Verfahrens- und Systemtechnik
der Otto-von-Guericke-Universität Magdeburg

Promotionskommission: Prof. Dr. Dieter Schinzer (Vorsitz)
Prof. Dr.-Ing. Kai Sundmacher (Gutachter)
Prof. Dr. Uwe Schröder (Gutachter)
Prof. Dr. Mihai Christov (Gutachter)

eingereicht am: 13 März 2012

Promotionskolloquium am: 28 Juni 2012

Acknowledgements

The elaboration of this doctoral thesis would not be possible without the help of many people who I would like to acknowledge.

First of all, I am grateful to Professor Kai Sundmacher for giving me the opportunity to work in his group on this rather challenging topic and for his kind academic guidance. I would like especially to thank Dr. Tanja Vidaković-Koch for supervising my work and providing the most substantial support during my doctoral studies. This work could not be accomplished without her fundamental explanations and patience and the helpful discussions that we had.

I need to acknowledge the indispensable assistance from Bianka Stein, Markus Ikert and Torsten Schröder in the experimental work and for the nice time during the everyday work. Significant contributions to this thesis have made Leonardo Sarmiento, Alexander Domscheit, Jenny Evtimova and Ema Nemet, who were involved in some parts of the work as research assistant, diploma or master students. Special thanks to Dr. Hartmut Grammel for providing help with the HPLC and fluorescence microscopy and Dr. Liane Hilfert for the NMR measurements.

I would like to thank Isai Gonzalez Martinez, Do Thi Quynh Nga and Miroslava Varničić for sharing the office with me and being wonderful colleagues and friends. I would like to thank the other colleagues from the PCP group and especially Thomas Kadyk and Christian Oettel for the fruitful discussions and the nice time in the lab. In continuation I would like to thank all my other colleagues in the MPI for providing a friendly working and social atmosphere during the years.

Finally, I would like to express my gratitude for the big support from my family and especially my mother and friends throughout the years.

Abstract

The enzymatic biofuel cells are a type of fuel cells, which use biocatalysts (enzymes) instead of conventional noble metal catalysts. The utilization of enzymes offers various advantages such as mild operating conditions, variety of possible fuels and high catalytic selectivity, which can theoretically enable a membraneless design. However, the use of enzymes is associated also with significant disadvantages such as the difficulty in the establishing of efficient electron transfer between the enzyme and the electrode surface and the very low long-term stability of enzymatic electrodes.

The typical performance of enzymatic biofuel cells, which is in the microwatt range, and the short operational life still limit their practical applications. The research in this field has been mainly focused on the development of different procedures for immobilization and electrical coupling of enzymes, while less attention has been paid to the overall system design. The current study aims to show the systematic development of a glucose-oxygen enzymatic fuel cell. This dissertation comprises different steps in the engineering of a biofuel cell, from the selection and development of a suitable procedure for preparation of electrodes and the systematic investigation of the electron transfer mechanism to the optimization of the electrode performance and the coupling of the electrodes in a fuel cell configuration.

Zusammenfassung

Die enzymatische Biobrennstoffzelle ist eine Art von Brennstoffzelle, die statt konventionellen anorganischen Katalysatoren (Edelmetalle), Enzyme (Biokatalysatoren) benutzt. Die Anwendung von Enzyme bietet verschiedene Vorteile im Vergleich zu anorganischen Katalysatoren, wie zum Beispiel mildere Betriebsbedingungen, Vielfalt von möglichen Brennstoffen und höhere Katalysator-Selektivität, die theoretisch einen membranfreien Aufbau möglich macht. Allerdings ist die Anwendung von Biokatalysatoren auch mit verschiedenen Nachteilen verbunden, wie zum Beispiel die Schwierigkeit eine effiziente Elektronübertragung zwischen Enzym und Elektrodenoberfläche zu ermöglichen und der geringen Langzeitstabilität einer enzymatischen Elektrode.

Die typische Leistung der Brennstoffzellen im Microwattbereich und ihre sehr kurze Lebensdauer begrenzen die bisherigen praktischen Anwendungen. Die Erforschung auf dem Gebiet der enzymatischen Biobrennstoffzellen ist normalerweise mit der Entwicklung von verschiedenen Prozeduren für die Enzymimmobilisierung und der elektrischen Ankopplung verbunden, der Systemaufbau wurde eher weniger beachtet. Diese Doktorarbeit zeigt die systematische Entwicklung einer Glukose-Sauerstoff-bazierten enzymatischen Biobrennstoffzelle. Diese Arbeit umfasst alle Schritte, von der Auswahl einer geeigneten Prozedur für die Elektrodenpräparation und der systematischen Untersuchung des Elektronenübertragungsmechanismus, über die Optimierung der enzymatischen Elektrodenleistung bis hin zur Kopplung von Anode und Kathode zu einer gesamten Brennstoffzelle.

Table of contents

1. Introduction	1
2. Theoretical background	3
2.1 Enzymatic electrodes	3
2.1.1 Redox enzymes and electron transfer to the electrode surface	3
2.1.2 Electrode modification and typical electrode architectures	5
2.2 Enzymatic fuel cells	7
2.2.1 Working principle, advantages and disadvantages of biofuel cells	7
2.2.2 Types of biofuel cells.....	9
2.2.3 Fuels, oxidants and enzymes	10
2.2.4 Applications of biofuel cells	12
2.3 Current limitations of glucose-oxygen enzymatic biofuel cells	13
3. Aims of the study	15
4. Reconstitution of GOx on modified gold	17
4.1 Approach for electrode modification	17
4.2 Electrode modification and activity	18
4.3 Electrocatalytic activity and behavior of gold	24
4.4 Conclusions about the origin of the catalytic activity	33
4.5 Experimental details	35
4.5.1 Chemicals and materials	35
4.5.2 Synthesis of <i>N</i> ⁶ -(2-aminoethyl)-FAD	35
4.5.3 Preparation of apo-GOx	36
4.5.4 Electrode modification	36
4.5.5 Electrochemical experiments	37
5. Enzymatic electrode based on TTF-TCNQ	38
5.1 Historical background and advantages of TTF-TCNQ	38
5.2 Electrode modification and activity	40
5.3 Optimization of the modification procedure	45
5.3.1 Influence of CTC loading and morphology	45

5.3.2	Influence of GOx and gelatin loading	49
5.3.3	Interpretation of the influence of structural parameters	52
5.4	Electrode architecture involving a gelatin matrix	53
5.4.1	Influence of type of carbon black and loading	55
5.4.2	Influence of GOx and gelatin loading	58
5.4.3	Performance of the optimized electrode	63
5.5	Electron transfer mechanism and origin of activity	65
5.5.1	Mechanisms according to the literature and current approach	65
5.5.2	TCNQ as mediator	66
5.5.3	TTF as mediator	68
5.5.4	TTF-TCNQ as mediator	70
5.5.5	Conclusions about the electron transfer mechanism	76
5.6	Conclusions	77
5.7	Experimental details	78
5.7.1	Chemicals and materials	78
5.7.2	Modification procedure with polypyrrole layer	78
5.7.3	Modification procedure with a gelatin matrix	79
5.7.4	Electrochemical experiments	80
6.	Hybrid fuel cell	81
6.1	Concept of the hybrid fuel cell	81
6.2	Performance of the hybrid fuel cell	82
6.3	Influence of fuel cell architecture	85
6.3.1	Influence of gas-diffusion layer	86
6.3.2	Influence of separator and cathode hydrophobization	87
6.4	Influence of glucose concentration and oxygen	88
6.5	Stability of the hybrid fuel cell	90
6.6	Conclusions	93
6.7	Experimental details	93
6.7.1	Chemicals and materials	93
6.7.2	Preparation of the enzymatic anode	94
6.7.3	Preparation of MEA and fuel cell construction	94
6.7.4	Electrochemical experiments	95

7. Initial studies with enzymatic cathode	97
7.1 Concept of the cathode modification procedure	97
7.2 DET and MET performance of the biocathode	97
7.3 Enzymatic fuel cell	99
7.4 Experimental details	102
7.4.1 Preparation of the enzymatic anodes	102
7.4.2 Preparation of the enzymatic cathodes	103
7.4.3 Enzymatic fuel cell construction	103
7.4.4 Electrochemical experiments	104
8. Concluding remarks	105
9. Literature	107

List of abbreviations

3D	- three-dimensional
ABTS	- 2,2'-azino-bis(3-ethylbenzothiazoline-6-sulphonic acid)
ACN	- acetonitrile
AFM	- atomic force microscopy
BOD	- bilirubin oxidase
CDH	- cellobiose dehydrogenase
CLEAs	- cross-linked enzyme aggregates
CNTs	- carbon nanotubes
CTC	- charge transfer complex
DAD	- diode array detection
DET	- direct electron transfer
DMFC	- direct methanol fuel cell
EDC	- 1-ethyl-3-(3-dimethylaminopropyl) carbodiimide
ESI	- electrospray ionization
FAD	- flavin adenine dinucleotide
FTIR	- Fourier transform infrared spectroscopy
GC	- glassy carbon
GDH	- glucose dehydrogenase
GDL	- gas-diffusion layer
GOx	- glucose oxidase
HEPES	- 4-(2-hydroxyethyl)-1-piperazineethanesulfonic acid
HPLC	- high-performance liquid chromatography
HQS	- hydroxyquinoline-5-sulfonic acid
MEA	- membrane electrode assembly
MET	- mediated electron transfer
MP-11	- microperoxidase-11
MS	- mass spectrometer.
MWCNTs	- multi-walled carbon nanotubes
NAD	- nicotinamide adenine dinucleotide
NHS	- N-hydroxysulfosuccinimide
NMA	- N-methylacridinium
NMP	- N-methylphenazinium
NMR	- nuclear magnetic resonance
OCV	- open circuit voltage
PEM	- polymer electrolyte membrane
PQQ	- pyrroloquinoline quinone
PTFE	- polytetrafluoroethylene

PVS	- polyvinyl sulfate potassium salt
QCM	- quartz crystal microbalance
RDE	- rotating disc electrode
RG	- rough gold
SAM	- self-assembled monolayer
SCE	- saturated calomel electrode
SEM	- scanning electron microscopy
STM	- scanning tunneling microscopy experiments
SWCNTs	- single-walled carbon nanotubes
TBATFB	- tetrabutylammonium tetrafluoroborate
TCNQ	- tetracyanoquinodimethane
THF	- tetrahydrofuran
TTF	- tetrathiafulvalene

1. Introduction

The present work entitled “The development of a glucose-oxygen enzymatic biofuel cell” combines contributions from two contemporary research fields – fuel cells and bioelectrochemistry. Both research areas can be regarded as branches of electrochemistry but in comparison to the rather application-oriented energy-producing task of fuel cells, bioelectrochemistry has a more fundamental spectrum, associated with the investigation of electrical phenomena in biological systems (electrokinetic, membrane and electron transfer phenomena). However, this differentiation is interchangeable in the broader sense, since the practical optimization of fuel cells requires a solid theoretical background and can also generate basic knowledge. On the other side, the investigation and understanding of bioelectrochemical phenomena can result in technological applications (e.g. amperometric biosensors, which emerged from redox protein electrochemistry studies).

Fuel cells are electrochemical devices, which convert chemical energy into electrical energy. The direct energy transformation allows them to overcome the thermodynamic limitations of the combustion-based power systems, increasing their efficiency up to typically 50-60%. The concept of fuel cell dates back to the early 1839 [1] but just recently the increasing energy demands and supply limitations of fossil fuels have motivated the commercial endorsement of the fuel cell technology. On the other side, the historical development of bioelectrochemistry is tightly associated with the advancement of electrochemistry. It can be dated back to the 18th century with the experiments of Sulzer, Galvani and Volta [2] but it came to prominence in the second part of the 20th century and is exponentially expanding since then.

Major focus of the bioelectrochemical research is the biological electron transport and the electrochemistry of redox enzymes in particular [3]. Driving forces for these investigations have been some practical applications such as the development of biosensors and bioreactors as well as the need of fundamental understanding of enzymes redox chemistry. The possibility of electrical contacting of enzymes has naturally prompted their employment as catalysts in fuel cell systems and has initiated the concept and studies of enzymatic biofuel cells. Historically, the work of Yahiro et al. from 1964 has been usually considered as the first report of an enzymatic biofuel cell in the literature [4], although there is another paper by Davis et al. from 1962, where

the authors report electrical output in presence of *Escherichia coli* and glucose oxidase [5]. The utilization of enzymes in biological fuel cells provides several substantial advantages such as high activity at mild conditions, substrate selectivity and a high number of possible fuels. However, the biological nature of the catalysts is also associated with important drawbacks such as difficulty in the electrical coupling and insufficient stability. These features postulate specialized niche applications of enzymatic biofuel cells rather than direct competition with conventional fuel cells as larger scale electrochemical power sources.

Despite of the extensive research and numerous reports of enzymatic electrodes, the biofuel cells still suffer from low performance and stability and the continuously growing number of publications has not yet resulted in substantial improvement. The subject of this thesis is to present the development and optimization of a glucose-oxygen biofuel cell in a systematic way. The thesis includes overview of the existing enzymatic biofuel cells with focus on the glucose and oxygen based electrodes, screening and investigation of suitable electrode modification procedures and their testing in single electrode and fuel cell configurations. Among the numerous anode modification procedures, specific attention will be drawn to two well-known approaches, which have not been employed in a glucose-oxygen fuel cell configuration so far, in an effort to understand the electron transfer mechanism and influence of electrode architecture on the performance. In addition to the indispensable single electrode studies, focus will be put on the influence of the fuel cell design and operational parameters. The aim of this study is to optimize the performance of a glucose-oxygen enzymatic fuel cell and to show the importance of all steps in the process of development, from the clarification of the catalytic mechanism to the overall cell design, by addressing the particular examples.

2. Theoretical background

2.1 Enzymatic electrodes

2.1.1 Redox enzymes and electron transfer to the electrode surface

Enzymes are proteins with mostly spherical or ellipsoidal shape that are able to catalyze chemical reactions, typically accelerating the equilibrium constants by a factor of 10^8 - 10^{20} as compared with non-catalyzed reactions. There is a local cavity within the protein molecule with a characteristic constitution and stereoconfiguration that forms the catalytically active center, where a chemically and spatially congruent substrate (“lock-and-key principle”) is converted to a product (Fig. 2-1). The protein structure is capable of adapting conformationally to the substrate to a certain extent [2].

The roughly 3000 enzymes currently known are grouped into six main classes according to the type of reaction catalyzed. Relevant for bioelectrochemical applications is the class of the oxidoreductases, which catalyze oxidation and reduction reactions by transfer of hydrogen or electrons. Essential non-protein component of an oxidoreductase, required for its catalytic activity, is the redox co-factor (redox center), which can be tightly or loosely bound to the enzyme. Co-factors can be inorganic such as single metals (e.g. Cu), metal clusters (e.g. Ni-Fe) and organometallic compounds (e.g. heme) or organic such as flavin adenine dinucleotide (FAD), nicotinamide adenine dinucleotide (NAD) or pyrroloquinoline quinone (PQQ).

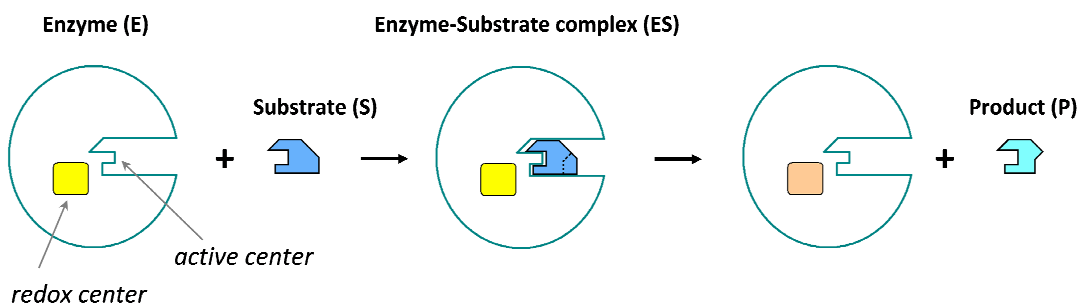
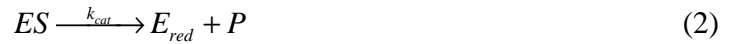


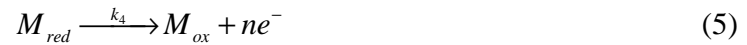
Figure 2-1: Schematic presentation of the “lock-and-key” principle for an oxidoreductase.

A key issue in the development of biofuel cells is the selection of a suitable electrode modification procedure, which would ideally preserve the activity of the enzyme by providing a suitable environment and enable highly efficient electron transfer from or to the electrode surface. It should be noted that in this respect the requirements for amperometric biosensors and electrodes for biofuel cells overlap to some extent [6]. The principal route of achieving electron transfer determines the electrode configuration. If an enzyme is capable of transferring (rendering or receiving) electrons to the electrode, the process is termed *Direct Electron Transfer* (DET). Less than 100 from over 1000 redox enzymes are known to feature DET [7]. In general, enzymes that tend to exhibit DET possess spatially exposed redox relay located near the protein periphery. In most of the cases, however, the redox unit is deeply buried into the protein structure and isolated with a thick carbohydrate shell. In order to overcome the kinetic barrier for electron transfer, a redox active species called *mediator* can be introduced to the bioelectrocatalytic system. It is used to shuttle electrons between the enzyme and the electrode and the process is referred to as *Mediated Electron Transfer* (MET). The basic electron transfer principles in the context of biosensors, applicable also to enzymatic biofuel cells, have been reviewed by Schuhmann et al. [8] and the main types of mediators used in biofuel cells research are summarized in recent reviews [9, 10].

The bioelectrochemical reaction can be regarded as consecutive reactions, which are schematically exemplified in the case of oxidation process (Fig. 2-2). The first one is an enzymatic reaction, which can be described by Michaelis-Menten kinetics (Eq. 1 and 2). The following reaction involves the regeneration of the reduced form of enzyme either by DET (Eq. 3) or MET (Eq. 4).



In the case of DET the current measured at the electrode is directly generated by the reoxidation of the reduced form of enzyme and in the case of MET the current is a product of the reoxidation of the reduced form of mediator at the electrode (Eq. 5).



Thus, the bioelectrochemical current depends not only on the rate of enzymatic reaction but also on the rates of enzymatic regeneration at the electrode in the case of DET and the rates of enzymatic regeneration by mediator and mediator reoxidation at the electrode in the case of MET. The same theoretical treatment with an inverted direction of electron flow can be applied in the case of reduction reactions.

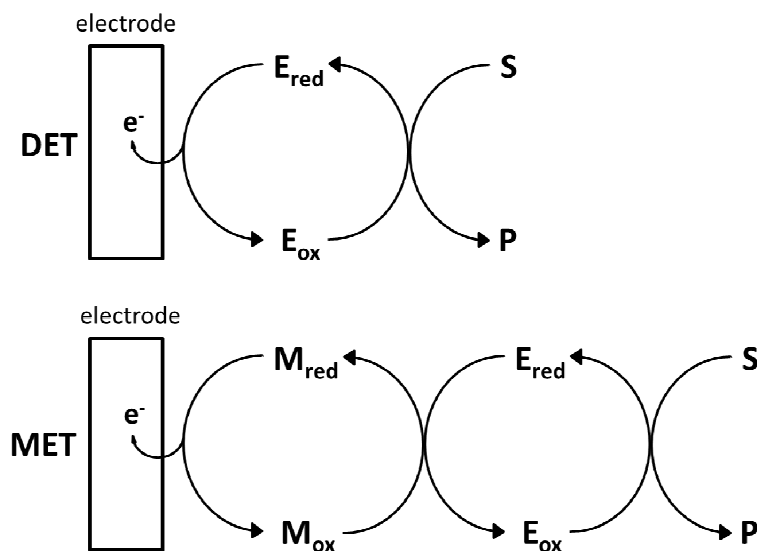


Figure 2-2: Reaction schemes for direct (DET) and mediated (MET) electron transfer.

2.1.2 Electrode modification and typical electrode architectures

There is a huge variety of immobilization strategies for both enzymes and mediators, which include simple physical adsorption, covalent attachment, cross-linking and entrapment in polymeric gels [2]. However, this is a rather formal differentiation since quite often the

immobilization approach is a combination of these methods. In general, monolayer configurations tend to be displaced by multilayers or other three-dimensional (3D) structures in order to increase the current output. 3D-structures can also provide suitable immobilization matrices for the enzymes and thus retain for longer time their activity. Provided that efficient electrical communication is achieved, essential problem that could possibly arise is the limited mass transport of the fuel. Compared to conventional fuel cell electrodes, the enzymatic electrodes exhibit higher complexity and the immobilization procedures are usually associated with complicated chemistry. Mediators tend to be very helpful for enabling or increasing the rate of electron transfer but the introduction of additional components raises further problems associated with the intrinsic properties of the mediator (stability, toxicity) as well as system design issues such as mediator diffusion or leaching.

DET enzymatic electrode configurations are usually realized with the help of carbon-based and/or nanostructured materials such as spectrographic graphite electrodes [11, 12] or carbon nanotubes (CNTs) [13-15]. The DET enzymatic electrode configurations are still outnumbered by MET-based configurations due to the fact that very few enzymes exhibit DET as discussed in the previous section. The MET enzymatic electrodes can be roughly divided into two groups: with free diffusive and immobilized mediators. Enzymatic electrodes involving diffusional mediators are expected to have less practical applications and such studies usually address a novel enzyme immobilization matrix [16-18]. More common in the area of biofuel cells is the application of immobilized mediator. Numerous strategies for immobilization of enzymes and mediators on the electrode surface have been reported in literature [10]. Worth noting are procedures, which use 3D matrices such as polymers, lipids and CNTs or combinations of these to incorporate enzyme and mediator.

As already discussed, the utilization of mediators has a significant role in the establishment of efficient electrical communication between the enzyme and the electrode surface but in many cases the electrode stability can be influenced by mediator leaching. A promising strategy, involving the covalent attachment of the mediator to a polymer backbone has been used in order to overcome this problem. The most notable example, originally introduced by Adam Heller, is the utilization of Os-based redox hydrogels as mediators and immobilization matrices [19-26]. So far, biofuel cells based on the concept of Os-based redox hydrogels exhibit probably the best

characteristics in the context of implantable applications and other groups have also adopted this procedure for immobilization of glucose oxidase (GOx) [27, 28] or other enzymes [29, 30].

2.2 Enzymatic fuel cells

2.2.1 Working principle, advantages and disadvantages of biofuel cells

Biofuel cells are conceptually equivalent of other types of fuel cells. The difference arises from the nature of the catalysts, which are employed instead of conventional noble metal catalysts, namely enzymes (biocatalysts). The utilization of biocatalysts results in different operating conditions and different fuels [3]. The working principle of biofuel cells is the same as in conventional fuel cells, namely fuel is oxidized at the anode side and the electrons which are released by the oxidation reaction are driven through an outer electrical circuit, thus generating electric current. Finally, the electrons reach the cathode, where they combine with an oxidant (typically oxygen) and protons to a product (typically water). The working principle and main components of the conventional polymer electrolyte membrane (PEM) fuel cell and an enzymatic fuel cell are compared in Fig. 2-3.

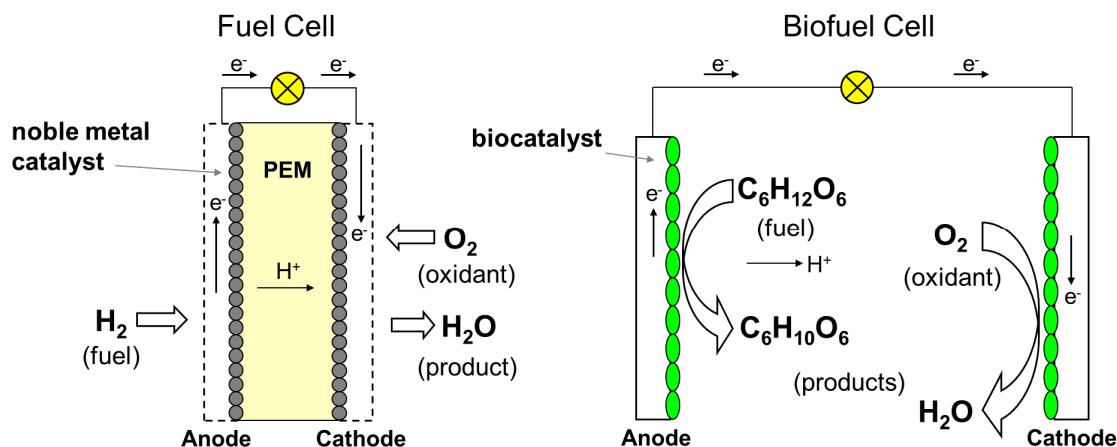


Figure 2-3: Schematic presentation and working principle of PEM fuel cell and an enzymatic biofuel cell.

The power of a biofuel cell is a product of its voltage and current ($P = U \times I$). The voltage of a biofuel cell is determined by the potentials of its electrodes (Fig. 2-4). For this reason, it is

desired that the oxidation potential is kept as negative as possible and the reduction potential is kept as positive as possible. The introduction of mediators often enables or increases the rate of electron transfer and the currents, respectively, but decreases the voltage that can be produced by the fuel cell. The reason is that the potential of enzymatic electrodes involving MET is influenced mainly by the potential of the respective mediator, which has to be more positive than the enzyme potential in the case of oxidation or more negative in the case of reduction in order that electron transfer takes place. In this respect the utilization of DET approach is more favorable for biofuel cell applications [7] but often there is a trade-off between the potential and the rate of electron transfer.

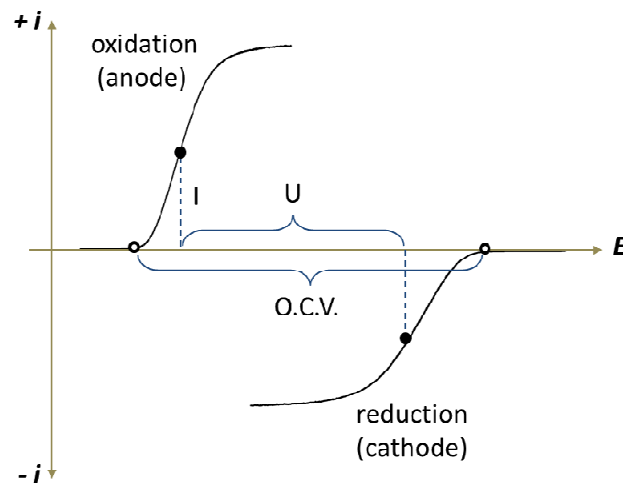


Figure 2-4: Polarization curves of anode and cathode in a fuel cell. Features which determine the performance are marked: current (I), voltage (U), open-circuit voltage ($O.C.V.$).

The utilization of biocatalysts provides several advantages over the conventional noble metal catalysts. Biocatalysts are inexpensive and their extended usage is expected to lower the cost of production, opposed to transition metal catalysts due to their limited availability. They are highly efficient systems exhibiting high turnover numbers, selectivity and activity under mild conditions (neutral pH and near-body temperature). The substrate specificity diminishes reactants crossover, which theoretically enables a membraneless fuel cell, which reduces the costs and simplifies the design. In addition, biocatalysts allow the utilization of more complex fuels (as their natural substrates abundant in nature), opposed to the relatively poor chemistry of hydrogen and methanol as typical fuels for conventional fuel cells.

Though, the biocatalysts have some disadvantages compared to transition metal catalysts. In general, redox proteins tend to exhibit their superior catalytic properties exclusively in their natural environment or, in other words, nature did not evolve enzymes for bioelectrocatalytical applications. This is usually manifested by the difficulty in establishing electrical communication between the protein and the electrode surface and by the limited stability of the biocatalyst-electrode assembly. Another drawback of enzymes from a chemical engineering point of view is the lower volumetric catalyst density. Enzymes are large molecules, so the number of active sites per volume is usually lower compared to conventional metal electrodes.

2.2.2 *Types of biofuel cells*

According to the traditional definition, enzymatic fuel cells are a type of biofuel cells, which utilize isolated enzymes [6]. If the biocatalysts are located inside living cells, the biofuel cells are referred to as *microbial*, although in a recent report [31] it was shown that not only bacteria but also human cells can be employed as catalysts in a fuel cell device. The use of single enzymes (or enzyme cascades) allows to have defined reaction pathways on the electrode surface and to overcome the limited output performance of microbial biofuel cells, which is considered to be due to mass transfer resistances across the cell membranes [6]. On the other side, enzymes still cannot compete with microbes in terms of long-term stability and fuel utilization (complete oxidation).

There are also examples in the literature, where an enzymatic electrode has been combined with a conventional catalyst electrode. Provided that an abiotic electrode usually exhibits higher stability, metal catalysts for the anodic reaction [32-38] and more often for the cathodic reaction [17, 30, 39-49] have been employed in order to complete the electrical circuit and to test the bioelectrodes under “fuel cell” conditions. The presence of one biocomponent (either anode or cathode) commonly allows the authors to refer to the studied systems as biofuel cells. Just recently, a fuel cell incorporating silicon nanoparticles for the electrooxidation of glucose and microperoxidase-11 (MP-11) for the reduction of hydrogen peroxide has been stated as a “hybrid cell” [50].

2.2.3 Fuels, oxidants and enzymes

The nature of employed catalysts in enzymatic fuel cells allows the utilization of numerous fuels including variety of sugars and low aliphatic alcohols. The most common and intuitive fuel for enzymatic biofuel cells is glucose due to its high abundance in nature and essential role in human metabolism [10]. Glucose is an important metabolic intermediate and a source of energy for a variety of living organisms. From the enzymes that are capable of glucose oxidation, glucose oxidase (EC 1.1.3.4, GOx) is the most widely employed in the area of biosensors and biofuel cells. GOx is a dimer, composed of two identical subunits with a mean total molecular mass of 160 kDa, an average diameter of 8 nm and isoelectric point of about 4.2 [51]. The redox co-factor responsible for the catalytic function of GOx is FAD. GOx catalyzes the conversion of glucose to gluconolactone, which spontaneously hydrolyzes to gluconic acid. The natural electron acceptor for GOx is oxygen, which in the course of the natural reaction is reduced to hydrogen peroxide [51]. Although GOx is a robust enzyme with high activity, there are two major drawbacks, which complicate its use in biofuel cells. First is the difficulty in establishing DET due the thick insulating carbohydrate shell [10], which usually necessitates the use of a mediator and consequently shifts the anodic potential to more positive values. The second drawback is its high reactivity with oxygen, which complicates the utilization of GOx-based electrodes in membraneless fuel cell configurations since oxygen competes for the released electrons with the electrode or the mediator and causes a decrease of the anodic current density. In addition, the generation of hydrogen peroxide in the vicinity of the electrode should be avoided since hydrogen peroxide is a highly reactive oxygen species with strong oxidizing properties and can be harmful to biological components such as enzymes.

Another enzyme that has been widely used in biofuel cell applications is glucose dehydrogenase (EC 1.1.1.47, GDH) [47, 52-54]. It has some advantages over GOx because its natural electron acceptor is not oxygen but is expected to find limited application since it requires a soluble NAD co-factor. A promising enzyme, recently introduced by Gorton and collaborators for biofuel cell applications is cellobiose dehydrogenase (EC 1.1.99.18, CDH) [30, 55]. Its natural substrate is cellobiose but CDH isolated from *ascomycete fungi* can also oxidize other disaccharides such as lactose as well as variety of monosaccharides including glucose. The enzyme is a monomer containing a flavin and a heme domain. Other enzymes from the family of

dehydrogenases that have been used in enzymatic biofuel cells are PQQ-dependent GDH [56] and fructose dehydrogenase [15, 57] for oxidation of glucose and fructose respectively.

Other possible fuels for enzymatic fuel cells are aliphatic alcohols such as methanol, ethanol and glycerol, the important metabolic intermediate pyruvate and hydrogen as a non-carbon containing fuel, which is known as a prominent substrate for conventional fuel cells. Different dehydrogenases have been employed for the oxidation of alcohols. Worth noting here are the enzyme cascades that allow complete oxidation of the substrate. For instance, a sequence of NAD-dependent dehydrogenases has been used for oxidation of methanol to CO₂ [49]. The commonly reported anodic systems use only one enzyme, which catalyzes partial oxidation of the fuel. The redox process is associated with the breakage of one chemical bond, which limits the number of electrons that can be gained from the anodic reaction to two. The employment of enzyme cascades allows better utilization of the chemical energy of the fuel and allows summation of the electrons from every single reaction and thus increases the total current density delivered by the fuel cell [58]. Other, PQQ-dependent dehydrogenases have been used for partial oxidation of ethanol [59] as well as for full oxidation of glycerol together with oxalate oxidase [60]. Hydrogen oxidation has been achieved by employing membrane-bound hydrogenase, which contains a Ni-Fe catalytic center and exhibits high tolerance to oxygen and carbon monoxide [61].

The most widely employed oxidant in enzymatic biofuel cells is oxygen and there are only few reports of other compounds. Oxygen is the typical oxidant in conventional fuel cells, where it is used in form of pure gas or air. In the case of enzymatic fuel cells it is usually used dissolved in aqueous electrolyte, whereby its low water solubility raises additional mass transport problems. The four-electron reduction to water catalyzed by the respective enzymes represents the cathodic half-cell reaction [11, 12]. The typical enzymes used for oxygen reduction are plant and fungal laccases and bilirubin oxidase (EC 1.3.3.5, BOD). These are multi-copper oxidases that can oxidize variety of substrates and possess four metal ions classified into three types: T1, T2, and T3. The T1 site is known to bind the organic substrate and the T2/T3 cluster catalyzes the four-electron reduction of oxygen to water [11, 12]. Laccases usually exhibit activity at slightly acidic conditions and are commonly employed at pH 5, while BOD has activity in more alkaline media, which allows its utilization at neutral pH. Another enzyme system used for

oxygen reduction is based on cytochrome oxidase and cytochrome c, both containing heme as the catalytic center [62].

Other oxidant that has been rarely employed is hydrogen peroxide. From the enzymes capable of hydrogen peroxide reduction microperoxidase-11 [63] and horseradish peroxidase [64] have been employed in biofuel cells. MP-11 has been also used for the reduction of cumene peroxide in a biofuel cell based on two immiscible solvents [65].

2.2.4 Applications of biofuel cells

The variety of intended enzymatic biofuel cell applications suggested in the literature tends to be roughly broken into two classes: implantable power and general power. In general, the utilization of such systems as possible power generating devices is slightly disputable since state-of-the-art enzymatic fuel cells cannot compete with the conventional energy generators in terms of power output and stability [66]. Nevertheless, in the context of electrochemical power, worth noting is the prototype bio battery introduced by Sony® in 2007, which is based on the enzymatic biofuel cell configuration reported by Sakai et al. [52].

The unique properties of biocatalysts suggest the employment of biofuel cells in uncommon, niche applications and the most evident are for implantable power, based on glucose and oxygen [6, 67]. The recent advances in the development of implantable electrically operated devices raise the need of new power sources that would fit their specific requirements. The miniaturization of biomedical devices demands miniaturization of their power sources, since the size of the electrical device is usually dominated by the size of the battery [68]. Theoretically there are number of biomedical accessories that would take advantage of a small implantable power source such as the biofuel cell, including the cardiac pacemaker, neurostimulators, hearing and vision devices, drug pumps, glucose sensors, bladder-control valves, etc. [6, 67]. However, according to Adam Heller, one of the pioneers in the field, biofuel cells could not compete with conventional Li-based batteries as power supplies for a pacemaker (due to short operational life) or neurostimulators (due to limited power output) [66]. He proposes particular applications in autonomous and disposable sensor-transmitter systems for monitoring bodily functions [66] or the integration in medical feedback systems for drug-delivery, e.g. for diabetes monitoring and

control [69]. It should be noted that just recently, the possibility of such applications has been demonstrated by the implantation of a biofuel cell in a living rat [70].

2.3 Current limitations of glucose-oxygen biofuel cells

The typical enzymatic fuel cell demonstrates power in the microwatt range and low long-term stability. Biofuel cell tests are often performed under quite different conditions (concentration, temperature, pH, mass transport conditions, etc.), which complicates or hampers the comparison between different configurations and the identification of the electrodes and fuel cells with the best performance. It is obvious that for straightforward characterization some standardization is needed and the logical way is adoption of methods from conventional fuel cells research. Regarding the electrochemical experiments the importance of steady-state measurements should be underlined. Once an unambiguous characterization of the biofuel cell performance under steady-state conditions has been done, dynamic experiments for simulation of real applications can be performed.

Essential for the future application of enzymatic fuel cells is their long-term stability. The utilization of a batch container as the conventional electrochemical cell or a beaker raises the problems of substrate depletion and product accumulation. Most of the reported configurations are based on a simple batch type system with focus on the chemistry and processes occurring at the bioelectrode interface. Flow-through systems offer possible solution for the long-term stability investigation of biofuel cells.

Quite often the stability of biofuel cells is not evaluated at all, or in an inappropriate manner. Numerous studies evaluate the long-term performance by recording the respective polarization curves in different intervals of time, meanwhile storing the fuel cell in the respective solution. These conditions do not represent the actual working conditions of such power-generating devices. More realistic information about the long-term stability can be obtained by constant polarization at potentiostatic or galvanostatic conditions.

Amongst the variety of enzymatic fuel cells based on different fuels and oxidants, glucose-oxygen fuel cells are the most renowned type and subject of most extensive research. Their major intended application is associated with implantation and use as power sources for other implantable devices. However, the problem with the low power density is especially pronounced

in this case since glucose and oxygen are present in very low concentrations in the human body, which still restrains any realistic practical applications. Therefore, in the development of glucose-oxygen biofuel cells, apart from the fine tuning and increase of the voltage, a major focus is the establishment of efficient electron transfer and increase of the currents. On the other side, the low stability is affected by the intrinsic nature of enzymes as biocatalysts as well as some issues associated with the electrode architecture (leaching of enzyme, leaching of mediator, pH change, etc.). The desire for electron transfer efficiency and stability constitute the electrode design as the essential step in the development of efficient biofuel cells. Consequently, most of the research until now has been focused on this issue and less attention has been drawn to the overall system design.

3. Aims of the study

In this work the systematic development of a glucose-oxygen enzymatic biofuel cell, including selection of a suitable electrode modification procedure, electrode preparation, characterization in single electrode studies and optimization, and, finally, combination of the electrodes in fuel cell devices and its testing under different operating conditions, is studied.

As discussed in sections 2.1.2 and 2.2.1, the ideal glucose oxidizing enzymatic electrode should exhibit as negative as possible oxidation onset potential and high current densities. The electrode potential is limited thermodynamically by the potentials of the respective half-reactions. The standard potential of the glucose oxidation to gluconolactone is -0.37 V (-0.61 V vs. SCE) and the standard potential of the oxidation of reduced FAD is -0.22 V (-0.46 V vs. SCE). These values have been calculated under standard conditions, assuming pH 7 and an ionic strength of 0.25 M, according to the data in [71]. Since GOx in general does not tend to exhibit DET with electrode surfaces, in order to establish an electrical communication, a mediator is required. The redox potential of the mediator has to be more positive than the potential of FAD in order that electron transfer takes place. The development of enzymatic electrodes based on GOx has been associated to a great extent with the search of suitable mediators, which have both favorable potential and fast kinetics with the enzyme and the electrode surface according to Eq. (4) and (5), respectively.

Additional requirement with respect to practical and especially implantable applications is the use of immobilized mediators. Some examples of such enzymatic electrodes, which have found an application in glucose biofuel cells are ferrocene [72, 73], tetrathiafulvalene (TTF) [74, 75], 8-hydroxyquinoline-5-sulfonic acid (HQS) [76] and Os redox hydrogels [20]. So far, Os hydrogels with redox centers attached to a polymer backbone overpower other configurations as discussed in [10]. However, the procedure of synthesizing Os redox hydrogels is usually complicated and involves several steps [22]. In addition, with respect to the application of enzymatic biofuel cells as implantable power sources, some issues, associated with the toxicity of Os-containing compounds may arise [6].

After a thorough screening of different procedures for preparation of glucose-oxidizing anodes, two other alternatives for electrical wiring of GOx have been identified as potential

candidates for application in a biofuel cell. The first one is the notorious procedure, proposed by Willner and Katz, which involves the reconstitution of apo-GOx (enzyme lacking co-factor) over a gold electrode chemically modified by a PQQ/FAD redox relay [77, 78]. The sophisticated approach based on the optimized structural orientation of mediator, co-factor and enzyme at the electrode surface, which has been proposed by the authors, should result in effective electron transport, sufficiently negative onset, fast kinetics and negligible dependence on oxygen [77].

The second procedure that will be investigated is based on the utilization of a specific electrode architecture based on a polymer film, charge transfer complex (CTC) and gelatin layer. This approach should enable efficient electron transfer between GOx and the electrode surface, according to the authors [79]. This procedure results also in sufficiently negative anode potential, high current densities, minor response to the oxygen in normal buffer solutions and remarkable stability. The detailed description of the procedures and their advantages and disadvantages will be presented in the corresponding sections.

The current thesis aims to demonstrate the gradual development of an enzymatic glucose-oxygen fuel cell with focus on some aspects of the optimization at both anode and fuel cell level. Less attention will be paid to the oxygen-reducing cathode, which will be addressed only in the context of the fuel cell performance. First, the two electrode modification procedures will be investigated in detail in order to clarify their working mechanisms and the influence of the electrode architecture. Afterwards the anode with better characteristics will be combined with an inorganic cathode in a hybrid biofuel cell. This will allow for testing of the anode under “fuel cell” conditions as well as for investigation of the influence of design and operating parameters on the performance of the hybrid device. At the end the enzymatic anode will be combined with an enzymatic cathode and some aspects, associated with the latter will be discussed.

4. Reconstitution of GOx on modified gold

4.1 Approach for electrode modification

The electrode modification procedure proposed by Willner and Katz [77, 78] involves several successive steps, which are schematically depicted, together with the assumed electron transfer mechanism, in Figure 4-1. The first step is roughening of the smooth gold surface by contacting with liquid mercury and subsequent dissolving of the amalgam layer in concentrated nitric acid (1). The second step involves the functionalization of the rough gold electrode with a cysteamine monolayer, which introduces free amino groups at the surface (2). In the next step a mediator molecule, PQQ, is attached to the functionalized surface (3). Then a modified FAD molecule: *N*⁶-(2-aminoethyl)-FAD is attached directly to PQQ through its functional aminoethyl moiety (4). Finally, apo-enzyme is reconstituted over the PQQ-FAD redox relay (5). The functional electrode utilizes PQQ as a two-electron mediator, which transfers the electrons from FAD to the electrode surface.

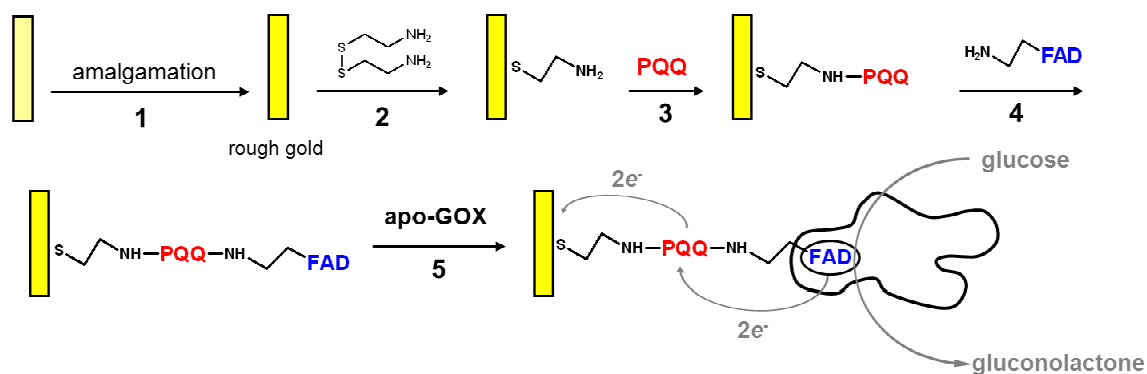


Figure 4-1: Schematic presentation of the electrode modification procedure and the respective working principle. Adopted from [77, 78].

The concept of the procedure, shown above is a logical follow-up of the initial efforts of the authors for reconstitution of apo-enzyme over a ferrocene-modified FAD in solution in order to obtain a site-specific modified “electroenzyme” [77]. By assembling the PQQ-FAD redox relay

and reconstituting the enzyme directly on the electrode surface, proper alignment and optimized positioning is achieved, which should result in an effective electron transfer between the biocatalyst redox co-factor and the electrode. Indeed, the authors reported current density of about $300 \mu\text{A cm}^{-2}$ at 80 mM glucose, which was in the range of the calculated theoretical current density, corresponding to the limiting turnover rate of the enzyme in a monolayer. In addition, the electron transfer efficiency was demonstrated by less than 2 % decrease of the amperometric signal in presence of air when the electrode was polarized at 0 V vs. SCE [77]. Similar reconstitution procedure has been also successfully applied for construction of enzymatic electrodes comprising of PQQ-boronic acid-FAD assembly [80], FAD-functionalized Au nanoparticles [81] and FAD-functionalized carbon nanotubes [82].

Despite of the apparent advantages, the group of Professor Willner reported only the employment of the reconstituted electrode together with a microperoxidase-11-based cathodes in biofuel cells based on hydrogen peroxide and cumene hydroperoxide as oxidants [63, 65]. The high performance of the proposed enzymatic anode design has motivated our initial efforts to reproduce the procedure (and optimize it further if possible) and then to employ it for preparation of an anode for use in a glucose-oxygen biofuel cell.

4.2 Electrode modification and activity

The method for electrode modification reported by Willner and Katz was adopted in the present study with slight modifications, regarding the procedure for preparation of apo-GOx and the carbodiimide coupling, which was used to assist the covalent attachment of PQQ and N^6 -(2-aminoethyl)-FAD to the electrode surface. All steps of the modification were followed by cyclic voltammetry.

Essential part in the procedure for preparation of apo-GOx is acidified salt treatment to unfold the spherical rigid protein by precipitation, so the FAD co-factor can be split off. The variations mainly concern the type of salt solution and the way of recovery of the dissolved protein. In this work the method proposed by Swoboda [83] was preferred over the method originally employed by Willner and co-authors [77] due to the simpler realization. The reconstitution ability of the apo-enzyme was checked in control experiments in solution at conditions identical to the surface reconstitution experiments. In a spectrophotometric assay the native enzyme exhibited activity

stated on the label and was used as a reference (100 %). Activity of reconstituted enzyme in solution was measured to be 86 % in the case of FAD and 63 % in the case of N^6 -(2-aminoethyl)-FAD.

The carbodiimide coupling is a common activation method for the reaction between amino and carboxylic groups, widely used in peptide chemistry. However, the carbodiimide reactive intermediate suffers from limited lifetime in aqueous solutions. This is the reason why the coupling reaction was further assisted by N-hydroxysulfosuccinimide in the present case, which was expected to improve the overall efficiency [84, 85].

In the first step the smooth gold electrode was subjected to amalgamation and consequent dissolving of the amalgam layer in concentrated nitric acid, according to the published procedures [86, 87]. This treatment leads to roughening of the gold surface as can be seen in Fig. 4-2. The highly developed gold structure observed in scanning electron microscopy (SEM) images is similar to the reported in the literature [86, 87].

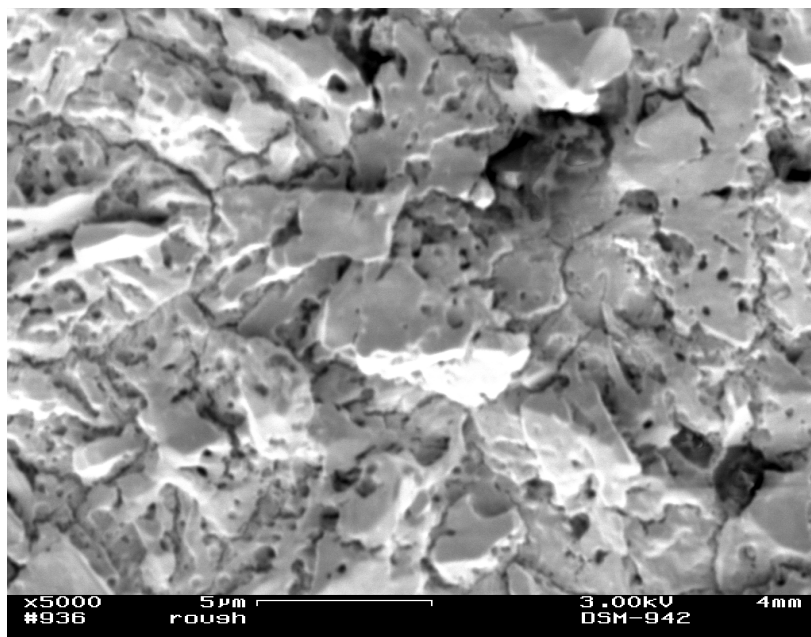


Figure 4-2: SEM image of rough gold.

In control experiments the real surface of the electrodes was determined by integration of the gold oxide reduction peak, according to [88] and a roughness factor of 25 ± 5 has been

determined. Voltammogram of the rough gold surface recorded immediately after amalgamation is shown in Fig. 4-3a. The observed voltammetric features have been assigned to OH layer formation on different single crystal domains [89], which will be discussed in detail in the next section. In the next step, a self-assembled monolayer (SAM) of cysteamine was formed on the roughened gold surface. Gold modification by thiol-containing compounds is a widely used approach for preparation of SAMs, which can be used to ensure selective access to the underlying surface and to introduce functional groups for further electrode modification [90, 91]. The voltammogram of the resulting cysteamine-modified surface is shown in Fig. 4-3a.

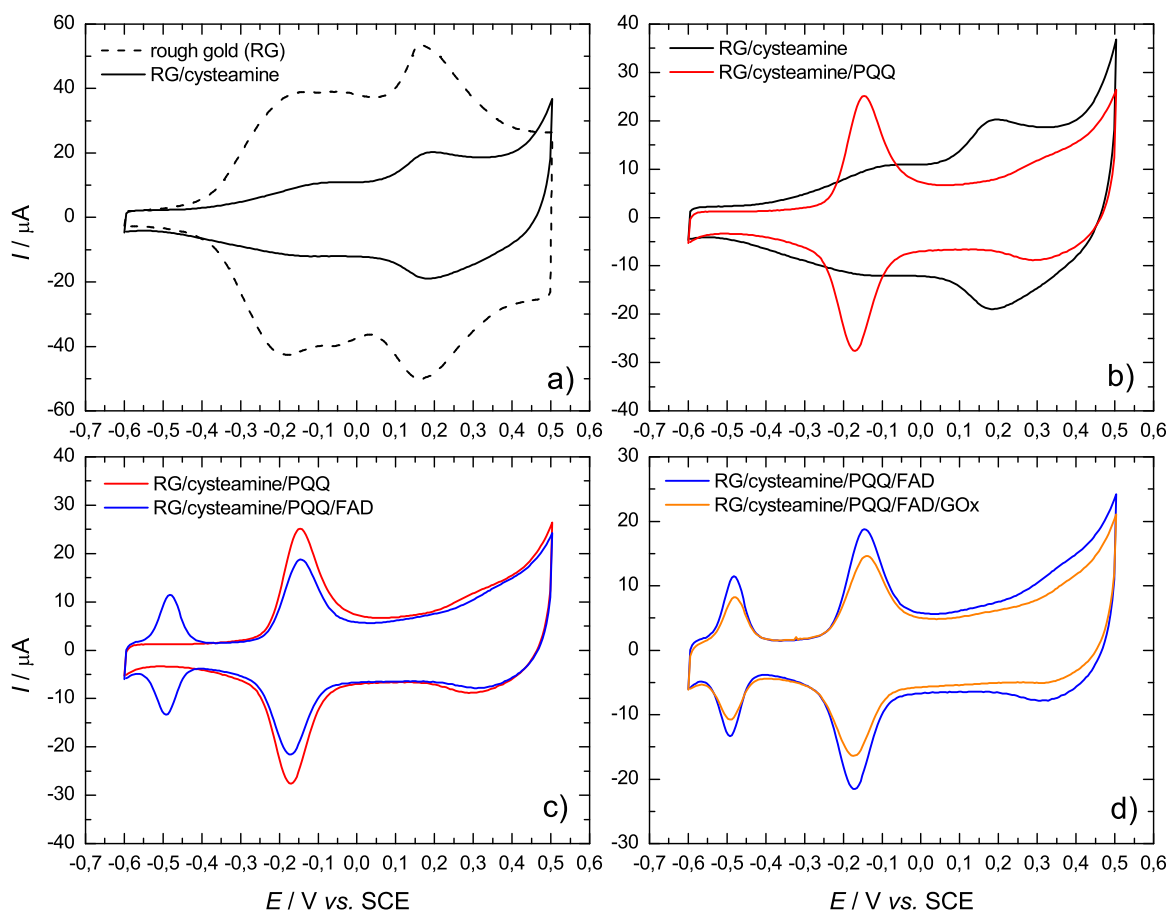


Figure 4-3: Cyclic voltammograms at different stages of the electrode modification. Conditions: 0.1 M phosphate buffer, pH 7.2, room temperature, N_2 atmosphere, scan rate: 20 mV s^{-1} .

The incomplete suppression of gold redox properties indicates successful SAM formation but incompact monolayer. The voltammetric features, accompanied by reductive desorption

experiments (discussed in the next chapter) indicate that the observed electrochemical behavior can be tentatively assigned to free Au(111) domains [89].

The electrode was further modified by PQQ, which presence on the surface could be followed by the appearance of a redox peak at -0.16 V vs. SCE, which value is close to the literature reported data (-0.13 V vs. SCE) [78] (Fig. 4-3b). The deviation can be due to the slight difference in pH and buffer composition since the formal redox potential of PQQ is pH dependent and an increase in pH decreases the potential, as shown in [86]. The value in the present case corresponds to the value, which can be roughly estimated from the pH dependence in the latter publication. In addition, the formal potential of immobilized PQQ is expected to be influenced also by the properties of the buffer due to its influence on the acid-base equilibrium of the polyelectrolyte mediator. The formation of PQQ layer is associated by additional suppression of the redox processes on gold. A surface coverage of 54 pmol cm^{-2} has been estimated based on the charge associated with the PQQ anodic peak assuming a two-electron process and a roughness factor of 25. This value is one order of magnitude lower compared to the previously reported values [78]. In general this method gives a rough estimation of the surface coverage, since it is difficult to determine precisely the real surface area and the limits for PQQ peak integration.

In the next step N^6 -(2-aminoethyl)-FAD has been attached to the surface. The presence of FAD on the surface was evidenced by the appearance of a redox peak at -0.49 V vs. SCE, which is in accordance to the value reported by Willner [78] and Gooding [92] (Fig. 4-3c). A surface coverage of 14 pmol cm^{-2} was calculated. The attachment of FAD was followed by a decrease of the PQQ peak charge with 3.8×10^{-5} C, which corresponded approximately to the charge associated with the FAD unit (3.2×10^{-5} C). This phenomenon can be taken as an indication that the modified PQQ molecules are accessible in the FAD peak during the voltammetry experiment and that the observed PQQ redox peak is associated only with non-functionalized PQQ molecules. It is likely that not all PQQ molecules are functionalized with FAD due to steric hindrance and other limitations. To our best knowledge, the behavior and intermolecular electron transfer in electrodes with redox components attached covalently in series has not been investigated in the literature so far.

In the last step of the modification apo-GOx was reconstituted over the FAD/PQQ functionalized electrode. The surface reconstitution was followed by additional suppression of

both FAD and PQQ peaks (Fig. 4-3d). Willner and co-workers observed only FAD peak suppression and ascribed it to insulation or “switching off” of FAD [77]. They assumed that not only FAD units within the protein but also external free FAD sites were shielded. In this respect, having in mind the large size of the protein and the short length of the spacer between PQQ and FAD, we assume that screening of PQQ molecules is also possible. The significantly smaller suppression of the FAD (and PQQ) peaks in the present case, compared to results in the original work [77], could be taken as an indication of inefficient reconstitution. However, as discussed above, the ability of the apo-enzyme for reconstitution in solution was proved by a spectrophotometric assay. In addition, despite of the smaller suppression, the surface coverage for GOx was estimated based on the depleted charge of the FAD peak, assuming two FAD units per one molecule of GOx, and a value of 2 pmol cm^{-2} was obtained, which was close to the literature reported value of 1.7 pmol cm^{-2} [78]. It should be noted that we used an identical approach for the estimation of the GOx coverage in order to compare our results with the results published in the literature. The active enzyme is a dimer composed of two sub-units, each containing one FAD molecule, which in our opinion significantly complicates the successful reconstitution of GOx on the electrode surface in a fully active form. However, in another study Willner and co-authors have demonstrated that the enzyme is reconstituted in a biologically active configuration on the electrode surface [80]. This conclusion was based on experiments with electrodes lacking a PQQ unit that exhibited electrical response to glucose only in presence of a diffusional mediator.

The enzymatic electrode in the present study exhibited high catalytic activity towards glucose oxidation with current density (based on geometrical surface area), reaching about $700 \text{ } \mu\text{A cm}^{-2}$ at 20 mM glucose (Fig. 4-4). The presence of one oxidation wave and the oxidation onset was in accordance with previously reported results. However, as can be seen in Fig. 4-4, the onset of glucose oxidation in the present case is shifted to more negative potentials with glucose concentration. At 20 mM or higher the onset coincides with the PQQ redox peak. This is in good agreement with the behavior at 80 mM glucose, originally shown in [77, 78], which has been ascribed to a PQQ-mediated electron transfer mechanism. It should be noted that Willner and co-workers investigated the activity for glucose oxidation in a limited (compared to the present case) potential range: up to 0.2 V [77] and up to 0.35 V vs. SCE [65] and in both cases the oxidation curves had different shape.

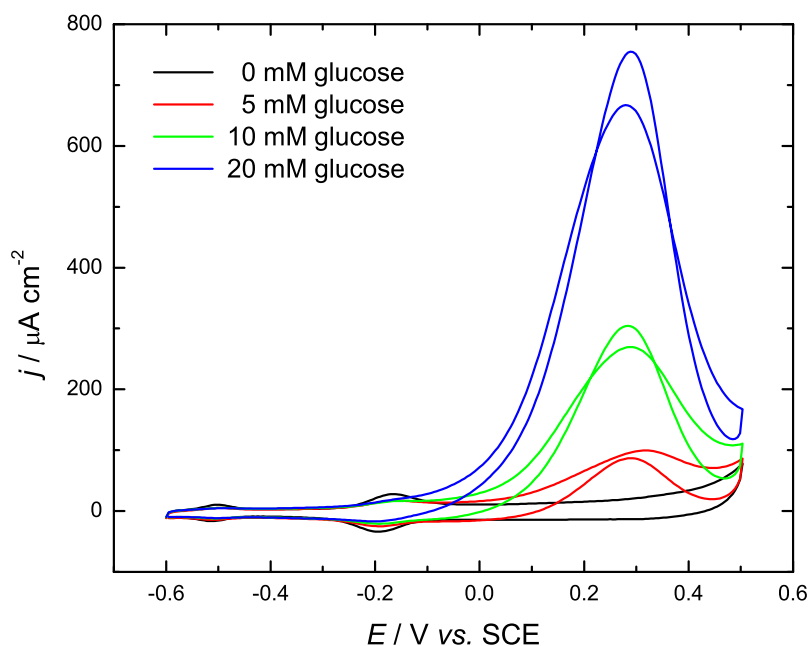


Figure 4-4: Cycling voltammograms, showing the oxidative activity of the enzymatic electrode in presence of different glucose concentrations. Conditions: 0.1 M phosphate buffer, pH 7.2, 37 °C, N₂ atmosphere, scan rate: 20 mV s⁻¹.

In the present case the upper potential limit of the voltammogram was extended to 0.5 V vs. SCE in order to obtain a fully developed limiting current region. However, a peak was observed instead of limiting current. It can be speculated that a similar behavior was shown in some of the original publications [77, 78] but the comparison is difficult due to the difference in the potential range. In the latter publications the upper potential limit was limited to 0.2 V vs. SCE and a peak was observed. Though, in another publication by the same authors, the upper potential limit was extended to 0.35 V vs. SCE and a well-expressed limiting current was observed [65]. However, it should be noted that in both series of publications the same electrode modification procedure has been addressed with no apparent difference, except the buffer composition. 0.1 M phosphate buffer has been used in the publications with upper potential limit of 0.2 V vs. SCE. In the case of a limiting current behavior, 0.01 M phosphate buffer with 0.05 M tetrabutylammonium tetrafluoroborate (TBATFB) has been used but the authors have not provided an explanation why the quaternary ammonium supporting salt changes the shape of the oxidative curve.

The behavior in the present case (well-defined peak) is in general not characteristic for bioelectrochemical systems. Such peak has been observed only in the case of hydrogen oxidation by hydrogenases [93] due to deactivation at higher anodic potentials, associated with redox changes of the NiFe catalytic center. However, this is not characteristic for GOx-based electrodes. Even in the case of mass transport limitations in the system, the current after the peak is expected to level off and not to decrease so dramatically. Moreover, well defined oxidation peaks were present even at very low sweep rates, suggesting that substrate depletion is not responsible for the electrochemical behavior of the enzymatic electrode.

On the other side, it is known that gold surfaces are able to catalyze the oxidation of different sugars including glucose [87, 94]. The onset potential for glucose oxidation and the number of peaks are correlated with the formation of AuOH species and the sharp current decrease at more positive potentials is attributed to oxide formation [94]. In order to clarify the origin of electrocatalytic activity in the enzymatic electrode, the behavior of smooth and rough gold, as well as rough gold modified with different layers has been investigated.

4.3 Electrocatalytic activity and behavior of gold

The behavior of the freshly prepared rough gold surface has been studied at room temperature and at 37 °C (Fig. 4-5). The voltammogram at room temperature is characterized by two peaks, which appear at approximately -0.19 and 0.17 V vs. SCE, which shape is identical to the reported in the literature [87]. At 37 °C the two very distinct peaks, observed at room temperature, merge into one peak. Additionally a decrease of capacitance in the double-layer region is observed. It was observed that this process occurs at room temperature as well but it takes several hours, while at 37 °C it is accelerated and occurs within several minutes. Similar change is observed when the electrode is kept in an inert gas atmosphere in absence of liquid.

The surface formed at 37 °C is stable under electrochemical conditions, but only in a limited potential range. If the potential region is extended to the region of gold oxide formation the features observed at room temperature are regenerated (Fig. 4-5). This process is referred in the text as electrochemical activation and the respective curves are denoted as “activated” in the figures. However, the regeneration is not complete since a decrease of the surface area is observed. The decrease can be due to a similar phenomenon as reported in [95] in the case of

gold surface after stripping of underpotential-deposited silver. The authors referred to the process as “self-annealing” and explained it by the tendency of a rough surface to reduce surface energy by merging smaller defects into larger ones.

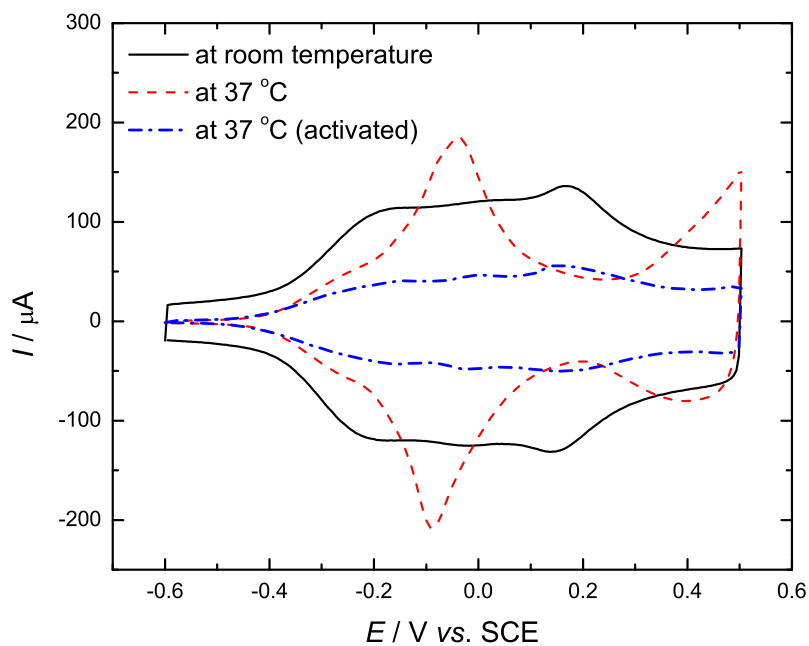


Figure 4-5: Cyclic voltammograms of rough gold at different conditions. Conditions: 0.1 M phosphate buffer, pH 7.2, N_2 atmosphere, scan rate: 50 mV s^{-1} .

The polycrystalline gold surface can be roughly considered as a combination of three low index single crystal planes. In this respect the observed voltammetric features can be assigned to OH formation on different single crystal domains of the polycrystalline surface (Fig. 4-6, data for single crystal surfaces based on reference [94]). In [87] similar voltammetric features were obtained after amalgamation but the authors correlated it to Au(110)-like structure. According to our analysis it is more likely that the fresh rough surface, characterized at room temperature, contains contributions of all three planes.

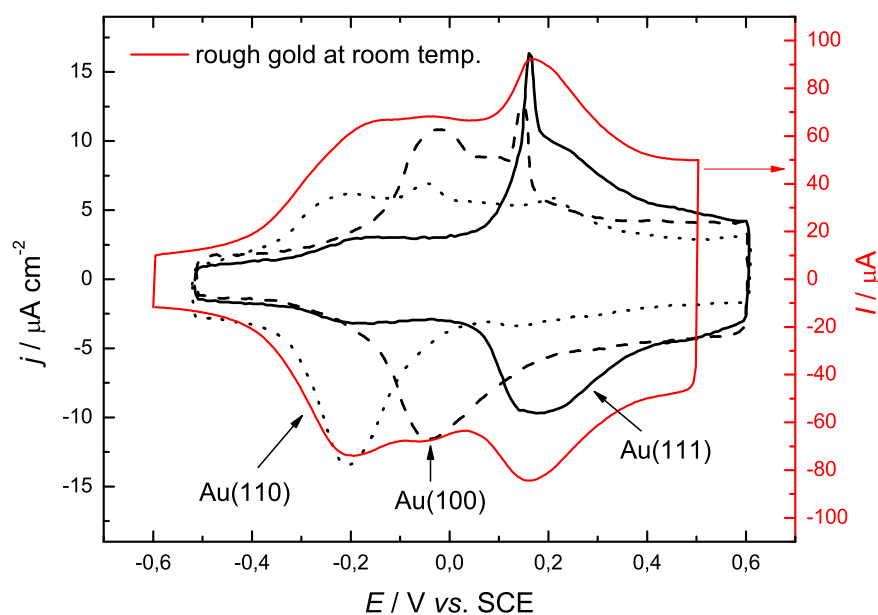


Figure 4-6: Cyclic voltammograms of rough gold and three types of single crystal gold. Conditions: 0.1 M phosphate buffer, pH 7.2, room temperature, N_2 atmosphere, scan rate: 50 mV s^{-1} . Data for single crystal surfaces based on [94].

The observed changes of surface properties of rough gold at elevated temperature can be assigned to some kind of surface restructuring. The peak position in the voltammogram of rough gold at $37 \text{ }^\circ\text{C}$ (Fig. 4-5, 4-6) resembles Au(100)-like surface but without additional microscopic studies it is difficult to draw a final conclusion.

The activity of smooth and rough gold for glucose oxidation has been investigated at $37 \text{ }^\circ\text{C}$. As can be seen in Fig. 4-7, smooth gold (flame annealed to melting) appears relatively featureless, with low current intensities and low activity for glucose oxidation at $37 \text{ }^\circ\text{C}$ (oxidation onset at about 0.05 V vs. SCE and very low peak current). The negligible activity of annealed gold is in accordance to the results in the literature [87]. If the electrode is electrochemically activated, the activity is enhanced and the oxidation onset is shifted to approximately -0.35 V vs. SCE . However, the peak current density reaches only about $7 \mu\text{A cm}^{-2}$. The shape of the voltammogram is identical to the behavior of alumina polished gold at room temperature [96].

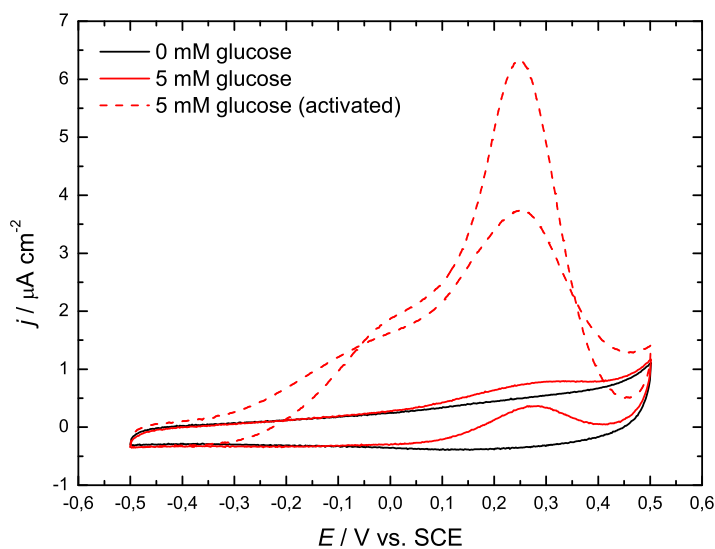


Figure 4-7: Cyclic voltammograms showing the activity of smooth gold before and after electrochemical activation. Conditions: 0.1 M phosphate buffer, pH 7.2, 37 °C, N₂ atmosphere, scan rate: 5 mV s⁻¹.

Similar to smooth gold, rough gold also exhibits very low activity in the limited potential range (Fig. 4-8). Nevertheless, the associated currents are higher and the reaction starts at more negative potential values. The catalytic effect of roughening has been shown in [87] and it has been attributed to the exposure of active sites on the gold surface. The activity in the latter case was significantly higher compared to present case and was increasing with an increase in amalgamation treatment length. However, experiments in [87] were performed only at room temperature, whereby the process of surface restructuring observed in Fig. 4-5 occurs with significantly lower rate as discussed above.

Analogous to the case of smooth gold, when the rough gold surface is electrochemically activated, the activity for glucose oxidation at 37 °C is significantly enhanced and the voltammogram is characterized by much higher current densities and faster kinetics. Current density of about 300 μA cm⁻² is reached already at -0.15 V vs. SCE (Fig. 4-8). The voltammetric behavior in presence of glucose of the electrochemically activated gold is identical to the behavior of rough gold reported in the literature at room temperature [96] and the behavior of smooth polycrystalline gold, which has been investigated in an extended potential range (corresponding to electrochemical activation in the present case) [94]. If the electrochemically activated rough gold surface is kept in buffer or is cycled only in the limited potential range, its

activity decreases rapidly and soon falls down to the level observed before electrochemical activation in Fig. 4-8.

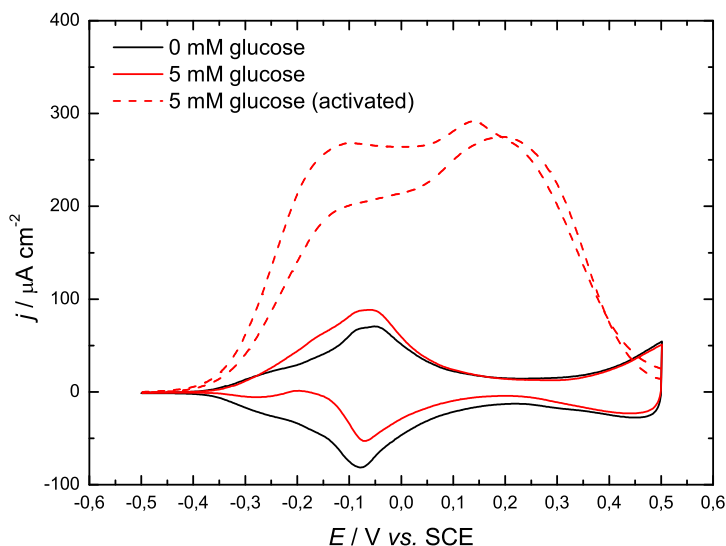


Figure 4-8: Cyclic voltammograms showing the activity of rough gold before and after electrochemical activation. Conditions: 0.1 M phosphate buffer, pH 7.2, 37 °C, N₂ atmosphere, scan rate: 5 mV s⁻¹.

The polycrystalline gold surface has been subjected to two different treatments (amalgamation and electrochemical activation), which have different effects. On the one side amalgamation has a pronounced influence on the catalytic properties. It increases the surface area and shifts the oxidation onset to more negative values. The latter effect is ascribed to the selective exposure of active sites, which can be tentatively interpreted in terms of different single crystal planes, since the activity of gold is known to be dependent on the crystallographic orientation [94].

On the other side the activity of both smooth and rough gold surfaces at 37 °C and in a limited potential range is low and it is restored only after electrochemical activation. The reason for this low activity is difficult to identify unambiguously without additional investigations. In the case of rough gold the surface restructuring at elevated temperature, leading to inactivation, can be clearly observed by the characteristic change of the voltammogram shape (Fig. 4-5) and the resulting features can be tentatively assigned to Au(100)-rich surface (Fig. 4-6). Electrochemical treatment is one of the procedures that can be used to alter the properties of a metal surface and to achieve certain crystallographic orientation. This process is referred to as electrochemical faceting [97]. In the case of polycrystalline gold it has been demonstrated that the formation of

an oxide layer and its subsequent reduction (controlled by a square-wave potential perturbation) significantly changes the ratio of different single crystal planes and increases the fraction of Au(111) [98]. The electrochemical activation in the present case involves the same processes and differs only in the type of potential perturbation – potentiodynamic versus potentiostatic. Consequently, it can be anticipated that it will have a similar effect on the gold surface.

However, it is difficult to assign the low activity solely to Au(100)-like surface, since it is also expected to have a significant activity for glucose oxidation, according to [94], at least at room temperature. Unfortunately, the simultaneous influence of temperature and potential range of single crystal and polycrystalline gold surfaces has not been studied in the literature.

The reduced activity might be also associated with the adsorption of phosphate anions at the gold surface, which process probably occurs in parallel with the change in the gold surface crystal structure. Anions from the buffer solution can adsorb on the electrode surface and partially block the initial stage of oxidation of gold, as discussed in [99], thus impeding the formation of Au(OH) layer, which is responsible for the catalytic activity of gold [94]. It has been shown that glucose oxidation is inhibited by anion adsorption [100, 101]. Phosphate anions were found to have the least influence from the investigated anions in neutral media [100] but major impact in acidic solutions [101], outperformed only by chloride anions. The inhibiting effect of chloride has been demonstrated also in the case of rough gold, prepared by amalgamation [87]. In addition, it should be noted that the geometrical conformity between the anions and the different crystal lattices plays a role on the rate of adsorption, as discussed in [101]. According to these considerations, it can be assumed that the reduced catalytic activity of gold in the limited potential range can be ascribed to the simultaneous effects of surface restructuring, associated with different single crystal planes, and/or phosphate adsorption. Potential cycling in an extended region (formation and dissolution of an oxide layer) is expected to clean the surface and change the ratio of different crystal lattices, which will lead to restoration of the catalytic activity but only for a limited time.

After the activity of bare gold has been discussed, in order to investigate further whether the catalytic activity of the enzymatic electrode has electrocatalytic or bioelectrocatalytic origin, the behavior of the rough gold electrode has been checked at different stages of modification. First, the activity of freshly prepared rough gold, modified by a SAM of cysteamine has been tested in presence of glucose at 37 °C (denoted as “active RG/cysteamine” in Fig. 4-9; not the same as

“activated” in previous figures). In control experiments the rough gold surface has been first exposed to elevated temperature in phosphate buffer for a given time to enhance the surface restructuring, shown in Fig. 4-5 and then modified by SAM. This surface has been referred to as “inactive RG/cysteamine”. As can be seen in Fig. 4-9, the rough gold, which has been modified by a SAM right after the amalgamation, exhibits high activity towards glucose oxidation.

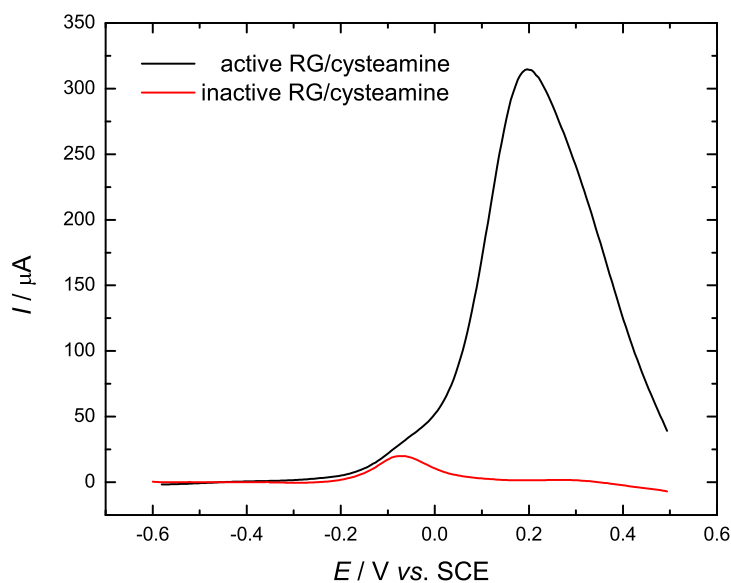


Figure 4-9: Linear sweep voltammograms of different rough gold (RG) surfaces, modified by cysteamine in presence of 5 mM glucose. Conditions: 0.1 M phosphate buffer, pH 7.2, 37 °C, N₂ atmosphere, scan rate: 20 mV s⁻¹.

The catalytic activity has been tentatively ascribed to exposed Au(111) domains [89], based on the position of the peak and the characteristic form of the oxidation wave (a pre-peak and a main peak at about 0.2 V vs. SCE), which is in accordance to the behavior of Au(111), shown in [94]. Contrary to the fresh rough gold, the “inactivated” rough gold, modified by SAM has a negligible activity, which is evidenced by a small peak at about -0.1 V vs. SCE, which position coincides with the position of the pre-peak in case of the “active” gold. The major peak is, however, completely suppressed.

The hypothesis of exposed Au(111) domains on the “active” rough gold surface has been further assisted by reductive desorption experiments [89]. The position of reduction peaks depends on the presence of different single crystal domains on the surface due to different binding strength with the chemisorbed thiol [102]. In the case of single crystal surfaces, the

Au(111) exhibits the lowest affinity for thiol chemisorption and consequently the most positive potential for its reductive desorption. It has been shown that in the case of polycrystalline gold, due to presence of different single crystal domains, multiple peaks are obtained and only the peak corresponding to Au(111) can be clearly observed at about -0.7 V vs. Ag/AgCl, while the other peaks at more negative potentials merge into a broader one [102].

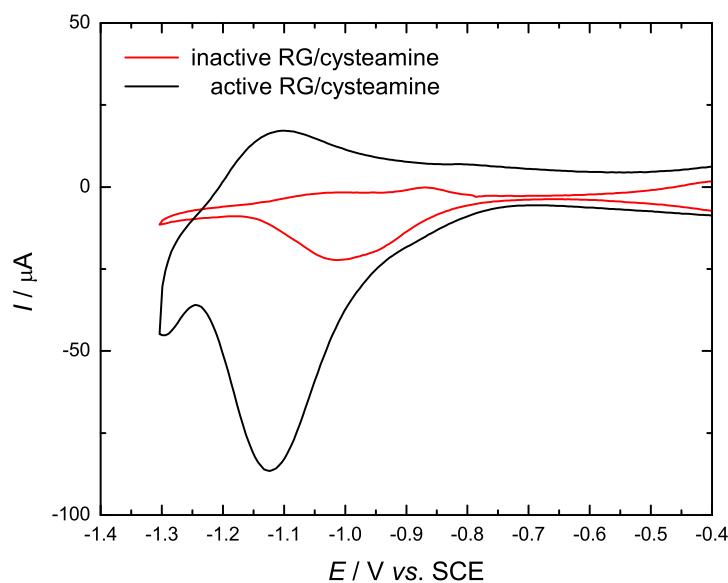


Figure 4-10: Cyclic voltammograms (1st scans) for the reductive desorption of cysteamine formed on different rough gold surfaces. Conditions: 0.5 M KOH, room temperature, N₂ atmosphere, scan rate: 20 mV s⁻¹.

As can be seen in Fig. 4-10, the rough gold surface modified by cysteamine lacks a peak at the position, which would correspond to cysteamine reductive desorption formed on Au(111). This hypothesis is also in accordance to the behavior in buffer (Fig. 4-3a), which indicates not compact SAM and the observed peaks can be assigned Au(111)-like surface. On the other side, the absence of the corresponding reductive peak in the case of “inactivated” rough gold and the respective behavior in buffer (Fig. 4-5) can be tentatively assigned to lack of Au(111) domains. In addition, the area of the desorptive peak in the latter case is significantly smaller, which indicates smaller affinity of this type of surface towards the self-assembly, as discussed in [89]. The results shown above clearly indicate that the SAM preserves the catalytic activity of rough gold at elevated temperatures even in the limited potential range. This effect can be tentatively

ascribed to the selective exposure of Au(111) domains at the rough electrode surface and/or to the prevention of anion adsorption.

The catalytic activity of the rough gold surface, modified further with different layers, according to the electrode modification procedure has been also investigated (Fig. 4-11). Similar to the cysteamine modified surface, gold functionalized by PQQ, FAD and GOx, exhibit electrocatalytic activity toward glucose oxidation (Fig. 4-11) but the addition of further layers decreases the activity, shifting the oxidation onset to more positive potentials and decreasing the peak intensity.

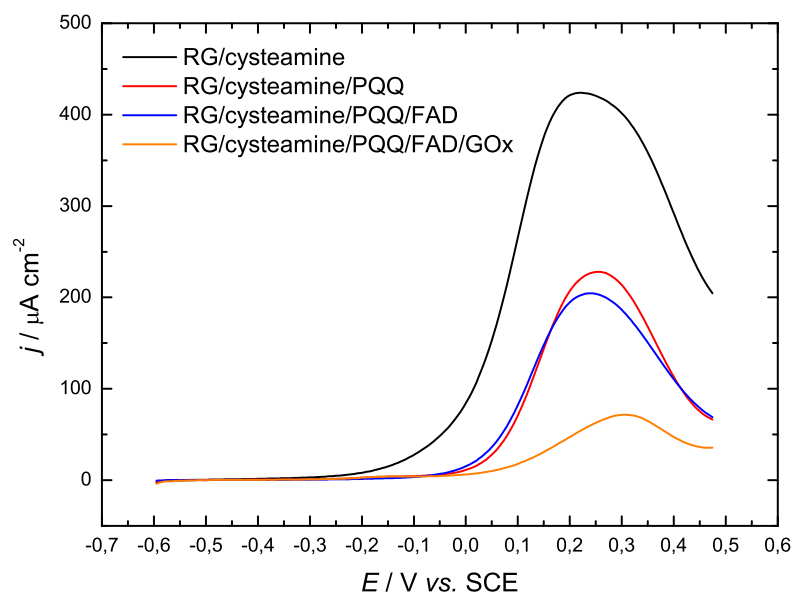


Figure 4-11: Cyclic voltammograms showing the activity for glucose oxidation of gold electrodes at different stages of the modification. Conditions: 5 mM glucose in 0.1 M phosphate buffer, pH 7.2, 37 °C, N₂ atmosphere, scan rate: 5 mV s⁻¹.

For example, the rough gold modified only by a SAM shows an oxidation onset at about -0.3 V vs. SCE and peak current density of approximately 400 $\mu\text{A cm}^{-2}$, while the GOx-reconstituted electrode has an oxidation onset at about -0.1 V vs. SCE and peak current density of approximately 70 $\mu\text{A cm}^{-2}$. These results are in contradiction to the original results, where the authors stated that the PQQ-FAD monolayer alone does not stimulate oxidation of glucose [78].

4.4 Conclusions about the origin of catalytic activity

The enzymatic electrode prepared according to the modification procedure, proposed by Willner and co-workers has a significant activity for glucose oxidation, even at concentrations as low as 5 mM. However, the results shown in the previous section indicate that it is difficult to ascribe this activity solely to the catalytic action of glucose oxidase due to the apparent activity of the underlying gold substrate. Smooth gold has a negligible activity for glucose oxidation at 37 °C in the limited potential range of interest (Fig. 4-7). Under the same conditions rough gold also exhibits low activity (Fig. 4-8). The high activity of rough gold can be observed either at room temperature as demonstrated in [87] or after electrochemical activation by cycling in an extended potential range. The loss of activity in the limited potential range is ascribed to some kind of surface restructuring, which is evident by the change of the voltammogram shape, and possibly by anion adsorption. The formation of a SAM on the rough gold surface preserves the activity even at elevated temperatures and shifts the oxidation wave to more positive potentials, resembling the behavior of Au(111). Based on these results it can be concluded that the largest part of the activity of the enzymatic electrode comes from the underlying gold surface.

This conclusion implies that in previous studies, where the same electrode modification procedure was used [63, 65, 77, 78], the possibility of an electrocatalytic (opposed to bioelectrocatalytic) mechanism should be considered. This can explain the unrealistically high turnover rate numbers (in the range of native enzyme) that have been estimated in the original publications [77, 78]. In addition, the authors have reported a minor decrease in current in air-saturated solutions. The negligible response to oxygen has been taken as an indication of very efficient electron transfer.

In order to investigate this unusually high tolerance to oxygen, the behavior of the rough gold electrode modified by PQQ and FAD has been tested in presence of glucose and oxygen (Fig. 4-12). The modified electrode is active for oxygen reduction and the activity can be tracked down to the bare and the cysteamine-modified rough gold surface as it has been shown in [103]. As can be seen in Fig. 4-12, the oxygen reduction activity of the PQQ-FAD-modified electrode has an onset potential around 0 V vs. SCE, which, having in mind the similar experimental conditions, can explain the little dependence on oxygen, originally observed by the authors [77].

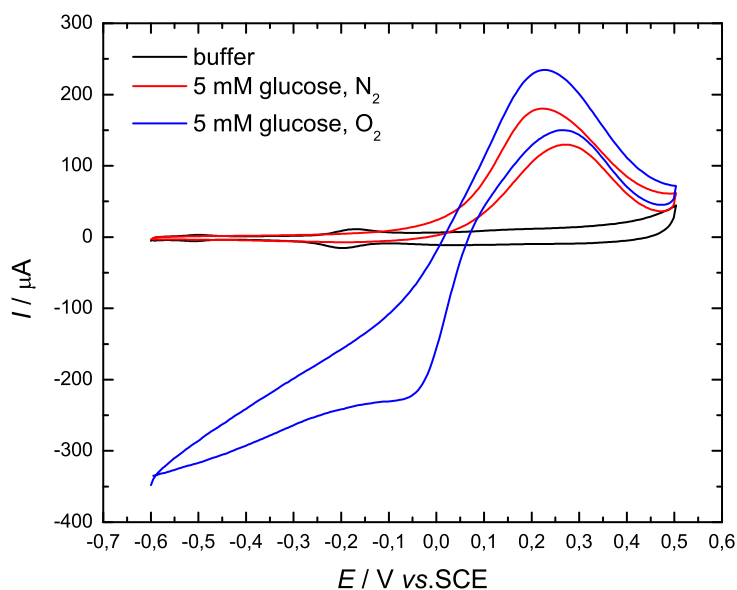


Figure 4-12: Cyclic voltammograms of the PQQ-FAD assembly, showing the catalytic activity for glucose oxidation in presence and absence of oxygen. Conditions: 5 mM glucose in 0.1 M phosphate buffer, pH 7.2, 37 °C, scan rate: 5 mV s⁻¹ (Response in buffer is also shown for clarity).

The results shown in Fig. 4-11 contradict the observation by Willner and co-authors that the PQQ-FAD assembly does not stimulate glucose oxidation [78]. A possible explanation of this lack of activity, which they observed, can be the use of smooth instead of rough gold surface. This can be speculatively concluded by the experimental description of the electrode modification in another publication: “Prior to the modification and measurements they (gold wire electrodes) were cleaned according to ... and, if required, roughened by treatment with mercury followed by dissolution of the amalgam layer in nitric acid.” [77]. However, this ambiguous description impedes the straightforward analysis of the previously reported results.

The results shown above indicate that the bioelectrochemical origin of the current in the reconstituted enzymatic electrode in the present study cannot be unequivocally confirmed and compromise to a certain extent the original works. Based on these conclusions, the procedure, involving reconstitution of apo-GOx on a modified gold surface has been abandoned and another electrode modification route has been investigated.

4.5 Experimental details

4.5.1 Chemicals and materials

Polycrystalline gold wires (0.5 mm diameter, 0.47 cm² working area) were used as platforms for electrode modification and electrochemical measurements. The polycrystalline gold was first subjected to electrochemical polishing [104] and then to flame annealing until the gold surface was slightly melted. This surface has been referred to as smooth gold. Rough gold electrodes were fabricated from a smooth gold surface by amalgamation [86, 87], which consisted of typically 10 s long contact with liquid mercury, followed by dissolving of the formed amalgam layer in concentrated nitric acid. In some experiments the gold electrodes were subjected to electrochemical preconditioning, which consisted of 10 potential cycles from -1 V to 1.3 V vs. SCE in 0.1 M phosphate buffer and has been referred to as electrochemical activation.

4.5.2 Synthesis of *N*⁶-(2-aminoethyl)-FAD

The modified FAD was synthesized according to the procedure of Bückmann [105]. Briefly, in the first step FAD was reacted with ethyleneimine (aziridine) in water at 30 °C in dark to give a *N*¹-functionalized FAD analog. The reaction was monitored by HPLC system, equipped with DAD (Diode Array Detection) and ESI-MS (Electrospray Ionization Mass Spectrometer). After 100 h reaction time the 60 % conversion rate, which was cited in the literature was reached and the reaction mixture was washed several times with cold ethanol to remove the unreacted aziridine. In the next step the conversion of the chemically unstable *N*¹-derivative to the desired *N*⁶-(2-aminoethyl)-FAD, known as Dimroth rearrangement, was performed under mild aqueous conditions (pH 6.5, 40 °C). After 7 h the reaction was terminated and the reaction mixture was subjected to preparative chromatography. The desired product was identified in the largest fraction, lyophilized and characterized by MS and ¹H and ¹³C Nuclear Magnetic Resonance. Further details of the synthetic modification and analysis can be found in the Master's thesis of Ivan Ivanov, submitted to the Department of Organic Synthesis, UCTM Sofia in 2006.

4.5.3 Preparation of apo-GOx

Apo-GOx was prepared from native GOx from *Aspergillus niger* (198 U mg⁻¹ activity as stated on the label), according to the procedure described by Swoboda [83]. Briefly, GOx was added slowly to an acidified saturated ammonium sulfate solution (pH 1.4) at -5 °C. The yellow supernatant was removed after centrifugation at 15000 rpm for 20 min at -5 °C and the precipitate was redissolved and neutralized with sodium acetate solution at 0 °C. The neutralized solution was subjected to one more cycle of acidified salt treatment, centrifugation and neutralization and when colorless, the enzyme was precipitated with neutral 90 % saturated ammonium sulfate solution and redissolved to concentration approximately 10 mg ml⁻¹ in 0.1 M phosphate buffer (pH 6.2), containing small amounts of bovine serum albumin and sodium azide.

In control experiments, apo-enzyme was reconstituted with FAD and N⁶-(2-aminoethyl)-FAD in solution. The apo-GOx was dissolved to concentration 1 mg ml⁻¹ and reacted with the respective co-factor for 4 h at 25 °C and 12 h at 4 °C. The activity of native and reconstituted enzymes was measured spectrophotometrically by a glucose oxidase assay kit (K-GLOX, Megazyme).

4.5.4 Electrode modification

The enzymatic electrode has been modified according to the published procedures [77, 78]. Briefly, the freshly prepared rough gold electrode was soaked in 0.02 M cystamine solution for 2 h at room temperature, which resulted in a SAM-modified surface. In the next step the electrode was incubated for 1.5 h in 0.003 M solution of PQQ in the presence of 0.01 M 1-ethyl-3-(3-dimethylaminopropyl) carbodiimide hydrochloride (EDC) and 0.005 M N-hydroxysulfosuccinimide (NHS) in 0.01 M HEPES aqueous buffer solution (pH 7.5) at room temperature. The PQQ-modified electrode was further functionalized by reaction with 0.0004 M N⁶-(2-aminoethyl)-FAD in 0.01 M HEPES buffer solution in the presence of 0.001 M EDC and 0.001 M NHS for 1.5 h at room temperature. Finally, the FAD-modified electrode was reacted with 1 mg ml⁻¹ apo-GOX solution in 0.1 M phosphate buffer solution (pH 6.2) for 4 h at room temperature and for 12 h at 4 °C. The buffer solution contained also 0.1 %

w/v bovine serum albumin and 0.1 % w/v sodium azide as stabilizers and preservatives. After that the electrode was left for 1 h more in buffer solution without apo-enzyme in order to remove the physically entrapped protein.

4.5.5 Electrochemical experiments

Electrochemical experiments were carried out in a three-electrode electrochemical cell with saturated calomel electrode (SCE) as a reference electrode by the use of potentiostat PGSTAT302 (Autolab, Netherlands). The gold wires were used as working electrodes and Pt wire as a counter electrode. Measurements were performed in 0.1 M phosphate buffer (pH 7.2) under nitrogen or oxygen atmosphere.

5. Enzymatic electrode based on TTF-TCNQ

5.1 Historical background and advantages of TTF-TCNQ

Charge transfer complexes (CTCs) are molecular complexes, characterized by partial transfer of electron from a donor to an acceptor. CTCs can be in general classified as a type of organic conductor together with organic conductive polymers [106]. The history of conductive organic molecules could be dated back to 1954, when the first molecular crystal (perylene-bromine complex) with high conductivity was reported [107]. However, the field of organic conductors was practically initiated by the discoveries of the tetracyanoquinodimethane (TCNQ) and the tetrathiafulvalene (TTF) molecules [108] and benchmarked by the first report of near-metal conductivity of the TTF-TCNQ complex [109]. TTF-TCNQ is a CTC (also known as organic salt or organic metal) with a room temperature conductivity in the range of $400 \pm 100 \text{ S cm}^{-1}$ [110] due to efficient overlapping of the π -orbitals of the respective molecules. The conductive salt is composed of segregated parallel stacks of TTF and TCNQ and the π -orbitals interact mainly along the stacking direction, which results in a quasi-one-dimensional conductor [108].

The unique electrical properties of TTF-TCNQ have naturally prompted studies on its utilization as an electrode material. Jaeger and Bard first studied the behavior of TTF-TCNQ electrodes in different aqueous solutions and found a stable potential range of about 0.7 V [111]. Since this groundwork, the TTF-TCNQ complex evolved as a highly efficient electrode material for more specific, namely bioelectrocatalytic applications. Pioneering works in this direction were done by Kulys and co-workers with other organic salts – complexes between N-methylphenazinium (NMP^+) or N-methylacridinium (NMA^+) and TCNQ [112, 113]. Later on, Albery and co-workers investigated different CTCs as electrode materials for the oxidation of GOx. They found that the best performance had the TTF-TCNQ salt [114] and exploited it further as an electrode material for the regeneration of other flavoenzymes [115].

Since then, the enzymatic electrocatalysis on TTF-TCNQ electrodes has been a subject of extensive research, almost exclusively for biosensor applications. TTF-TCNQ has been mostly used in combination with GOx for the determination of glucose concentration but studies,

involving other substrates and enzymes have been also reported. The efforts in the development of amperometric biosensors based on TTF-TCNQ have been summarized in a recent review [116].

In our opinion CTC-based enzymatic electrodes have a great promise for biofuel cell applications. Glucose biosensors based on TTF-TCNQ exhibit high current densities, high oxygen tolerance and remarkable stability under continuous operation [79, 117]. In addition, CTC has several other advantages. Enzymatic electrodes based on TTF-TCNQ do not require complicated modification procedures, in fact they can be prepared as simply as carbon paste electrodes by mixing of the respective components [118]. The TTF-TCNQ salt is commercially available and has high electronic conductivity, which is beneficial for lowering the ohmic resistance within the electrode layer. The morphology of the CTC-crystals can be tuned by variation of the experimental conditions [119]. They can be also prepared in form of nanoparticles [120]. These strategies can be applied to tune the catalytic properties of the CTC and/or to increase the catalytically active surface area. Both TTF and TCNQ have low toxicity, which is attributed to their low solubility in water and physiological fluids [121]. In addition, the catalytic properties of the CTC and the overpotential for glucose oxidation can be further improved by lowering of the redox potentials of its components, e.g. of TTF [122]. However, despite these promising features, TTF-TCNQ anode, to our best knowledge, has not been employed in an enzymatic fuel cell so far.

There are several reports describing the electrical contacting of GOx through TTF-TCNQ but our attention has been drawn by the approach, proposed by Khan [79]. This modification procedure should ensure high current densities, relatively negative oxidation onset and fast kinetics. Especially beneficial for biofuel cell applications is the remarkable stability, which has been reported in the literature. Khan et al. have shown that glucose biosensors based on TTF-TCNQ can retain up to 40 % of their initial response after 100 days of continuous operation [79]. Therefore, we have decided to adopt the procedure, to investigate it in detail and optimize it and finally, to employ the resulting enzymatic anode in a biofuel cell.

5.2 Electrode modification and activity

The electrode modification involves several steps, which are schematically depicted in Fig. 5-1 [79]. In the first step a conducting polymer film is electrochemically grown on a stainless steel electrode (1). In the second step a layer of TCNQ is applied on the polymer surface (2). After that, a TTF solution is cast over the TCNQ layer, thus allowing for a direct growth of CTC crystals (3). In the next step, enzyme solution is adsorbed at the TTF-TCNQ crystal structure (4). Finally, the whole assembly is covered with a gelatin solution to form a stabilizing gelatin film and after drying the film is cross-linked with glutaraldehyde (5).

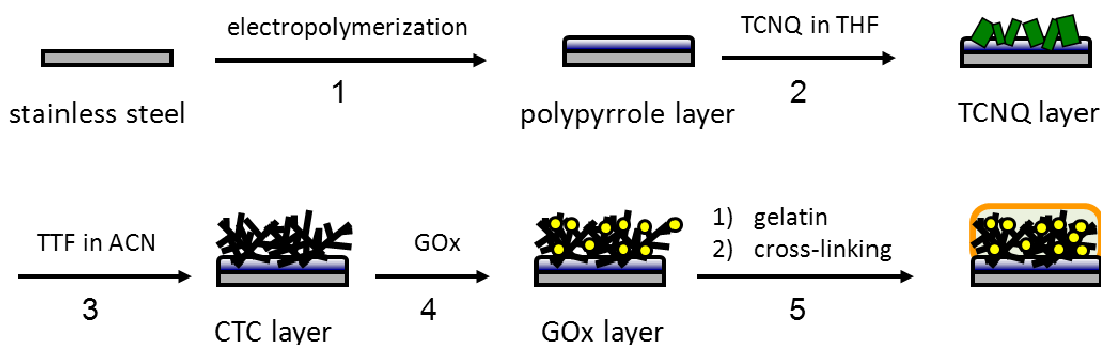


Figure 5-1: Schematic presentation of the electrode modification procedure, according to [79].

The underlying chemically inert polymer film should ensure mechanical stability of the electrode assembly. According to the authors, the polymer film swells in presence of tetrahydrofuran (THF) in which TCNQ is dissolved by the casting procedure and TCNQ crystals penetrate the polymer, thus providing strong roots for the TTF-TCNQ crystal structure [79]. The polymer film, referred to as “shapable electroconductive” film in the original publications, is based on galvanostatically synthesized polypyrrole doped by a sulfated poly(β -hydroxyethers) polyanion and has a conductivity in the order of $15\text{-}20\text{ S cm}^{-1}$ [79]. In the present study, a commercially available polyvinyl sulfate was used as a dopant anion since it is known that larger surfactant polyanions provide films with better electrical and mechanical properties [123]. The film was grown on a stainless steel support under galvanostatic conditions from aqueous

solution, containing pyrrole and the polyanion. This resulted in a highly developed surface with the characteristic cauliflower structure as shown in Fig. 5-2. It should be noted that the film was not peeled off from the support as in the original work but used for further modification attached to the steel electrode.

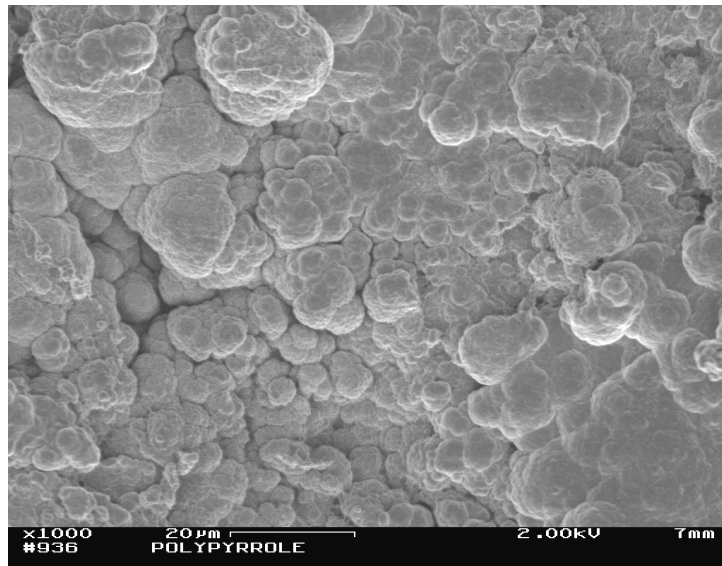


Figure 5-2: SEM image of the polypyrrole layer.

A SEM image of the CTC grown in two consecutive steps directly over the polypyrrole surface is shown in Fig. 5-3. As can be seen the CTC crystals have the characteristic elongated shape and form dendritic structures. These structures have been also referred to as “nanowires” in the literature [119].

In order to characterize further the electrode architecture, after the electrode modification has been completed, the enzymatic electrode assembly has been peeled off from the stainless steel support and a cross-section cut has been made. The corresponding SEM image is shown in Fig. 5-4. The side, which is oriented to the viewer, corresponds to the polypyrrole layer. This is evident from the imprints left by the stainless steel surface, which has been polished with emery paper before the electropolymerization.

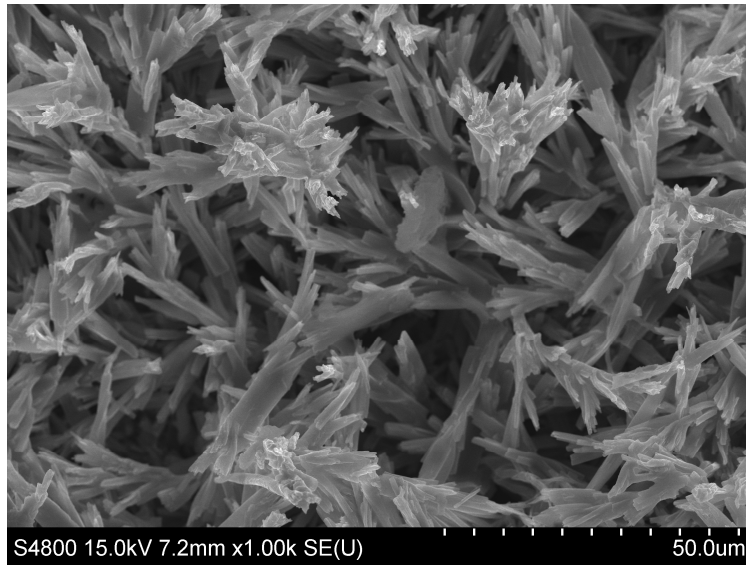


Figure 5-3: SEM image of the CTC crystals (top view).

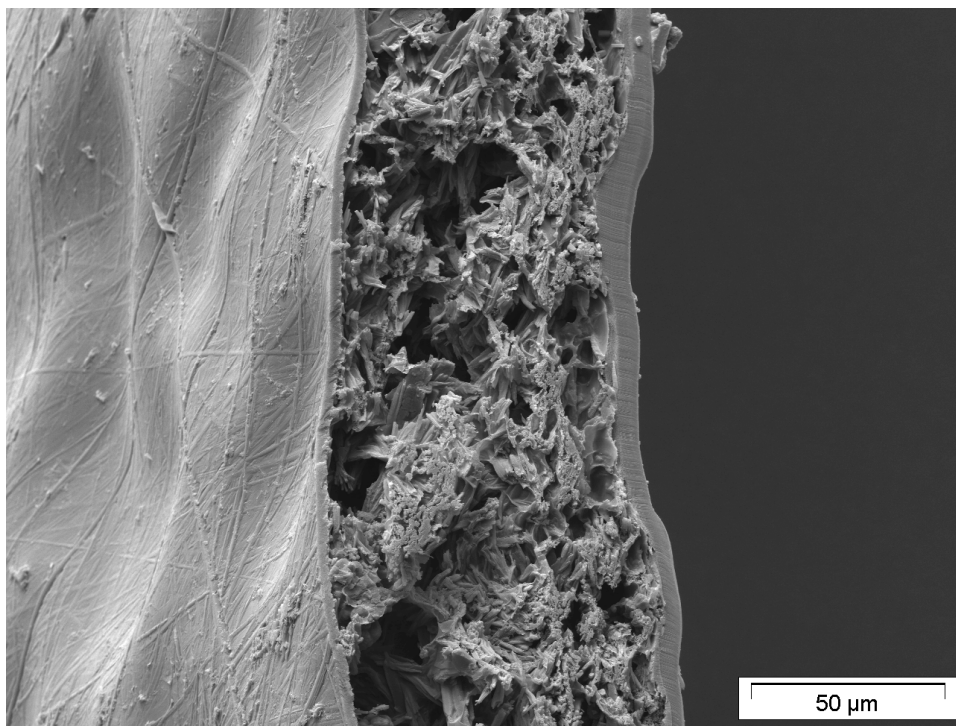


Figure 5-4: SEM image of the cross-section of the enzymatic electrode.

Three layers can be clearly distinguished and the thickness of every layer has been estimated from the micrograph as follows: 2 μm polypyrrole layer, 60 μm catalyst layer, composed of CTC crystals with adsorbed GOx, and 5 μm gelatin layer. The thickness of the polypyrrole layer, determined from the SEM image corresponds to the thickness, estimated from the deposition charge according to empirical dependence reported in [124]. As can be seen in Fig. 5-3 and 5-4 the catalyst layer of the enzymatic electrode is characterized by randomly distributed CTC bundles and cavities, forming a highly irregular porous structure, which serves as a matrix for enzyme immobilization. According to previous reports, this matrix was described as a standing highly-branched tree-like structure emerging from the polymer layer with a size of 40-50 μm [79, 117]. This presentation seems to be unrealistic taking into account the present results for electrodes with a similar CTC loading. SEM observations in the present case do not indicate CTC crystals penetrating the polypyrrole layer as reported in [117] or structures, vertically standing on the electrode surface [79]. Another important observation is that unlike the previously reported presentation of gelatin, penetrating the CTC crystals and stabilizing the respective structure [79], the gelatin layer in the present case penetrates little in the catalyst layer and forms a well-defined membrane on top. This phenomenon will influence the transport properties of glucose in the enzymatic electrode and has significance for the modeling. According to the SEM observations in the present case, the concentration of glucose can be described by diffusion through a membrane (gelatin) layer and further diffusion and reaction in a catalyst layer.

The electrochemical behavior of the enzymatic electrode has been studied between -0.2 and 0.2 V vs. SCE in 0.1 M phosphate buffer (pH 7.2), since this potential region is regarded as “stable”, where no CTC decomposition occurs [111]. As can be seen, despite the low sweep rate, large capacitive currents, exceeding the reaction currents, are observed. According to experiments with electrodes lacking polypyrrole, the pronounced capacitive behavior is ascribed to the underlying polymer surface and not to the high surface area of the CTC crystals or to the underlying stainless steel support, as shown in Fig. 5-5 (note the axis scales). The voltammograms in buffer indicate some oxidative process occurring at the stainless steel surface at more positive potentials but the associated currents are negligible.

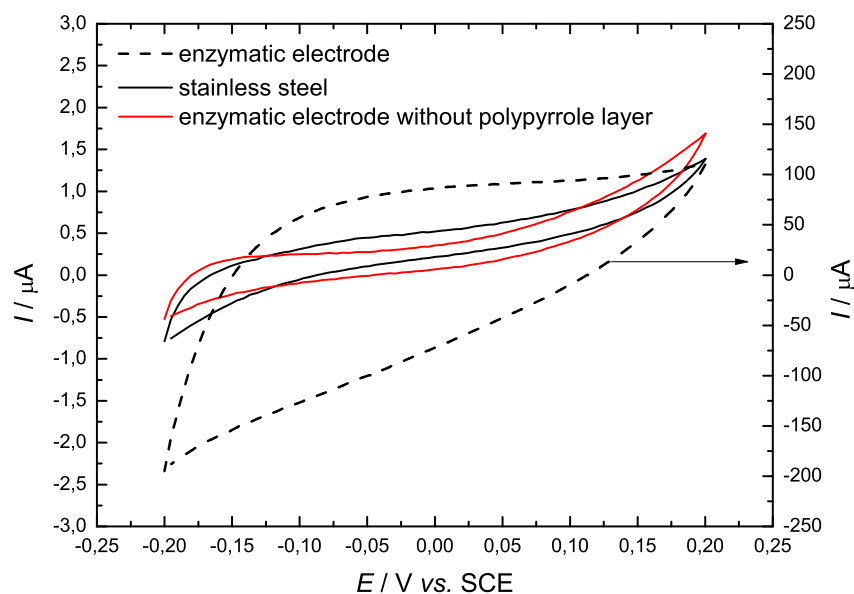


Figure 5-5: Cyclic voltammograms of the stainless steel support and the enzymatic electrode with and without a polypyrrole layer. Conditions: 0.1 M phosphate buffer, pH 7.2, room temperature, N_2 atmosphere, 400 rpm, scan rate: 5 mV s^{-1} .

The oxidative activity of the enzymatic electrode is demonstrated in Fig. 5-6. Similar voltammetric behavior, exhibiting large capacitive and significantly smaller faradaic currents, has been reported by Pauliukaite et al. in the case of a TTF-TCNQ-based carbon paste biosensor for determination of glutamate [118]. The pronounced capacitive behavior in the latter publication can be ascribed to the graphite powder, which has been used to prepare the paste, while in the present case the major capacitive contribution comes from the polypyrrole layer. As can be seen in Fig. 5-6, the enzymatic anode exhibits activity for glucose oxidation and the currents increase with substrate concentration. Maximum current in presence of 5 mM glucose reaches ca. $110 \mu\text{A}$ (corrected for the background current), which corresponds to nearly $400 \mu\text{A cm}^{-2}$ current density (calculated with respect to the geometrical surface area). The open circuit potential of the enzymatic electrodes after equilibration in the electrochemical cell under rotation in presence of glucose has been typically around -0.2 V vs. SCE , while as can be seen in Fig. 5-6 the oxidation onset observed in the positive scans is at ca. -0.1 V vs. SCE . In general, the onset potential for the glucose oxidation reaction is mainly related to the type of mediator used in the system. Further analysis of the oxidation onset and the mechanism will be presented below.

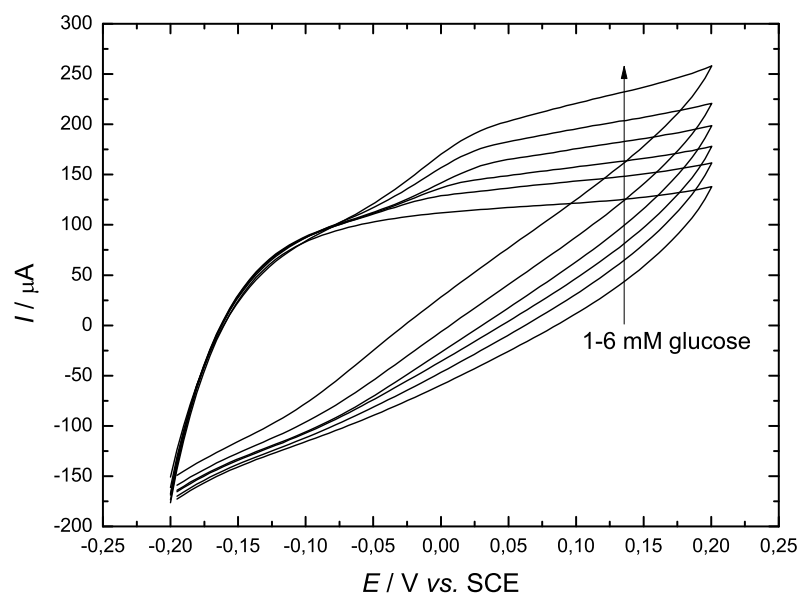


Figure 5-6: Cyclic voltammograms of the enzymatic electrode in presence of different glucose concentrations. Conditions: 0.1 M phosphate buffer, pH 7.2, 37 °C, N₂ atmosphere, 400 rpm, scan rate: 5 mV s⁻¹.

5.3 Optimization of the modification procedure

As already shown in Fig. 5-4 the catalyst layer has a highly irregular porous structure and it can be anticipated that the enzyme distribution within this layer will have significant effect on the activity of the enzymatic electrode. To optimize the performance of the electrode, the ratio between CTC and GOx has been varied in a systematic way. In addition the influence of the thickness of the gelatin layer has been also checked.

5.3.1 Influence of CTC loading and morphology

The concentration dependencies of the current at 0.2 V vs. SCE (corrected for the background current) of two enzymatic electrodes with different CTC loadings are shown in Fig. 5-7a. The CTC loading was found to have a minor influence at lower glucose concentrations and higher impact at higher glucose concentrations, shifting the currents at 30 mM glucose from ca. 150 μA

for 1 mg cm^{-2} CTC to ca. $310 \text{ } \mu\text{A}$ for 2 mg cm^{-2} CTC. Also, the linear region in the concentration dependence was extended with an increase of the loading.

The influence of the CTC loading has been additionally investigated at 5 and 20 mM glucose (Fig. 5-7b). 5 mM glucose has been chosen as the operational concentration of interest (normal glucose concentration in the human body) and 20 mM has been chosen as a concentration, close to saturation.

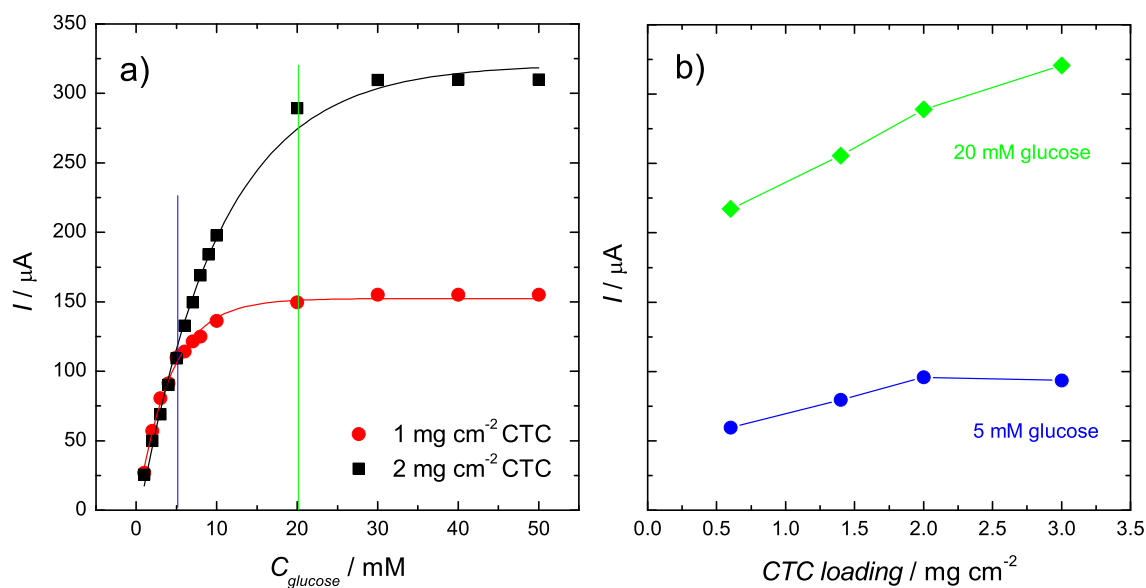


Figure 5-7: a) Concentration dependencies of two enzymatic electrodes with different CTC loadings; b) Dependence of the current on the CTC loading at two different glucose concentrations. Conditions: 0.1 M phosphate buffer, pH 7.2, 37 °C, N_2 atmosphere, 400 rpm. Data extracted from cyclic voltammetry experiments and corrected for background current.

At 5 mM a CTC loading, higher than 2 mg cm^{-2} does not influence the current output anymore, while at 20 mM the current increases in the whole investigated range. Based on these results, 2 mg cm^{-2} has been chosen as the optimum CTC loading for further tests in presence of 5 mM glucose. Similar investigation of the influence of CTC loading has been presented in the original work, where the authors also reported an optimum value of about 2 mg cm^{-2} for the CTC loading [79]. It should be noted that in the latter case the electrode modification procedure involved adsorption of the enzyme on the CTC crystals and subsequent removal of the excess enzyme solution. This implies a combined effect of both loadings, whereby the amount of adsorbed GOx increases with the CTC loading (shown by

spectrophotometric measurements) and limits the discrimination between both effects. In the latter work the authors reported also mechanical instability of the crystal structure by loadings higher than 2 mg cm^{-2} , which was not observed in the present case.

In addition to the loading, the influence of the morphology of CTC on the performance of the electrode has been studied. The morphology of the CTC crystals determines the active surface area and therefore has a direct effect on the current density. The procedure, which has been used for growth of the CTC crystals, is basically a precipitation reaction, which is performed directly on the electrode surface. It has been demonstrated that the experimental conditions of the precipitation reaction determine to a great extent the morphology of the crystals, ranging from simple nanowires to complicated helical dendrites [119]. However, the effect of the surface area, influenced by the morphology has not been studied before.

The growth of the CTC crystals, which is depicted in Fig. 5-1 proceeds in two steps. This type of precipitation procedure has been used in the literature [79, 117] and has been adopted in the present case. In the first step, a layer of dry TCNQ is formed at the electrode surface and in the second step a solution of TTF in acetonitrile (ACN) is applied in several castings over the TCNQ layer. In this way, the dry TCNQ dissolves in the TTF solution and immediately reacts, thus forming the precipitate organic salt. This kind of crystal growth corresponds approximately to a stepwise addition of solid TCNQ crystals to a TTF solution and maintains low concentration of TCNQ.

However, it is known that the higher concentration of reactants leads to faster nucleation, which results in smaller crystal size [125]. Therefore, the precipitation procedure has been performed also in one step in order to check whether it would influence the morphology and the activity, respectively. The CTC crystals have been grown by simultaneous casting of TTF and TCNQ solutions over the polypyrrole-modified electrode, which ensures high concentration of both reactants. A SEM image of the corresponding surface is shown in Fig. 5-8. Indeed, the one-step procedure results in needle-shaped crystals with smaller size (compare Fig. 5-3 and 5-8) and consequently higher surface area. The increase in surface area is manifested by an increase in currents, which has been observed by constant polarization at 0.1 V vs. SCE (Fig. 5-9).

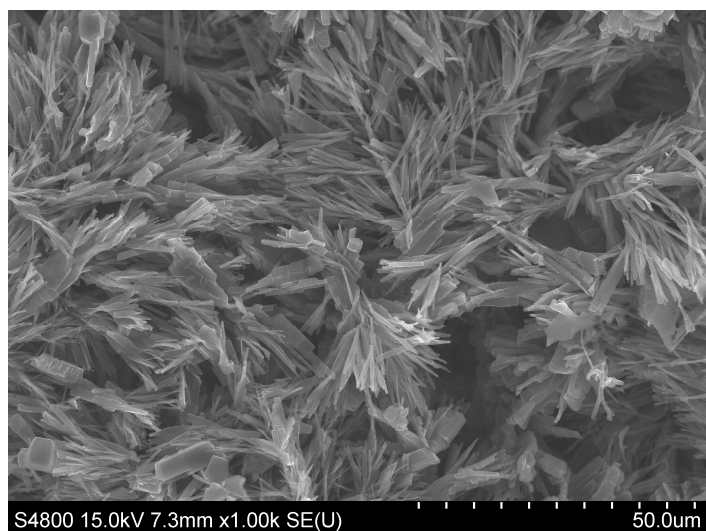


Figure 5-8: SEM image of the CTC crystals formed by one-step precipitation, which is based on simultaneous casting of TTF and TCNQ (top view).

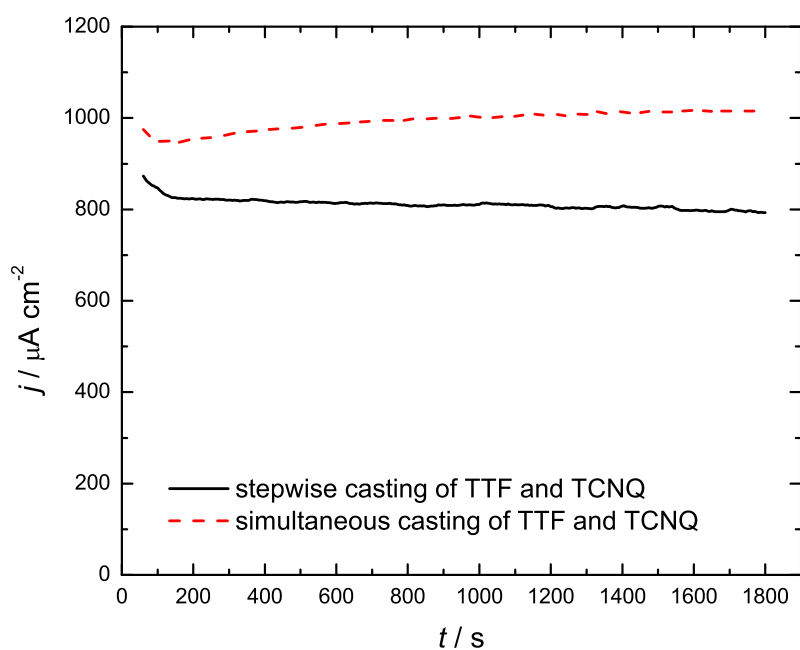


Figure 5-9: Chronoamperometric response at 0.1 V vs. SCE of two enzymatic electrodes, employing CTC crystals prepared in two different ways. Conditions: 20 mM glucose in 0.1 M phosphate buffer, pH 7.2, 37 °C, N₂ atmosphere, 400 rpm.

As can be seen in Fig. 5-9, the precipitation of the CTC crystals in one step increases the steady-state response with approximately 200 $\mu\text{A cm}^{-2}$ at 20 mM glucose.

5.3.2 Influence of GOx and gelatin loading

The influence of the GOx loading on the anode performance in the present study has been tested at constant CTC loading (Fig. 5-10). The effect is similar to the effect observed in the case of CTC. Decreasing the GOx loading twice suppresses the currents at higher glucose concentrations, decreases the linear region and shifts the saturation concentration to lower values (ca. 10 mM).

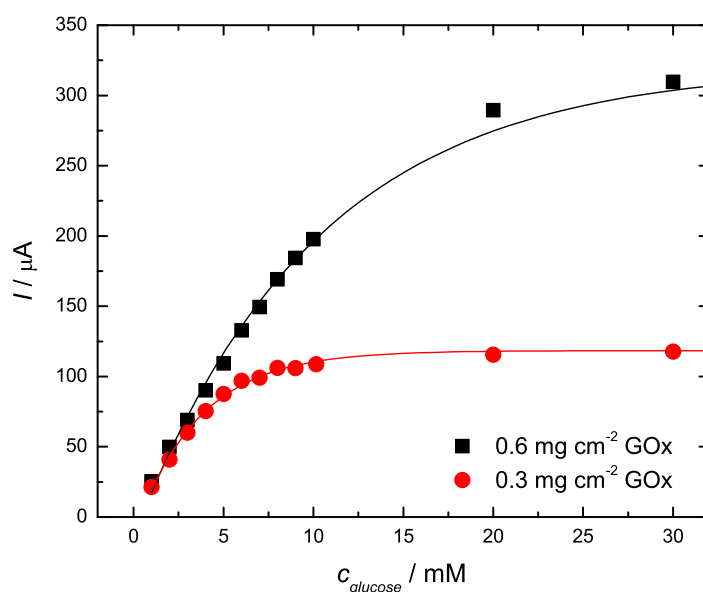


Figure 5-10: Concentration dependencies of two enzymatic electrodes with different GOx loadings. Conditions: 0.1 M phosphate buffer, pH 7.2, 37 °C, N₂ atmosphere, 400 rpm.

In a similar manner, the gelatin loading has been varied by keeping the other two structural parameters constant. Doubling of the gelatin loading decreases the currents as can be seen in Fig. 5-11. The current decrease is more pronounced at higher glucose concentrations but the relative current ratio is approximately 60 % in the whole concentration range. This effect has been ascribed to limited mass transport of glucose through the gelatin layer. Similar change in the concentration dependence was reported also in the case of polysiloxane membranes for controlling the ratio between glucose and oxygen permeability in a glucose biosensor based on hydrogen peroxide detection [126]. In the latter reference the increase of membrane thickness

also decreased the currents, which was ascribed to limited supply of glucose. However, the biosensors with thicker polysiloxane membranes exhibited greater linearity range at the expense of the lower currents. This was ascribed to the decreased ratio between glucose and oxygen permeability, which resulted in comparatively higher oxygen concentration (sufficiently high to allow for a stoichiometric reaction with reduced enzyme in an extended glucose concentration range) [126]. In the present case oxygen is not involved in the regeneration of reduced enzyme and the increase of gelatin thickness causes a decrease of both currents and linear region.

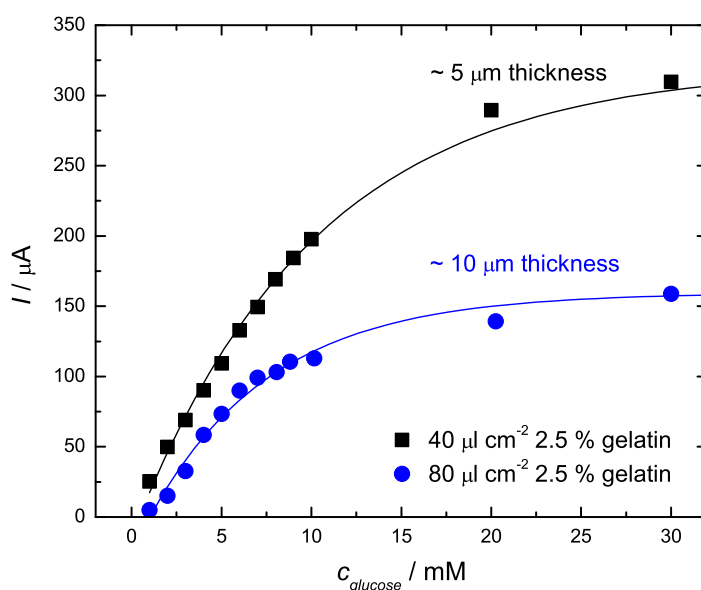


Figure 5-11: Concentration dependencies of two enzymatic electrodes with two different gelatin loadings. Conditions: 0.1 M phosphate buffer, pH 7.2, 37 °C, N₂ atmosphere, 400 rpm.

Another aspect from the modification procedure, which has been investigated, is the influence of gelatin cross-linking. Cross-linking is a common and simple technique, used for enzyme immobilization but often with the expense of reduced enzyme activity due to alteration of the natural protein conformation [127]. However, in the present case the cross-linking procedure is beneficial for the quality of the gelatin film and thus for the whole electrode assembly. The relative activity under constant polarization and rotation of the electrode assembly with and without cross-linking treatment is shown in Fig. 5-12. As can be seen from the graph, the cross-linked electrode exhibits stable pH response during the course of the experiment, while the activity

of the untreated electrode decreases more significantly. The reason for the decreasing activity is assumed to be correlated with the solubility of gelatin. Gelatin films, which are not cross-linked, are soluble in aqueous solvents [128] and it can be anticipated that the dissolution is enhanced by the elevated temperature and the rotation during the experiment. In this way the structural integrity of the enzymatic anode is deteriorated and CTC and enzyme can leach from the electrode surface.

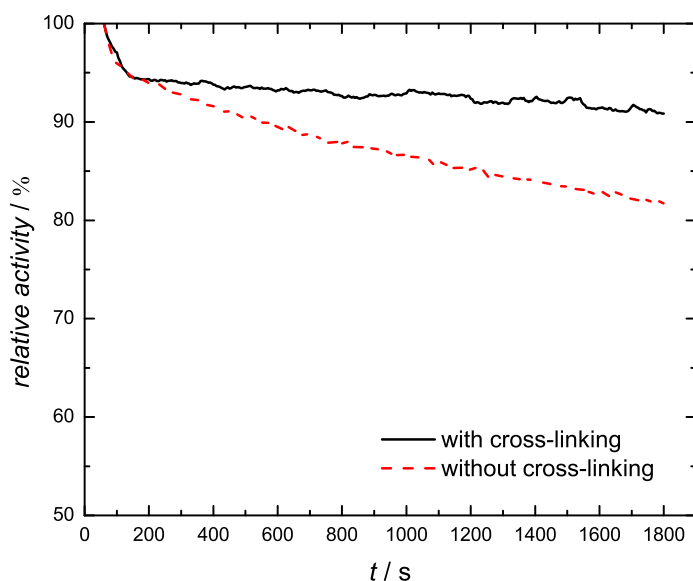


Figure 5-12: Chronoamperometric response at 0.1 V vs. SCE of two enzymatic electrodes, showing the influence of cross-linking. Conditions: 5 mM glucose in 0.1 M phosphate buffer, pH 7.2, 37 °C, N₂ atmosphere, 400 rpm

In addition to the solubility effect, cross-linking decreases the swelling of the film [128], which is expected also to be beneficial for preserving the stability of the electrode assembly. In control experiments, cross-linked and non-cross-linked thin layers of gelatin have been formed on flat mica surfaces and the respective surfaces have been analyzed by atomic force microscopy (AFM). The resulting images (50 $\mu\text{m} \times 50 \mu\text{m}$) are shown in Fig. 5-13.

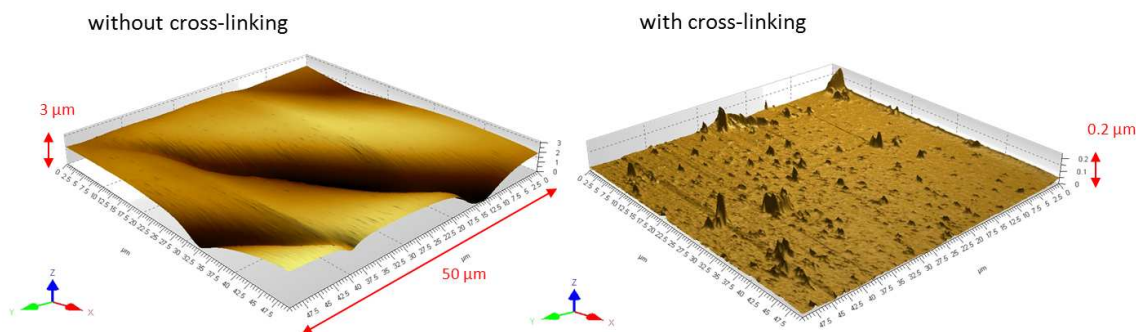


Figure 5-13: AFM images (tapping mode) in 0.1 M phosphate buffer of two types of gelatin films, formed on flat mica substrate.

Cross-linking results in rigid films with better mechanical properties. The apparently flat surface of the cross-linked gelatin layer (note the z scale in Fig. 5-13) implies that its profile is determined to a great extent by the underlying flat mica substrate. It should be noted that the thickness of the gelatin film on mica corresponds approximately to the thickness in the case of the enzymatic electrode since the same loading ($40 \mu\text{l cm}^{-2}$ 2.5 % gelatin) has been used. On the other side, the AFM image of the gelatin, which has not been treated with glutaraldehyde, can be considered as rough (deviations in surface profile up to $3 \mu\text{m}$). This roughness can be attributed to the higher degree of swelling, which is expected to take place, according to the results shown in [128]. In addition, the AFM images in the case of the untreated gelatin film were not completely reproducible. This can be tentatively ascribed to changes in the surface of the layer due to dissolution during the experiment. AFM images have been recorded in tapping mode in order to minimize the possibility of mechanical damage. The mild imaging mode should prevent scratching of the gelatin layer by the cantilever but local dissolution may be also induced by fluctuations in the liquid caused by the AFM tip. Although it can compromise the experiment to some extent, the low reproducibility of the AFM images in the case of untreated gelatin can be taken as an indication for instability of the layer due to dissolution of gelatin.

5.3.3 Interpretation of the influence of structural parameters

The influence of the investigated structural parameters on the bioelectrode response can be interpreted in terms of the mechanism of enzymatic glucose oxidation. Previous studies

regarding electrodes with similar architecture assumed direct regeneration of the reduced enzyme at the CTC surface [79, 117, 129]. For instance, Khan discussed the influence of CTC loading only from the point of view of surface area for adsorption and electrical contacting of GOx [79]. Contrary to previous reports, in the present study a MET mechanism has been assumed and CTC has been considered as the mediator (M in Eq. 4 and 5). At the moment, for the analysis of the respective effects there is no need of detailed clarification of the mechanism. This topic will be discussed further in the text. The sensitivity of the electrode response in the limiting current region on all three investigated parameters suggests a mixed reaction-mass transfer limitation. The change of the gelatin loading effectively changes the thickness of the membrane layer, which increases the mass transfer resistance for glucose transport and decreases the glucose concentration at the electrode surface.

The increase of enzyme loading will increase the rate of the reaction between glucose and enzyme. It can be easily anticipated, even in terms of simple Michelis-Menten kinetics that the increase of the enzyme loading will increase the slope of the concentration dependence in the linear region ($K_M \gg [S]$) and it will change the value of the current response in the limiting region ($K_M \ll [S]$), which has been qualitatively observed (see Fig. 5-10). The increase of the CTC loading and surface area will effectively increase the concentration of the mediator in the catalyst layer, which will lead to increase in the electrode response. At lower substrate concentrations the change of CTC loading has less influence, which means that under these conditions the total reaction rate is not dominated by the enzyme-mediator reaction. At higher substrate concentrations (e.g. 20 mM) the increase of the CTC loading produces the continuous increase of the electrode response.

5.4 Electrode architecture involving a gelatin matrix

The results, shown in the previous chapter clearly demonstrate the importance of the structural parameters on the performance of the enzymatic electrode. In addition to the loadings of the different components (CTC, GOx, gelatin) and the procedures, used in the preparation of the electrode (precipitation conditions, cross-linking), the overall anode architecture is also expected to have a major impact on the activity for glucose oxidation. In this respect, the same constituents of the enzymatic electrode (GOx, CTC and gelatin) have been tested in another

architecture with the addition of high surface area carbon (carbon black). In this case all components have been dispersed in a gelatin solution and applied as film on the stainless steel surface. Conductive high-surface area carbon materials such as Vulcan are well established as catalyst supports in fuel cell research and recently adopted in the preparation of enzymatic electrodes for biofuel cell applications as a mean to facilitate electron transfer and to increase current densities [57, 130]. Gelatin, on the other side, has a hydrophilic nature and swells in presence of water, whereby the degree of swelling depends on the degree of cross-linking as discussed in [128]. The biocompatible hydrogel polymer network provides a suitable environment for the entrapped enzymes, in addition to good film-forming properties, non-toxicity and mechanical stability [131]. In the present case the utilization of carbon and gelatin results in 3D stable electrode architecture. The main difference with the procedure described in the previous chapter is that the gelatin does not form a protective membrane on top but constitutes a network within the entire volume of the electrode and provides its structural integrity. However, the difference of the electrode structure is expected to change the mass transport properties of glucose within the layer.

The electrode architecture, which involves a gelatin matrix, has two major advantages, regarding the practical preparation. First, it is much simpler and requires less time. The components are mixed together and an aliquot of the resulting ink is cast on the stainless steel surface and cross-linked after drying. Thus, the steps of electropolymerization and crystal growth, as well as all associated drying steps in-between are omitted. The second advantage is that commercial CTC or CTC, which has been precipitated previously, is used. As shown in Section 5.3.1 the experimental conditions of CTC growth on the electrode surface influence to a great extent its morphology and consequently the surface area. It was observed that small experimental variations during the CTC precipitation cause differences in the activity and it is difficult to obtain results with high reproducibility. Therefore, the use of CTC with defined and more uniform crystal size distribution should result in more reproducible behavior.

In order to optimize the modification procedure, the influence of several structural parameters has been tested. All electrodes have been characterized by steady-state measurements (chronoamperometry at different potentials) at 0, 5 and 20 mM glucose. This helps to eliminate the capacitive currents, which are present in the case of dynamic experiments such as cyclic voltammetry and provides more realistic information about the performance of the electrode.

Only curves at 20 mM of glucose (corrected for the background current) are presented since the effects, which are observed by the systematic variation of the ink components are more pronounced at higher concentrations. The presented curves are based on the mean values of three measurements.

5.4.1 Influence of type of carbon black and loading

Different types of commercial carbon blacks have been used to facilitate electron transfer and to increase surface area. For instance, Vulcan (Cabot) has been employed as a support matrix for BOD by the preparation of oxygen-reducing biocathode [130]. Ketjen Black (Akzo Nobel) has been used for immobilization of BOD, laccases and fructose dehydrogenase in a fructose-oxygen biofuel cell [57]. It should be noted that the utilization of carbon black materials in the literature has been usually associated with efforts to establish DET, as discussed in Section 2.1.2. In the present case GOx is not expected to exhibit DET and the electron transfer pathway is already defined through the CTC. Therefore the carbon particles should be regarded as a mean to facilitate electrical communication between the mediator and the electrode.

Three different types of carbon blacks have been tested and the resulting polarization curves are presented in Fig. 5-14. As can be seen Vulcan and Ketjen Black have similar performance, which significantly outreaches the performance of Printex-based electrodes. For instance, the current density, delivered by Vulcan and Ketjen Black at 0.2 V vs. SCE is around $1000 \mu\text{A cm}^{-2}$, while the current density when Printex is used is only about $200 \mu\text{A cm}^{-2}$. Vulcan has been identified as the most suitable material for electrode preparation since the Ketjen Black films had poor quality, larger carbon particles agglomerates and the electrode film often detached from the stainless steel surface. The higher structural stability of the films, based on Vulcan has been assigned to better dispersion of the Vulcan particles in the gelatin-based ink.

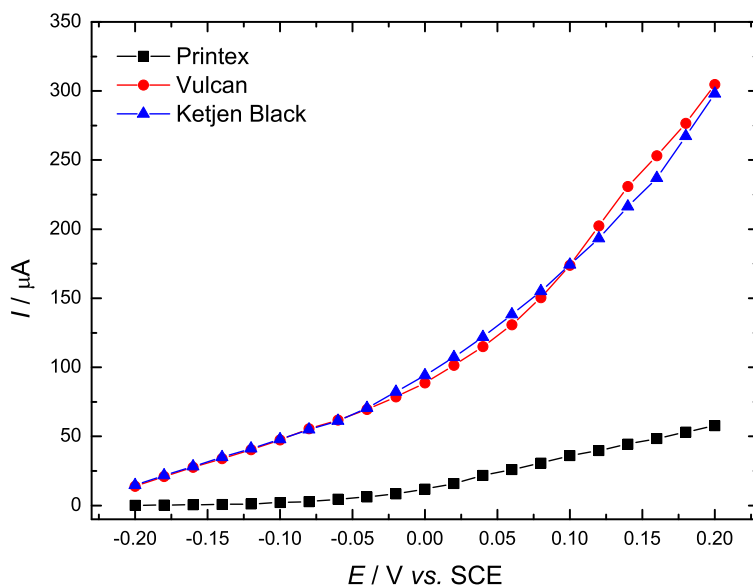


Figure 5-14: Steady-state polarization curves in presence of glucose of enzymatic electrodes employing different types of carbon blacks. Conditions: 20 mM glucose in 0.1 M phosphate buffer, pH 7.2, 37 °C, N₂ atmosphere, 400 rpm. Catalyst ink composition: 20 mg carbon black, 10 mg GOx, 10 mg TTF-TCNQ in 1 ml 2 % gelatin.

In the next step the influence of the Vulcan content in the ink composition has been checked. The performances of the enzymatic electrodes with different Vulcan loading are shown in Fig. 5-15. As can be seen in Fig. 5-15a, the increasing content of Vulcan in the catalyst ink improves the electrode activity. The addition of 5 mg Vulcan does not influence the performance of the electrode at potentials lower than -0.05 V vs. SCE. Further increase of the Vulcan content to 20 mg and 30 mg leads to a noticeable shift of the currents even more negative potentials. The precise identification of the oxidation onset at higher Vulcan loadings is difficult due to the limits of electrochemical stability of the CTC. At more negative potentials a process of TTF-TCNQ decomposition takes place [111] and the measurement of the onset potential becomes impossible without changing the surface properties.

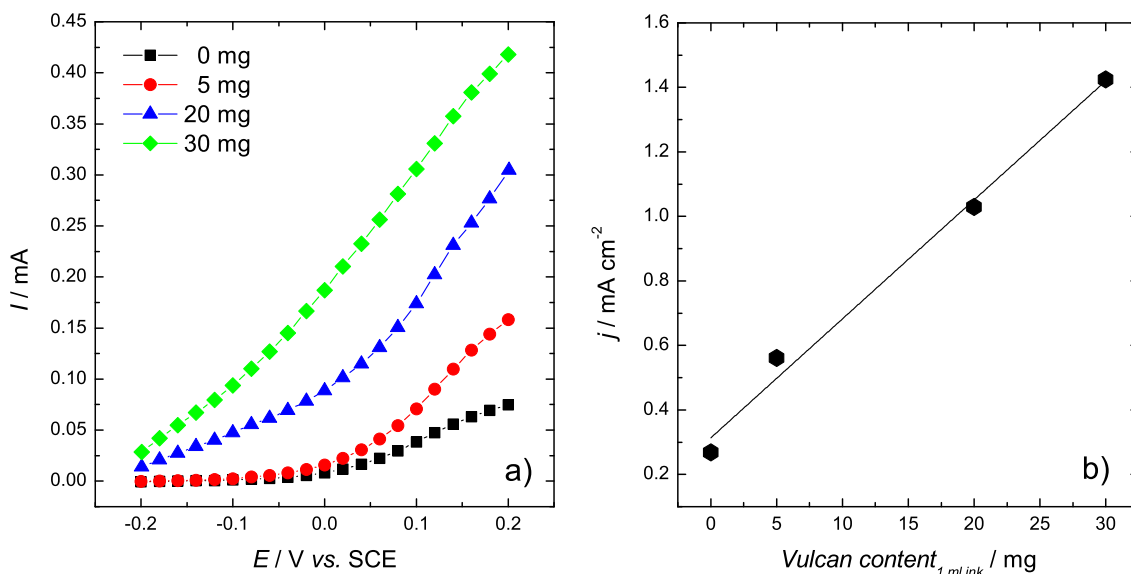


Figure 5-15: a) Steady-state polarization curves in presence of glucose for enzymatic electrodes with different Vulcan loadings; b) Dependence of the current density at 0.2 V vs. SCE on the Vulcan loading. Conditions: 20 mM glucose in 0.1 M phosphate buffer, pH 7.2, 37 °C, N₂ atmosphere, 400 rpm. Catalyst ink composition: 10 mg GOx, 10 mg TTF-TCNQ in 1 ml 2 % gelatin.

The catalytic effect of Vulcan can be tentatively ascribed to the increase of conductive surface area, which improves the electrical communication between the mediator and the electrode. At more positive potentials the increase in currents is more pronounced and the resulting current densities at 0.2 V vs. SCE are presented in Fig. 5-15b. As can be seen the increase in activity is almost linear in the investigated range and it can be expected that further increase of the Vulcan content will improve additionally the electrode performance. However, films with Vulcan content of 30 mg ml⁻¹ ink and higher were extremely unstable and deformed. They detached from the stainless steel surface due to film shrinking after drying.

It should be noted that the stainless steel electrodes in the present study have a geometrical surface area of 0.28 cm². In control experiments disc-shaped films with surface area of 0.07 cm² with higher Vulcan loading were found to be stable. However, electrodes with smaller surface area can result in a significant enhancement of the activity when translated into current density, which can compromise the realistic characterization of the electrodes. In order to ensure comparison for further fuel cell experiments and scaling-up of the electrode films, Vulcan

content of 20 mg ml⁻¹ in the catalyst ink has been chosen as an optimum loading, which gives reproducible films with good quality and better adhesion to the stainless steel surface.

5.4.2 Influence of GOx and gelatin loading

The performances of enzymatic anodes with different GOx loadings are compared in Fig. 5-16. Unlike the expectations, coming from the assumed reaction mechanism and the results, presented in Section 5.3.2, the increase of GOx content causes a decrease of the electrode performance in the case of enzymatic electrodes based on a gelatin matrix. The polarization curves at GOx concentration up to 5 mg ml⁻¹ show similar behavior with limiting current region (Fig. 5-16a). The electrodes with higher GOx concentration (10 and 15 mg ml⁻¹) exhibit qualitatively different behavior with no limiting currents and overall lower performance.

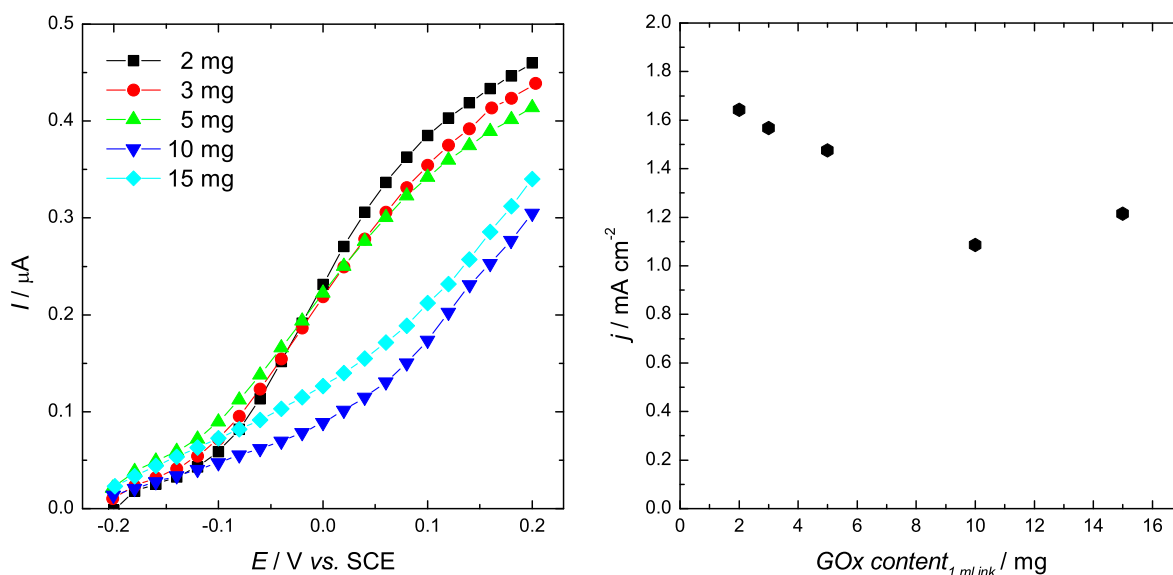


Figure 5-16: a) Steady-state polarization curves in presence of glucose for enzymatic electrodes with different GOx loadings; b) Dependence of the current density at 0.2 V vs. SCE on the GOx loading. Conditions: 20 mM glucose in 0.1 M phosphate buffer, pH 7.2, 37 °C, N₂ atmosphere, 400 rpm. Catalyst ink composition: 20 mg Vulcan, 10 mg TTF-TCNQ in 1 ml 2 % gelatin.

The dependence of the current density at 0.2 V vs. SCE versus the GOx loading is shown in Fig. 5-16b. As can be seen the currents increase with a decrease of enzyme content in the catalyst ink. This contradicts the behavior of enzymatic electrodes, which is expected, according to the Michaelis-Menten kinetics and has been shown in the case of polypyrrole-based electrodes in Fig. 5-10. It should be noted that the loadings of CTC and GOx in both cases are in a similar range.

The unusual dependence can be tentatively correlated with the distribution of enzyme within the catalyst layer. It can be assumed that higher enzyme loading will lead to inefficient enzyme distribution and formation of large enzyme agglomerates, which can impede the electrical contacting of all enzymes and also hamper the electrical communication of the mediators with the conductive Vulcan particles and the intact CTC crystals.

The addition of salts, organic solvents, polymers or protein solutions can lead to the precipitation of enzymes as physical aggregates, while preserving their native conformation and activity. Subsequent cross-linking of these physical aggregates by reaction of reactive groups on the enzyme surface (e.g., free amino groups of lysine residues) with reagent such as glutaraldehyde stabilizes the aggregates. The formed structures are known as cross-linked enzyme aggregates (CLEAs) and represent a method for enzyme immobilization, which is especially advantageous for industrial applications [132]. Common strategy in the preparation of CLEAs is the addition of an inert protein (e.g. bovine serum albumin) called proteic feeder. This additive serves to prevent the excessive cross-linking, which can produce too rigid conformation of the enzyme and consequently lead to poor activity and triggers the CLEA formation in case of lower enzyme concentrations.

It can be anticipated that the combination of enzyme (GOx), inert protein (gelatin) and glutaraldehyde during the procedure for electrode preparation in the present case can result in similar enzyme agglomerates. However, the precipitation of the enzymes is not induced by a precipitation agent as in the case of classical CLEAs, but by the simultaneous effect of gelatin and glutaraldehyde. Such agglomeration in presence of different proteic feeders and absence of precipitant has been demonstrated in the case of GOx [133] and it was found that low concentration of gelatin does not lead to formation of aggregates.

A promising tool for investigation of the distribution of enzymes within the 3D-structure of the catalyst layer and their interactions with the gelatin matrix is fluorescence microscopy, as

discussed in [134]. In order to prove the hypothesis of agglomeration, the influence of cross-linking and the distribution of the enzyme in the electrode architecture have been investigated by this technique. The tests have been performed with fluorescent-labeled GOx since the intrinsic fluorescence of GOx, measured by a fluorometer, has proved not to be sufficient for imaging. First, in control experiments, films of GOx in gelatin have been prepared on a glass substrate. It should be noted that the concentration, thickness and cross-linking conditions, correspond to the experimental conditions in the case of enzymatic electrodes. Fluorescence micrographs of GOx dispersed in gelatin before and after cross-linking are presented in Fig. 5-17.

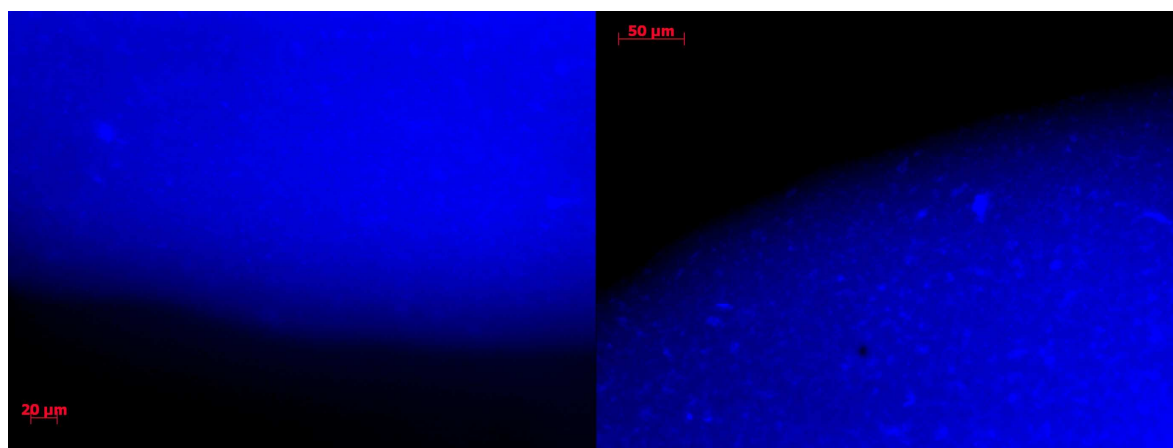


Figure 5-17: Fluorescent micrographs of GOx dispersed in a gelatin matrix before (left) and after (right) cross-linking.

As can be seen from Fig. 5-17, when the enzyme is dispersed in a gelatin matrix, cross-linking enhances the formation of enzyme agglomerates. Enzymes, which have not been subjected to cross-linking also form agglomerates but have more uniform distribution within the gelatin layer.

In the case of polypyrrole-based electrodes, the adsorption of enzymes and the casting of gelatin proceeds in different steps and the gelatin forms well-defined layer on top of the electrode. In this way the enzyme is adsorbed directly on the CTC surface and is expected to have little contact with the gelatin membrane and the cross-linking agent. Therefore less aggregate formation after cross-linking is expected and the resulting better distribution of GOx can be tentatively accounted for the increase in performance with increase of enzyme loading. In the case of enzymatic electrodes based on GOx, dispersed throughout the gelatin film,

glutaraldehyde is expected to cause more pronounced agglomeration and affect the distribution within the layer to a higher extent.

Fig. 5-18 shows fluorescent images of two enzymatic electrodes with different enzyme loadings. The dispersion of enzyme in the gelatin matrix and the subsequent cross-linking leads to aggregate formation in both cases. As can be seen in the graph, the Vulcan and CTC particles absorb the fluorescence of deeper buried enzyme structures unlike the images of GOx dispersed only in a gelatin matrix, shown in Fig. 5-17. The surface with lower enzyme loading (2 mg ml^{-1} GOx concentration in the catalyst ink) is characterized by more scattered and diffuse fluorescent signal, which indicates more uniform enzyme distribution within the catalyst layer. When the GOx concentration is increased to 10 mg ml^{-1} GOx, the agglomerates are more pronounced.

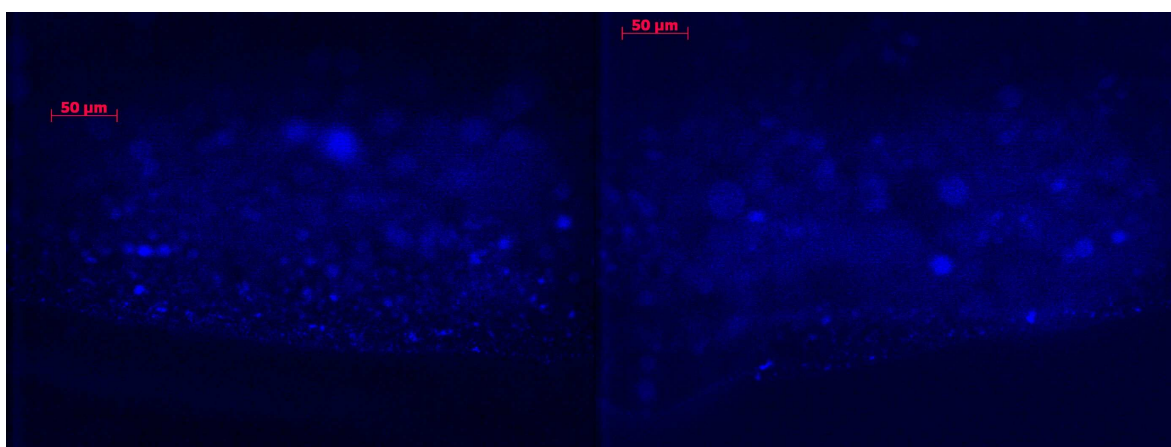


Figure 5-18: Fluorescent micrographs of enzymatic electrodes with 10 mg ml^{-1} (left) and 2 mg ml^{-1} (right) GOx concentration in the catalyst ink. Other concentrations are as follows: 20 mg ml^{-1} Vulcan, 10 mg ml^{-1} CTC in 1ml of 2 % gelatin solution.

The fluorescent images, shown above are in accordance with the hypothesis of not uniform distribution, which causes the the unusual influence of the enzyme loading in the case of the enzyme electrodes, based on a gelatin matrix. The existence of more enzyme agglomerates at higher GOx loading leads to hampering of the electrical communication with the conductive matrix as well as the substrate and mediator fluxes to enzymes within the aggregates. Consequently, despite of the higher overall loading of enzyme, the electrode exhibits lower performance as shown in Fig. 5-16.

The influence of gelatin concentration in the catalyst ink is shown in Fig. 5-19.

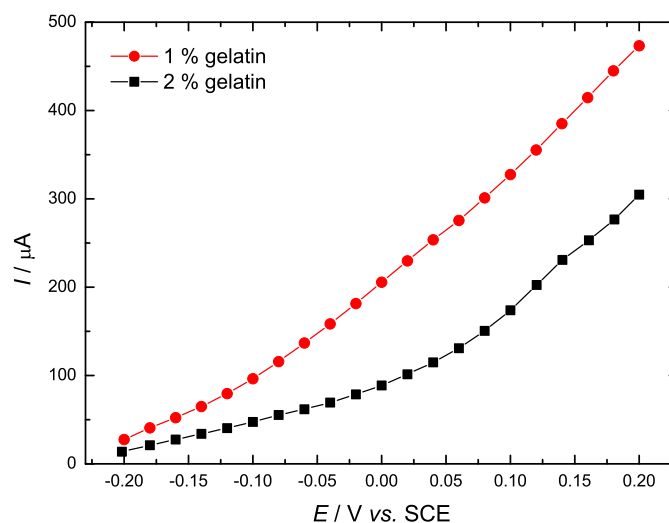


Figure 5-19: Steady-state polarization curves of two enzymatic electrodes with different gelatin concentration in the catalyst ink. Conditions: 20 mM glucose in 0.1 M phosphate buffer, pH 7.2, 37 °C, N₂ atmosphere, 400 rpm. Catalyst ink composition: 20 mg Vulcan, 10 mg GOx and 10 mg TTF-TCNQ in 1 ml gelatin.

As can be seen from the graph decrease of gelatin content to 1 % leads to a substantial increase in performance. This is in accordance to the effect observed in the case of polypyrrole-based enzymatic electrode and can be also explained by the limited diffusion of glucose through the gelatin matrix as discussed in Section 5.3.2. In addition to the diffusion effect, the lower gelatin concentration is expected to cause less enzyme agglomeration, as discussed in [133] and therefore it will improve the distribution of enzyme within the catalyst layer. However, although beneficial in terms of currents, the use of 1 % gelatin in the catalyst ink leads to unstable films, which detach from the stainless steel surface by the drying process (more than 50 % failure rate). This phenomenon demonstrates the trade-off between performance and ease of preparation, which has been already discussed in Section 5.4.1 in the case of different Vulcan loadings.

Based on the experiments shown above, the following catalyst ink composition has been identified as optimal: 20 mg Vulcan, 10 mg TTF-TCNQ and 2 mg GOx dissolved in 1 or 2 % gelatin aqueous solution.

5.4.3 Performance of the optimized electrode

The performance of the optimized enzymatic electrode has been tested in presence of different glucose concentrations and in presence of oxygen. The polarization curves of the enzymatic electrode in presence of different glucose concentrations are shown in Fig. 5-20. As can be seen from the graph, the polarization curves at lower glucose concentrations are characterized by limiting current regions, while at higher glucose concentrations the behavior is different (e.g. at 50 mM glucose the polarization curve is linear at potentials more positive than 0 V vs. SCE). This change can be tentatively attributed to a change in the rate-determining step of the overall reaction. At lower glucose concentrations, the substrate concentration limits the rate of the enzymatic reaction according to Eq. 1 and 2. At higher glucose concentrations, rate-limiting becomes either the enzyme-mediator reaction (Eq. 4) or the mediator reoxidation at the electrode surface (Eq. 5). The pronounced dependence of the current on the electrode potential suggests that rate-limiting is rather the electrochemical reaction. However, despite that the potential controls directly only the rate of mediator reoxidation, the enhanced consumption of reduced mediator can change the kinetics of the preceding chemical reaction as well.

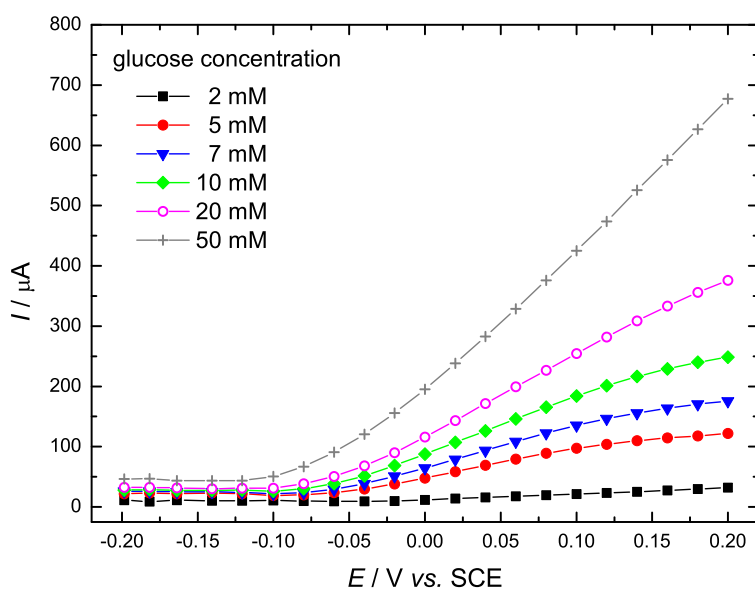


Figure 5-20: Steady-state polarization curves of the optimized enzymatic electrode in presence of different glucose concentrations. Conditions: 0.1 M phosphate buffer, pH 7.2, 37 °C, N₂ atmosphere, 400 rpm. Catalyst ink composition: 20 mg Vulcan, 2 mg GOx and 10 mg TTF-TCNQ in 1 ml 2 % gelatin.

It should be noted that the concentration dependencies are based on the values taken from individual polarization curves and the experiments have been performed with the same electrode with increasing glucose concentrations. This approach allows for a complete characterization of the electrode behavior in different potential ranges (opposed to e.g. flow-injection analysis at a single potential) but involves continuous potential cycling and prolonged polarization at different potentials. This kind of electrochemical treatment can be regarded as accelerated aging and could potentially lead to change in the electrode properties as it will be discussed in below.

Important prerequisite for the implementation of enzymatic anodes in membraneless fuel cell configurations is their oxygen tolerance. This issue is of special importance in the case of GOx electrodes since oxygen is believed to be the natural electron acceptor for the enzyme [10]. The activity of the optimized enzymatic electrode has been tested in absence and presence of oxygen at different glucose concentrations (Fig. 5-21). As can be seen from the graph, the presence of oxygen decreases the performance of the anode at both investigated concentrations. The currents at 0.2 V vs. SCE decrease from about 150 μA and 530 μA in absence of oxygen, to about 80 μA and 300 μA in presence of oxygen, at 5 mM and 20 mM of glucose, respectively. Both changes correspond to nearly 2 times activity decrease.

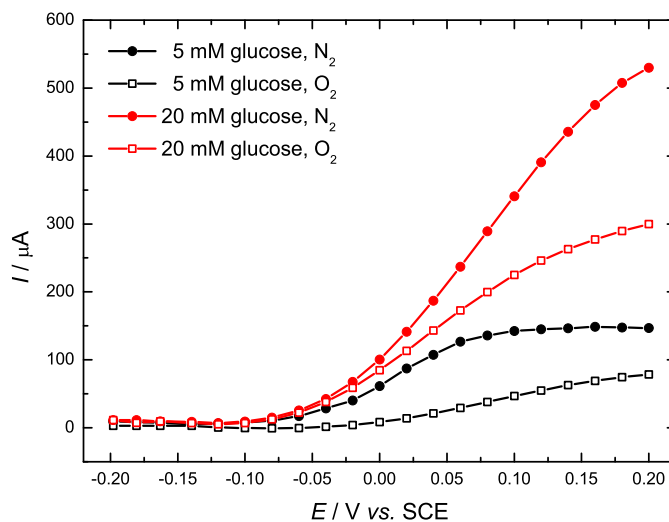


Figure 5-21: Steady-state polarization curves for an optimized enzymatic electrode in presence of different glucose concentrations under nitrogen or oxygen atmosphere. Conditions: 0.1 M phosphate buffer, pH 7.2, 37 °C, 400 rpm. Catalyst ink composition: 20 mg Vulcan, 2 mg GOx and 10 mg TTF-TCNQ in 1 ml 1 % gelatin.

5.5 Electron transfer mechanism and origin of activity

5.5.1 Mechanisms according to the literature and current approach

The electron transfer mechanism in enzymatic electrodes, employing TTF-TCNQ remains still controversial in the literature. GOx in general is believed to lack DET due to the carbohydrate shell that isolates its redox center (FAD), although there are some studies reporting DET in the case of GOx as discussed recently [10]. Deglycosylation of the enzyme partially exposes FAD, which facilitates DET, as demonstrated by Mano and co-workers [135]. TTF-TCNQ exhibits high electrical conductivity and no visible redox processes (e.g. due to salt decomposition) in the catalytically relevant potential region, so it can be regarded as an inert electrode material like carbon. On the other side both TTF [136] and TCNQ [137] are known to act as mediators for GOx.

Early studies on CTCs suggested mechanism based on homogeneous MET [112, 113]. Further works, specifically addressing TTF-TCNQ, claimed direct regeneration of the reduced enzyme by means of a DET [114]. Later on, the same group assumed a heterogeneous redox catalysis (opposed to the homogeneous case) with TCNQ as a mediator adsorbed on the CTC surface [138]. This hypothesis was further supported by electrochemical and quartz crystal microbalance (QCM) measurements and soluble TTF species were completely ruled out of the possible ET pathway [139]. Additional experimental observations indicated that TTF should be also involved in the mechanism and two independent modes of MET were suggested: homogeneous with TTF^+ and heterogeneous with TCNQ^0 [140]. Another study excluded the possibility of homogeneous MET or heterogeneous redox catalysis and propounded the hypothesis of electroactive enzyme, modified by incorporation of a hydrophobic mediator (TTF and possibly TCNQ), released from the CTC [141]. This suggestion was based on the successful modification of GOx with TTF by hydrophobic interactions [142]. Later on, Albery and co-workers developed a theory for a homogeneous MET with mediators being supplied from the bulk or generated *in situ* and considered the theoretical possibility to apply this mechanism in the case of organic salts [143].

After all, despite of the long debate, more recent works, reported third generation (mediatorless) glucose biosensors based on TTF-TCNQ, whereby the assumption of DET

corresponded well to the obtained experimental data [79, 117]. Contrary to the latter publications, a newer study exploited the concept of alternating MET mechanism with different mediator species, depending on the applied potential [116].

In order to provide a further insight into the mechanism, enzymatic electrodes based on TTF, TCNQ and TTF-TCNQ have been prepared in identical manner and tested towards their activity for glucose oxidation. The identical preparation route of the different types of electrodes allows for a direct comparison of their electrochemical behavior and performance. It should be noted that all potential values in the text below are referred to the scale of SCE.

5.5.2 TCNQ as mediator

TCNQ is a strong electron acceptor molecule, which can undergo two redox transformations: to the monovalent (TCNQ^-) and subsequently to the divalent (TCNQ^{2-}) radical anions and the respective redox reactions can be clearly distinguished in a suitable solvent, e.g. acetonitrile [144]. However, the low solubility of TCNQ in aqueous solutions obstructs the straightforward analysis of its electrochemical behavior in phosphate buffer. Fig. 5-22 shows voltammograms of the TCNQ-based enzymatic electrode in different potential windows with an increasing upper potential limit.

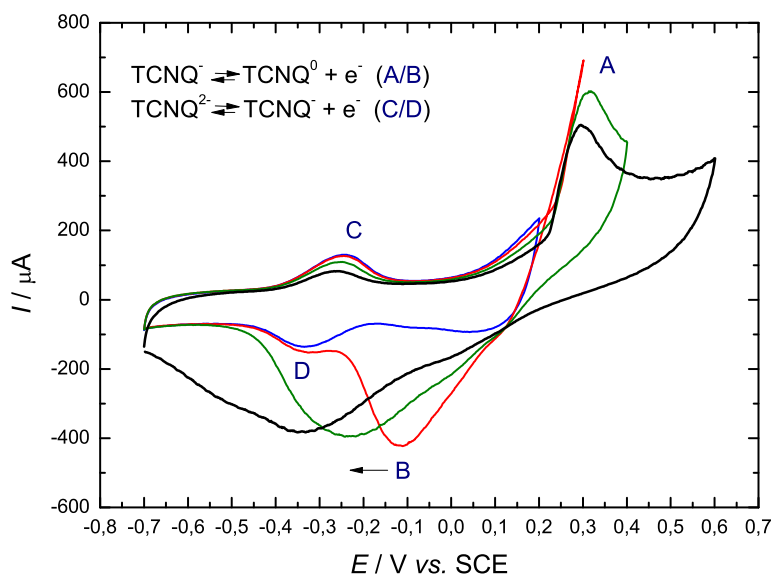


Figure 5-22: Cyclic voltammograms of the TCNQ electrode in different potential ranges. Conditions: 0.1 M phosphate buffer, pH 7.2, 37 °C, N_2 atmosphere, 400 rpm, scan rate: 5 mV s^{-1} . Catalyst ink composition: 20 mg Vulcan, 10 mg GOx and 10 mg TCNQ in 1 ml 2 % gelatin.

If the upper potential is kept negative enough (e.g. 0.2 V), two well-defined redox peaks, denoted as C and D, are observed. These peaks can be assigned to the redox couple $\text{TCNQ}^{2-}/\text{TCNQ}^{-}$ [144]. Another redox process is observed at potentials higher than 0 V. This process can be assigned to the $\text{TCNQ}^{-}/\text{TCNQ}^0$ redox couple. When the upper limit is further extended, two well-defined peaks (A and B) appear. Qualitatively similar behavior, with better defined redox processes and an “inert zone” between peaks A and B, has been shown in the case of TCNQ on pyrolytic graphite [144].

The behavior of the TCNQ enzymatic electrode in the present case was also similar to the behavior of a glucose biosensor based on carbon blacks [137]. In the latter case the two redox processes can be more clearly distinguished, despite of the broader peaks and the larger peak separation. In the present case the negative shifting of peak B ($\text{TCNQ}^0 \rightarrow \text{TCNQ}^{1-}$) with an increase of positive potential limit of the voltammogram impedes the differentiation between the two reductive processes in the negative scan when the upper potential limit is set more positive. In addition, a decrease in peak intensities is observed with cycling, which is regarded to be due to dissolution of TCNQ as reported in [144].

Cyclic voltammograms of the TCNQ-based electrode in absence and presence of glucose are presented in Fig. 5-23.

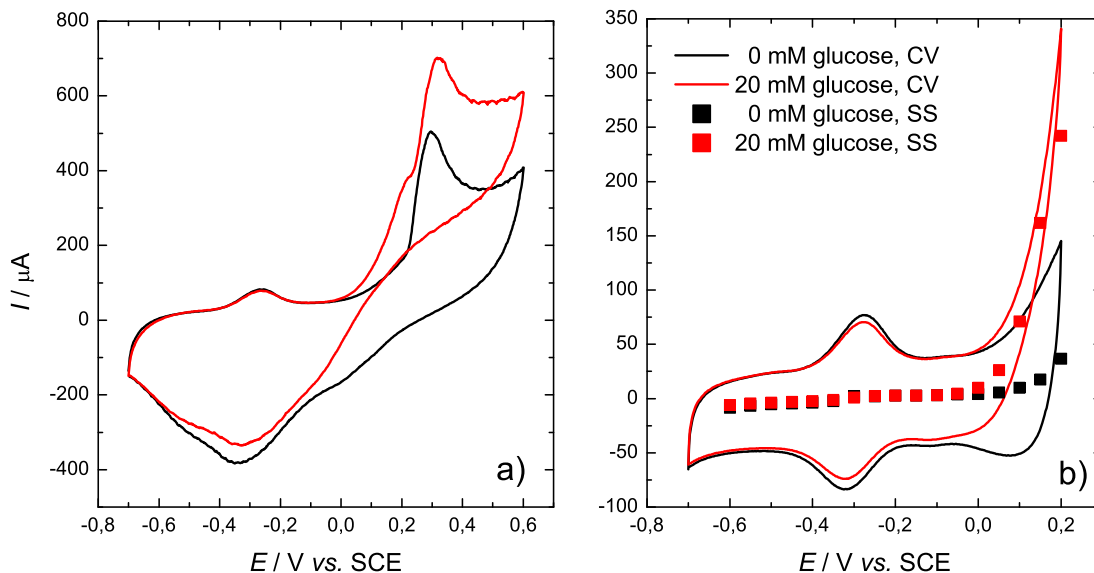


Figure 5-23: a) Cyclic voltammograms showing the activity of the TCNQ electrode in an extended potential range; b) Cyclic voltammograms and steady-state polarization curves of the TCNQ electrode showing the activity in a limited potential range. Conditions: 0.1 M phosphate buffer, pH 7.2, 37 °C, N_2 atmosphere, 400 rpm, scan rate: 5 mV s^{-1} . Catalyst ink composition: 20 mg Vulcan, 10 mg GOx and 10 mg TCNQ in 1 ml 2 % gelatin.

In the extended potential range the enzymatic electrode exhibits oxidation activity with an onset at about 0 V (Fig. 5-23a) and the ET process is assumed to be mediated by TCNQ⁰. The activity for glucose oxidation has been further investigated in a limited potential range, where the TCNQ²⁻/TCNQ⁻ process can be clearly observed (Fig. 5-23b). As can be seen in the graph, steady-state experiments (current values after 1 min) are in a good agreement with voltammetry. According to the literature, TCNQ⁻ species can theoretically act as potential mediators for GOx-catalyzed glucose oxidation, since its redox potential is more positive than the redox potential of the enzyme [116]. However, this is assumed not to be the case since the difference between the redox potential of the TCNQ²⁻/TCNQ⁻ couple and the glucose oxidation onset is about 300 mV.

5.5.3 TTF as mediator

TTF, analogous to TCNQ, is known to undergo two redox transformations, to the TTF⁺ and the TTF²⁺ radical cations, which can both act as redox mediators for the regeneration of reduced GOx [136]. Fig. 5-24 shows voltammograms of the TTF-based enzymatic electrode in different potential ranges in phosphate buffer. As can be seen from the graph if the potential window is kept until 0 V, the enzymatic electrode exhibits only capacitive behavior. When the positive potential limit is increased to 0.2 and 0.4 V, respectively, a redox process, assigned to the TTF⁰/TTF⁺ couple, occurs. The oxidation of TTF⁰ to TTF⁺ starts at about 0.05 V and no current peak in the positive scan is observed, regardless of the upper potential limit. However, a well-defined peak, corresponding to the reduction of TTF⁺ back to TTF⁰, is present in the negative scan. Its position is dependent on the positive potential limit, i.e. on the amount of TTF⁺ been generated during the oxidation.

It is assumed that due to the specific electrode architecture, the TTF⁺ cations, which are formed during the TTF oxidation at higher potentials, escape from the electrode surface. Therefore no mass transport limitation, evidenced by a peak in the positive scan, can be observed. As can be seen, when the upper potential limit of the voltammogram is extended, the positive currents clearly surpass the reductive currents, which can be attributed to TTF dissolution. Such behavior is typical for some metal electrodes, e.g. copper, where dissolution

(oxidation) in the positive scan and copper redeposition in the negative scan take place, respectively [145].

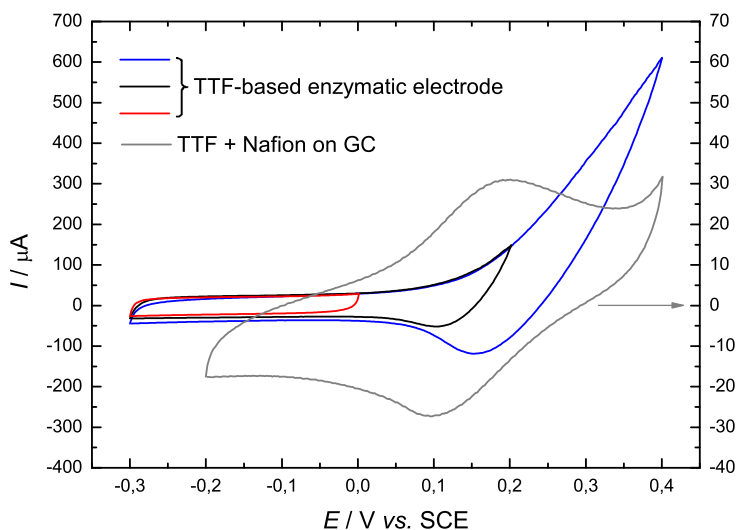


Figure 5-24: Cyclic voltammograms of the TTF enzymatic electrode and a glassy carbon (GC) modified with TTF in different potential ranges. Conditions: 0.1 M phosphate buffer, pH 7.2, 37 °C, N₂ atmosphere, 400 rpm, scan rate: 5 mV s⁻¹. Catalyst ink composition: 20 mg Vulcan, 10 mg GOx and 10 mg TTF in 1 ml 2 % gelatin.

In order to have an experimental reference for the redox potential of the TTF⁰/ TTF⁺ couple in the aqueous phosphate buffer employed in this study, in control experiments TTF has been dispersed in a Nafion solution and applied as a thin layer on a glassy carbon (GC) surface. The resulting voltammogram (see Fig. 5-24) shows the reversible oxidation of TTF and the peak position corresponds to the behavior of the TTF-based enzymatic electrode. The presence of a well-defined anodic peak can be tentatively attributed to the low amount of TTF in the Nafion film and the negative charge of the polymer, which will prevent TTF⁺ cations to escape from the surface. The reversible redox potential of TTF on GC is around 0.15 V, which is in accordance with the values, reported in the literature [75].

The voltammograms of the TTF electrode in absence and presence of glucose are shown in Fig. 5-25. The enzymatic electrode exhibits high activity towards glucose oxidation and the oxidation onset is at about -0.25 V. This value is well more negative than the value of the reversible potential, expected for the TTF⁰/ TTF⁺ couple.

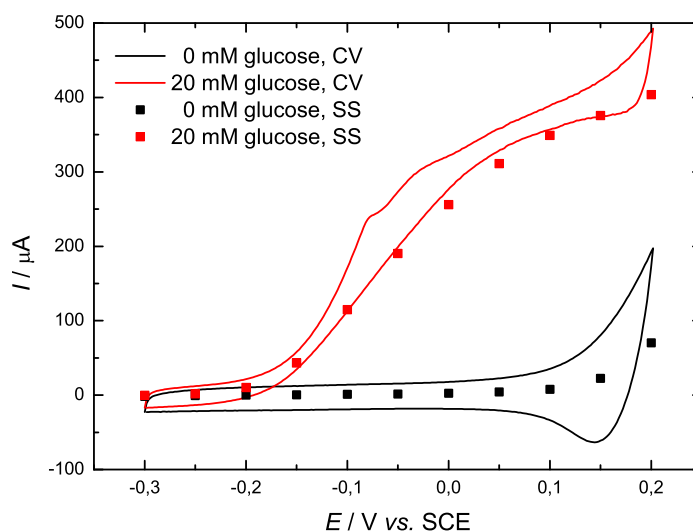


Figure 5-25: Cyclic voltammograms and steady-state polarization curves of the TTF enzymatic electrode showing the activity for glucose oxidation. Conditions: 0.1 M phosphate buffer, pH 7.2, 37 °C, N₂ atmosphere, 400 rpm, scan rate: 5 mV s⁻¹. Catalyst ink composition: 20 mg Vulcan, 10 mg GOx and 10 mg TTF in 1 ml 2 % gelatin.

As can be seen, steady-state curves follow the behavior observed in voltammogram. Similar oxidation onset and electrochemical behavior has been shown in the case of TTF-modified CNTs [75]. It should be noted that according to the literature TTF²⁺ species also can act as mediators but they are less stable and easily decomposed [136].

5.5.4 TTF-TCNQ as mediator

After the information about the electrochemistry and the glucose oxidation activity of the single components TTF and TCNQ has been obtained, the electrochemical behavior the CTC has been investigated and directly compared with the behavior of the TTF and TCNQ electrodes. Fig. 5-26a shows the voltammograms of the CTC electrode in buffer in different potential ranges, which have been compared with the responses of TTF and TCNQ electrodes at the same potential scale in Fig. 5-26b.

As can be seen, the shape of the voltammogram of CTC in the potential range between -0.2 and 0.2 V indicates that some redox processes are occurring at potentials close to both limits of the voltammetric experiment. It should be noted that this kind of response has been obtained in a reproducible manner with fresh CTC electrodes, which have not been subjected to any

pretreatment or conditioning. The respective voltammogram shows that a reduction process takes place at potentials negative to -0.1 V, and a small oxidation peak can be observed immediately upon scan reversal. According to the literature, the reduction currents can be assigned to cathodic salt decomposition, according to Eq. 6 as proposed by Jaeger and Bard [111] and the subsequent anodic peak has been previously ascribed to reversibility of the process at its initial stage [146].

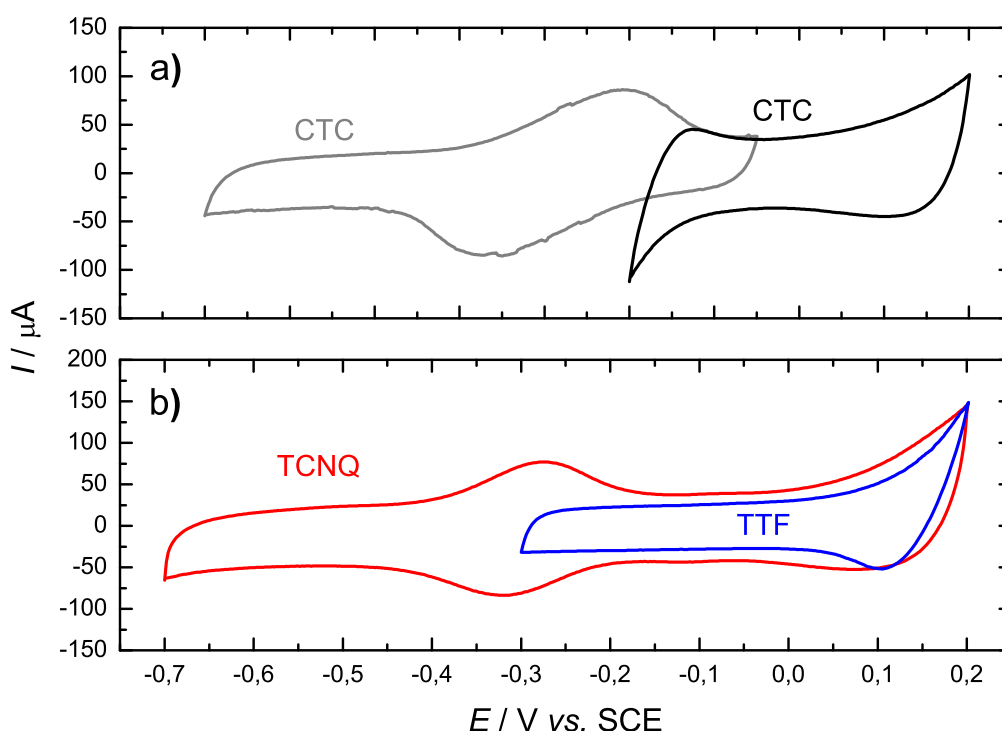


Figure 5-26: Cyclic voltammograms of TTF, TCNQ and TTF-TCNQ electrodes in different potential ranges. Conditions: 0.1 M phosphate buffer, pH 7.2, 37 °C, N₂ atmosphere, 400 rpm, scan rate: 5 mV s⁻¹. Catalyst ink composition: 20 mg Vulcan, 10 mg GOx and 10 mg mediator in 1 ml 2 % gelatin.

The CTC decomposition is accelerated when the electrode is subjected to cycling at low sweep rates in a more negative potential range. However, the associated cathodic currents decrease with the number of cycles until a reproducible response is obtained, which indicates possibly decomposition of all electrochemically susceptible TTF-TCNQ. The gradual cathodic decomposition is demonstrated in Fig. 5-27.

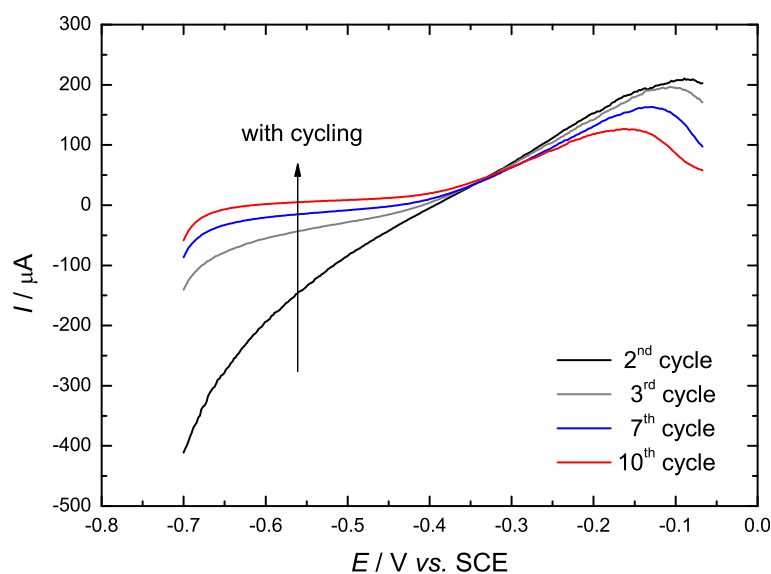


Figure 5-27: Consecutive linear sweep voltammograms of the TTF-TCNQ electrode, demonstrating gradual cathodic decomposition. Conditions: 0.1 M phosphate buffer, pH 7.2, 37 °C, N₂ atmosphere, 400 rpm, scan rate: 5 mV s⁻¹. Catalyst ink composition: 20 mg Vulcan, 10 mg GOx and 10 mg TTF-TCNQ in 1 ml 2 % gelatin.

After sufficiently long cathodic treatment, the resulting voltammogram from -0.7 to -0.05 V is characterized by a clearly developed redox peak (Fig. 5-26a). Based on its position and shape, it can be assigned to the $\text{TCNQ}^{2-}/\text{TCNQ}^-$ couple (see Fig. 5-26b) as discussed above. Therefore, it can be assumed that it is more likely that the small anodic peak upon scan reversal in the voltammogram between -0.2 and 0.2 V is rather due to TCNQ^{2-} oxidation to TCNQ^- , than to reversible salt decomposition. This implies that the redox behavior observed at potentials more positive than 0 V can be attributed both to the $\text{TTF}^0/\text{TTF}^+$ and the $\text{TCNQ}^-/\text{TCNQ}^0$ couples. Unfortunately, it is difficult to discriminate between both processes because of the similar onset potentials of TTF^0 and TCNQ^- oxidation, as can be seen in Fig. 5-26b.

The presence of TTF^0 and TCNQ^- species in the electrode architecture could be also explained by CTC dissolution. According to the literature, TTF-TCNQ has a stable potential window in aqueous media and shows no current peaks that could be attributed to salt decomposition [111]. The observation of redox processes in the potential region between -0.2 and 0.2 V (see Fig. 5-26a) challenges the assumption of a completely inert potential range

under the present experimental conditions. The release of electroactive species within the “stable” potential window has been discussed in [147] and demonstrated also by scanning tunneling microscopy experiments (STM) [148]. The authors in the latter study observed dissolution at potentials within the stable potential region and even at equilibrium potential. They assumed the presence of neutral TTF and TCNQ species dissolved in the aqueous solution, either reversibly at equilibrium, or irreversibly at non-equilibrium potentials (Eq. 7-9) and distinguished the nature of these species ($\text{TTF}_{(aq)}$, $\text{TCNQ}_{(aq)}$) from the nature of the surface-confined species (TTF^0 , TCNQ^0). This assumption corresponds to the observed behavior in the present study and can explain the fact that the voltammetric features of the single components TTF and TCNQ can be followed on the CTC electrodes without any special potential pretreatment.



As already discussed above, not only TTF-TCNQ but also TTF and TCNQ can act as mediators for GOx. The corresponding activities are compared in Fig. 5-28. For the sake of clarity the respective polarization curves in absence and presence of 20 mM glucose have been presented in the same potential scale and current range for all electrodes.

As can be seen the glucose oxidation activity of the CTC electrode in the range between -0.2 and 0.2 V (Fig. 5-28b) significantly resembles the behavior of the TTF electrode (Fig. 5-28a), in terms of oxidation onset and measured currents. The reduction currents at potentials negative to -0.2 V can be explained by the crystal lattice reduction, which has been discussed above, since the CTC electrode in Fig. 5-28b has not been subjected to any special pretreatment and has been investigated only in the range between -0.25 and 0.2 V.

Fig. 5-28c shows the polarization curves of the CTC in absence and presence of glucose in the potential range between -0.6 and 0.1 V after negative potential pretreatment. As can be seen, after pretreatment no reduction currents are observed and the glucose oxidation onset potential is at about -0.25 V, which corresponds to the behavior of CTC in Fig. 5-28b and the behavior of

TTF in Fig. 5-28a. This implies that the electrode pretreatment induces CTC decomposition and generates TTF species in the electrode architecture, which can act as mediators for the GO_x-catalyzed glucose oxidation.

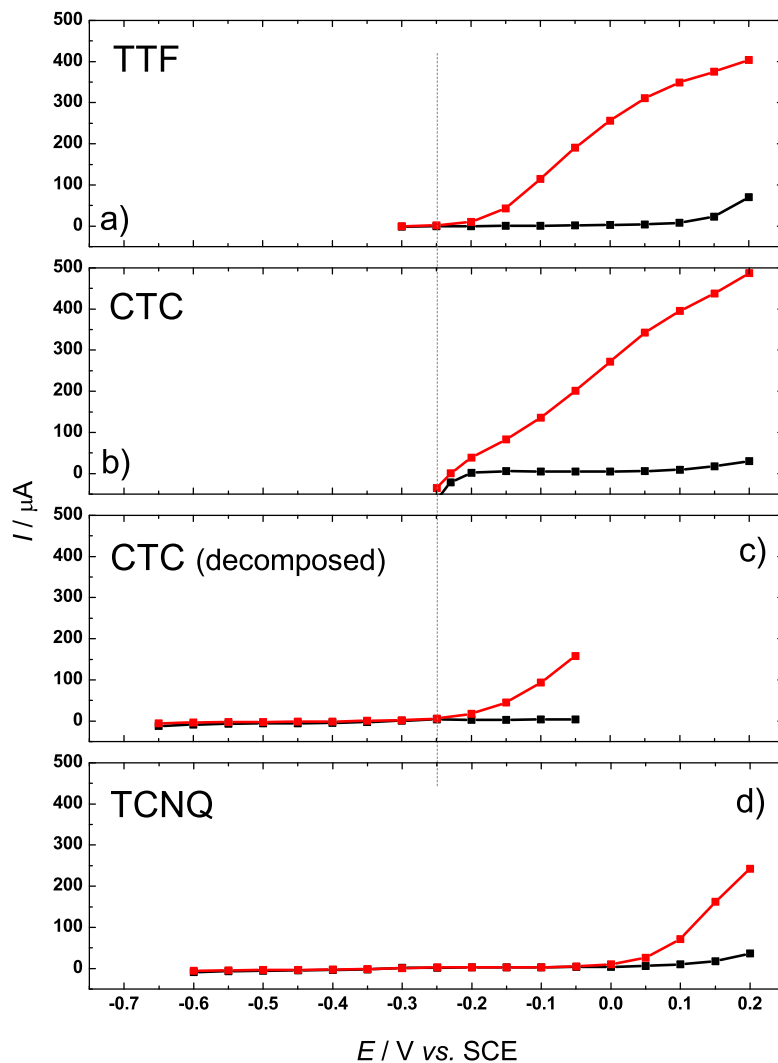


Figure 5-28: Steady-state polarization curves of TTF-, TTF-TCNQ- and TCNQ-based enzymatic electrodes in different potential ranges in absence and presence of glucose. Conditions: 0.1 M phosphate buffer, pH 7.2, 37 °C, N₂ atmosphere, 400 rpm. Catalyst ink composition: 20 mg Vulcan, 10 mg GO_x and 10 mg mediator in 1 ml 2 % gelatin. Dashed line is additionally drawn for guidance of the reader.

The glucose oxidation activity of the TCNQ electrode does not start earlier than 0 V (see Fig. 5-28d), which indicates that TCNQ cannot be accountable for mediation at the more negative potentials observed in Fig. 5-28b and 5-28c. On the other side, it is likely that at potentials more

positive than 0 V, both TTF and TCNQ act as mediators and the respective currents are superimposed, which is evidenced by a kink in the respective polarization curve (Fig. 5-28b) but the two processes cannot be distinguished. These findings correspond to the proposal of alternating ET mechanism, involving different mediator species [116] but restricted to more positive potentials.

In order to have additional experimental evidence that dissociated species are present on the CTC surface, the electrodes have been analyzed by Fourier Transform Infrared Spectroscopy (FTIR) after different treatments. The state of the TTF-TCNQ can be easily determined by the shift in the nitrile stretching band of TCNQ according to the empirical dependence demonstrated in [149, 150] due to the relation between the vibrational frequency and the degree of charge transfer, manifested in compounds with π -delocalized systems. The shift in the initial nitrile frequency of TCNQ in the case of TTF-TCNQ and KTCNQ corresponds to a degree of charge transfer of 0.59 and 1.00, respectively. Thus, it makes possible to identify in a simple way the nature of TCNQ species present at the electrode surface. Fig. 5-29a shows referent FTIR spectra of TCNQ, TTF-TCNQ and KTCNQ recorded between 2500 cm^{-1} and 2000 cm^{-1} .

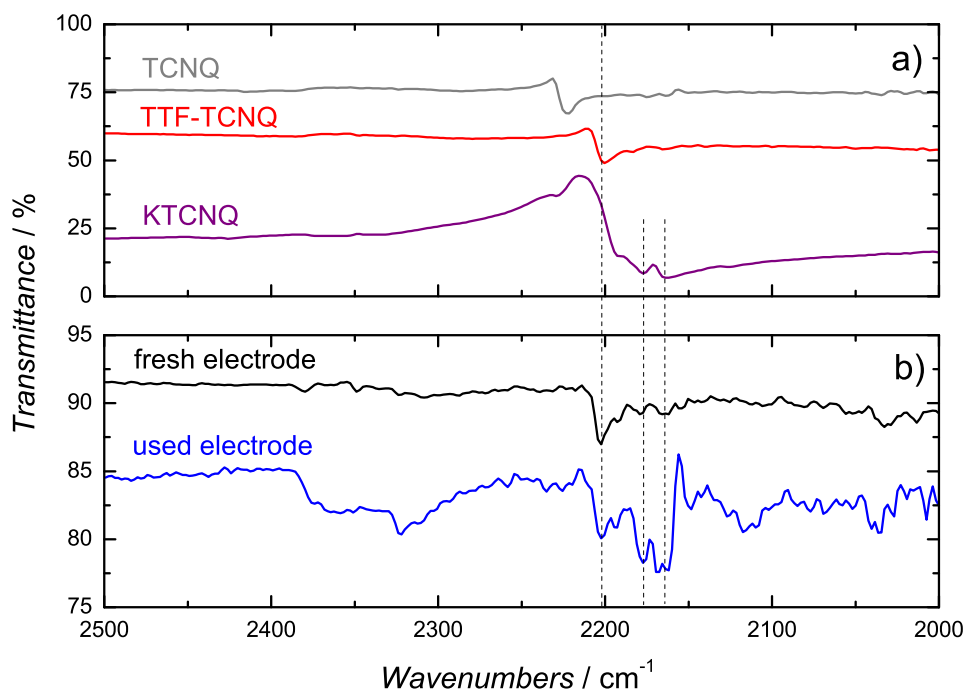


Figure 5-29: FTIR spectra of a) different TCNQ species; b) TTF-TCNQ enzymatic electrodes before after electrochemical characterization in absence and presence of glucose between -0.2 V and 0.2 V vs. SCE. Dashed lines are additionally drawn for guidance of the reader.

The values obtained for the charge transfer degree are 0.43 and 0.88 for the TTF-TCNQ and KTCNQ, respectively. These values slightly deviate from the literature reported values but the apparent shifts demonstrate that the respective peaks can be used for characterization of the nature of TCNQ species at the electrode surface. Fig. 5-29b shows spectra of the freshly prepared enzymatic electrode and after electrochemical characterization in presence of glucose. The value of the frequency (2200 cm^{-1}) of the fresh electrode indicates the presence of TTF-TCNQ in its original state. The peaks in the FTIR spectrum of the electrode, which has been subjected to electrochemical characterization in absence and in presence of glucose, indicate the presence of intact TTF-TCNQ as well as TCNQ anions. The peak at 2177 cm^{-1} is characteristic for TCNQ^- species, while the peak at 2163 cm^{-1} can be attributed to both TCNQ^- and TCNQ^{2-} species [151]. The presence of divalent anions can be also assumed due to the broad peak at about 2110 cm^{-1} (characteristic for TCNQ^{2-}) but this is rather speculative interpretation since the peak is poorly defined. Despite of this ambiguity, the FTIR spectrum of the used electrode confirms the presence of intact TTF-TCNQ crystals and TCNQ anions at the electrode surface. This observation is in accordance to the voltammetric data and further assists the hypothesis of TTF-TCNQ dissolution in the investigated potential range.

5.5.5 Conclusions about the electron transfer mechanism

The results shown above imply that in the present electrode configuration electroactive species are generated *in situ* from the CTC surface even within the “stable” potential range. The significant similarity in the glucose oxidation activity of CTC and TTF electrodes suggests MET with TTF species as the main mediators. The possibility of simultaneous activity of TTF and TCNQ at more positive potentials is also considered. It should be noted that the assumption of MET does not contradict the hypothesis of enzyme modified through hydrophobic interactions by TTF species and undergoing “direct” oxidation at electrode surfaces [141], whereby the difference arises from the different terminology used by different groups.

The interpretation in the present study is in accordance with most of the previous findings in the literature but extends the current understanding of the CTC electron transfer mechanism by discussion of the oxidation onset potential, which is an important parameter for practical applications of CTC-based anodes in biofuel cells. In this context, the results shown above

indicate that both CTC and TTF can be used as mediators for glucose oxidation and they show similar performance. However, the CTC electrodes overpower due to the smaller relative loading of TTF. For instance, enzymatic electrodes based on 10 mg loading of TTF and TTF-TCNQ show similar kinetics but in 10 mg of TTF-TCNQ only 5 mg of TTF are present, having in mind the 1:1 stoichiometric ratio of the components. The better performance of TTF-TCNQ can be tentatively ascribed to the higher conductivity of the enzymatic electrode (due to the intrinsic conductivity of the CTC) and/or some effects in respect to the difference in the dissociation rate of TTF^+ from the TTF^0 and $\text{TTF}^{\delta+}\text{TCNQ}^{\delta-}$. Another advantage is the simultaneous action of TCNQ as a mediator at more positive potentials.

To summarize, based on the experiments shown above it can be concluded that major part of the activity of TTF-TCNQ based enzymatic electrodes for glucose oxidation is due to TTF species, which are released from the CTC surface. TCNQ species can also act as mediators but only in a more positive potential range. The TTF and TCNQ species can be generated *in situ* either by simple dissolution or by potential induced crystal decomposition during the electrochemical tests. It should be pointed out that these conclusions are limited to the particular electrode architecture used in present study but they can be also extended for the theoretical treatment of results shown in previous works.

5.6 Conclusions

CTCs such as TTF-TCNQ are well-established materials for the preparation of glucose biosensors and enzymatic electrodes based on TTF-TCNQ exhibit high current densities, relatively low overpotential and high stability. In addition, they can be prepared by unpretentious procedures, which involve only commercially available materials. However, despite of these promising features, CTC-based anodes have never found an application in biofuel cell devices, which has motivated our studies with this kind of systems. Our results indicate that TTF-TCNQ forms a highly irregular porous structure, which serves as a matrix for immobilization of the enzyme, which underlines the importance of the optimization of the enzymatic electrode architecture. In order to improve the electrode performance with respect to fuel cell applications, the influence of various aspects of the preparation procedure has been studied in a systematic way and the respective findings extend the existing interpretation present in the literature. It was

found that the dispersion of the electrode components in a gelatin matrix together with a conductive high surface area material such as Vulcan XC72R has the most beneficial influence on the electrode performance. In addition, the results shown in the present study support the hypothesis of mediated electron transfer by species, released *in situ* from the CTC surface. These findings open and support further possibilities for optimization of the electrode performance such as chemical tuning the potentials of the donor and acceptor compounds forming the CTC, as well as more precise control of the CTC shape, size and distribution.

5.7 Experimental details

5.7.1 Chemicals and materials

All chemicals including glucose, TTF, TCNQ, TTF-TCNQ and polyvinyl sulfate potassium salt (PVS) as well as tetrahydrofuran (THF) and acetonitrile (ACN) were of analytical reagent grade and purchased from Sigma-Aldrich. Ultrapure water from Millipore was used in all experiments.

Stainless steel was used as a mechanical and electrical support for the preparation of enzymatic electrodes. Discs with a diameter of 11 mm and 1 mm thickness were used in the case of single electrode experiments (three-electrode set-up). The discs were mounted in a sample holder for rotating disc electrode (RDE) with an opening of 8 mm (0.5 cm² working area) for the electropolymerization and an opening of 6 mm (0.28 cm² working area) for the electrochemical tests.

5.7.2 Modification procedure with polypyrrole layer

The enzymatic electrode preparation procedure was similar to the procedure reported by Khan [79] and had several steps. The stainless steel discs were polished with emery paper and degreased with acetone before further modification. In the first step, a polypyrrole film was electrochemically deposited on the stainless steel surface. The electropolymerization was done galvanostatically at a current density of 4 mA cm⁻² until a charge of 1.2 C cm⁻² passed. The aqueous monomer solution contained 0.02 M (per monomer molecular weight) PVS and 0.15 M

pyrrole. The solution was agitated by the RDE. No attempts to exclude oxygen from the system during the electropolymerization were made.

In the next step, CTC crystals were grown directly on the polymer surface. First, TCNQ dissolved in THF was cast several times on the electrode until the desired loading was achieved. After that, TTF dissolved in ACN was applied in several successive steps over the TCNQ layer until TTF loading of slight excess compared to the TCNQ loading was obtained. The electrode was then gently washed with ACN in order to remove the unreacted TTF and dried under ambient conditions. After that GOx was adsorbed on the CTC crystals by applying an aliquot of 20 mg ml⁻¹ GOx solution in phosphate buffer (pH 7.2) and the electrode was left to dry. Subsequently, the CTC/GOx assembly was covered by an aliquot of gelatin solution (2.5 % w/v in water, incubated for 30 min at 30 °C before use) and dried again. Finally, the electrode assembly was cross-linked by dipping into a glutaraldehyde solution (5 % in water) for 60 s, washed with plenty of water and dried at room temperature. The enzymatic electrodes were kept in plastic bags at -20 °C before use. Cross-sectional scanning electron microscopy (SEM) analysis of the enzymatic electrode assembly was performed by AQura GmbH, Germany using XL30 FEG (FEI Company).

5.7.3 Modification procedure with a gelatin matrix

Stainless steel discs were used as a support of the enzymatic electrodes. Vulcan XC72R (Cabot) was supplied by QuinTech (Germany). Ketjen Black EC 300J was a kind gift by Akzo Nobel Chemicals and Printex XE 2B was gift by Evonik Industries. The ink used for modification of the enzymatic electrodes had typically the following composition: 20 mg Vulcan XC72R, 10 mg of the respective mediator (TTF, TCNQ or TTF-TCNQ) and 10 mg GOx (1920 U) in 1 ml of 2 % w/v gelatin aqueous solution (heated to 35 °C before use). In the case of tests for optimization of the modification procedure the type of carbon black material as well as the quantities of Vulcan, TTF-TCNQ, GOx and gelatin were varied. The mediators were ground in an agate mortar before use. Suspension of the ink components in the gelatin solution was assisted by mechanical stirring and ultrasonication for about 5 min. For preparation of the enzymatic electrodes 50 µl of the respective ink was applied on the stainless steel electrode (0.28 cm²) and left to dry under ambient conditions. After that the electrode assembly was cross-linked by

dipping into a glutaraldehyde solution (5 % in water) for 60 s, washed carefully with water and dried again. The enzymatic electrodes were kept in plastic bags at $-20\text{ }^{\circ}\text{C}$ before use.

In case of fluorescence experiments GOx was modified by fluorescent protein label (DyLight 350 NHS ester from Thermo Scientific) according to the supplier protocol.

5.7.4 Electrochemical experiments

Electrochemical experiments were carried out in a conventional double-jacketed Pyrex electrochemical cell (Radiometer Analytical). The RDE was used as a working electrode, platinum wire as a counter electrode, and saturated calomel electrode (SCE) as a reference electrode. The experimental solutions were saturated with nitrogen or oxygen. Electrochemical single electrode and fuel cell experiments were performed by a computer controlled potentiostat PGSTAT302 (Eco Chemie/Autolab). Steady-state polarization curves were obtained by extracting of the currents after 1 min at different potential values.

6. Hybrid enzymatic fuel cell

6.1 Concept of the hybrid fuel cell

Important aspect in the development of enzymatic biofuel cells, apart from the design and optimization of the individual electrodes, is the design of the whole fuel cell system. Little emphasis has been put on this issue in the past and most of the studies have been focused on single electrodes studies. For this reason, after the successful development of the anode modification procedure, the enzymatic anode has been combined with a Pt cathode in a hybrid biofuel cell device. The structure of the cathode comprises the membrane electrode assembly (MEA) design, which has been adopted from the conventional fuel cell technology. It should be noted that the term “hybrid” when referred to a fuel cell, is mainly associated with the combination of two power sources with different operational principles (e.g. fuel cell and battery). However, this term can be also used to denote the different nature of catalysts (e.g. biological catalyst at the anode and an inorganic catalyst at the cathode as in the present case) as discussed in [10]. The combination with a noble metal catalyst electrode allows for testing of the enzymatic electrode performance under fuel cell conditions. Similar strategy has been used both for anodes [32, 37, 152] and for cathodes [30, 48, 60]. Such systems have been usually referred to as biofuel cells, despite of the presence of a non-bio component. The hybrid fuel cell device in this study can be used as a platform for investigation of different enzymatic anodes and give additional information about their behavior in a whole fuel cell system when combined with a cathode with “known” catalytic properties.

The enzymatic fuel cell device, presented in this study comprises a parallel plate design (see the experimental details in Section 6.7.3 below). The bioanode operates in liquid phase and the flow-through design of the anodic chamber allows for perfusion of the fuel solution. The continuous flow diminishes substrate depletion and product accumulation and allows for mass transport investigations of the bioanode under fuel cell conditions. In case of a batch operation or when analysis of the oxidation products is required, the flow can be stopped and the anodic chamber can be isolated by closing the inlet and outlet valves.

The cathode operates in gas phase, which allows overcoming the limitations associated with the low oxygen solubility in aqueous solutions [52]. The use of pure oxygen instead of air and

the high flow rate (500 ml min^{-1}) should eliminate oxygen concentration effects along the flow field channels. The oxygen gas was not humidified due to the fact that the one side of the membrane is in contact with aqueous solution and should be sufficiently hydrated. The high platinum loading (5 mg cm^{-2}) should ensure high cathode performance as it was shown by Reshetenko et al. [153], who studied the influence of cathode optimization on the performance of a direct methanol fuel cell (DMFC).

In the following sections the influence of the fuel cell architecture and some operational parameters on the hybrid fuel cell performance will be investigated.

6.2 Performance of the hybrid fuel cell

Polarization and power curves of the hybrid enzymatic fuel cell at two different glucose flow rates are shown in Fig. 6-1. The polarization curve at 5 ml min^{-1} flow rate exhibits a small activation region and an OCV of 0.94 V .

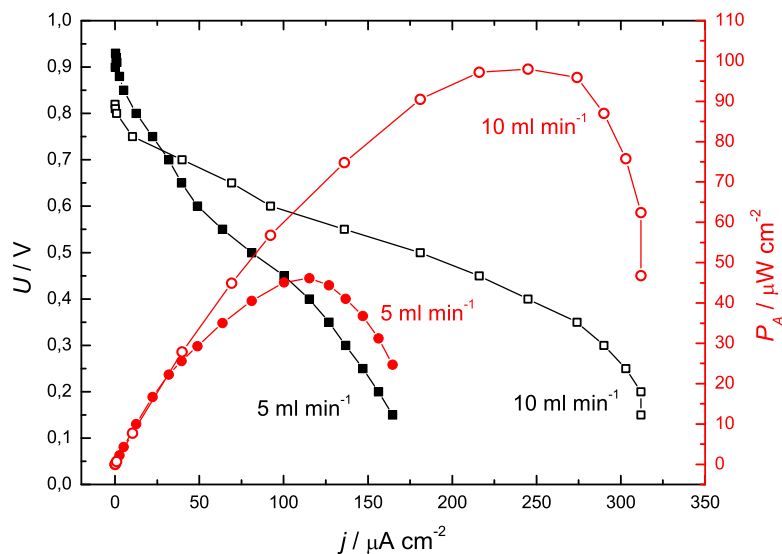


Figure 6-1: Polarization (black squares) and power curves (red circles) of the hybrid fuel cell at glucose flow rates of 5 ml min^{-1} (full symbols) and 10 ml min^{-1} (empty symbols). Conditions: Anode: 5 mM glucose in 0.1 M phosphate buffer, $\text{pH } 7.2$, $37 \text{ }^\circ\text{C}$, N_2 atmosphere; Cathode: 500 ml min^{-1} dry oxygen flow rate.

Different OCV values for glucose-oxygen biofuel cells have been presented in the literature. For example, 0.55 V was reported for a similar flow-through hybrid fuel cell with enzymatic anode

mediated by dissolved benzoquinone and a Pt cathode [46] or 0.8 V for a non-enzymatic direct glucose fuel cell based on Pt catalysts, which employed also a MEA design [154]. High OCV values (around 1 V) have been demonstrated in the case of glucose-oxygen enzymatic biofuel cells based on Os redox hydrogels [21, 23].

The theoretical cell voltage for glucose oxidation to gluconolactone in presence of gas-phase oxygen under standard conditions, calculated according to [71] and assuming ionic strength of 0.25 M is 1.18 V, which corresponds to the value calculated in [21]. If conditions deviate from standard conditions as in the present case (5 mM glucose concentration and not defined concentration of gluconolactone, which is consumed in a following hydrolysis reaction) even higher theoretical cell voltage can be expected according to the Nernst equation. Although reasonable from a thermodynamic point of view, the value of 0.94 V is unexpectedly high, compared to the typical performance of similar biofuel cells.

The OCV in a fuel cell is influenced by the open circuit potentials of the anode and the cathode. As it was already mentioned, the open circuit potential of the anode in the present case is around -0.2 vs. SCE. On the other side, control experiments with Pt black-modified electrodes revealed current onset of the oxygen reduction at about 0.3 V vs. SCE in phosphate buffer, which was in accordance with the literature values for Pt nanoparticles on multi-walled carbon nanotubes (MWCNTs) (ca. 0.26 V vs. SCE) [155]. According to these half-cell experiments one can expect much lower OCV. The high values obtained in the present study can be possibly explained by the specific architecture of the fuel cell, namely the enzymatic electrode is in contact with buffer, while the Pt cathode is in contact with Nafion. This implies pH difference between the electrodes. In control experiments the Pt black cathodes in 0.1 M sulfuric acid revealed reduction onset at approximately 0.7 V vs. SCE, which was similar to the value for Pt nanoparticles on MWCNTs in 0.1 M perchloric acid [156]. Furthermore, the oxygen reduction kinetics is significantly enhanced at the Pt/Nafion interface since Nafion is a superacid (due to the highly acidic protons attached to the sulfonate sites in the polymer structure) and exhibits negligible anion adsorption effects, in addition to high oxygen solubility [157], which implies even more positive onset potential for the Pt cathode than the one observed in the case of sulfuric acid. In light of this discussion, the measured OCV values can be expected in the present setup. Regarding the value of 0.55 V, reported for a similar hybrid setup [46], the difference can be possibly attributed to the different fuel cell architecture, the higher glucose concentration and the

different mediator. Higher glucose concentration is expected to increase the glucose crossover and consequently to decrease OCV, which will be discussed below. The possibility of crossover is taken into account since Pt has catalytic activity for glucose oxidation as demonstrated in [158].

In addition to the activation region, observed in Fig. 6-1, the mass transport and resistance limitation regions in the polarization curve can be also distinguished. The current values obtained in the present setup suggest that the fuel cell is limited by the enzymatic anode since the Pt cathode can easily reach the mA range under similar conditions, e.g. in a DMFC [159]. The fuel cell exhibits maximum power density of about $45 \mu\text{W cm}^{-2}$ at 5 ml min^{-1} glucose flow rate. Increasing the flow rate to 10 ml min^{-1} decreases the OCV to 0.82 V and changes the shape of the polarization curve. The region of ohmic polarization is significantly extended and the mass transport limitation can be clearly identified at current densities around $300 \mu\text{A cm}^{-2}$ (see Fig. 6-1). The decrease in OCV at higher flow rate can be attributed to crossover of glucose, which can be oxidized at the cathode, creating a mixed potential. Increase in flow rate is expected to enhance the mass transport of glucose at the anode but also to increase the rate of crossover. Such phenomenon has been also demonstrated in a recent study, where the influence of operational parameters such as fuel concentration and flow rate on the performance of a DMFC has been investigated [159]. The higher flow rate in the present case resulted in an improved overall performance of the fuel cell, raising the maximum power output to nearly $100 \mu\text{W cm}^{-2}$ at 0.4 V.

The performance of the fuel cell presented in this study is somewhat superior compared to other hybrid biofuel cells employing Pt cathodes, although a straightforward comparison is difficult due to the difference in experimental conditions as outlined in [10]. For instance, a hybrid fuel cell with similar MEA architecture, which delivered around $45 \mu\text{W cm}^{-2}$ at 100 mM glucose, was reported by Tamaki et al. [44]. The anode was based on GOx and a ferrocene-modified polymer, which redox potential resulted in lower OCV and moderate output despite the high fuel concentration.

Another compartmentalized hybrid fuel cell, which utilized GOx and dissolved benzoquinone as mediator generated similar output ($42 \mu\text{W cm}^{-2}$) also at 100 mM glucose [17]. In another study, highly efficient bioelectrodes based on Os redox hydrogels, single-walled carbon nanotubes (SWCNTs) and CDH were tested in a model membraneless configuration together

with a Pt black cathode and the resulting maximum power density was $157 \mu\text{W cm}^{-2}$ in presence of 100 mM glucose.

The performance of the hybrid biofuel cell presented in this study is also comparable to the performance of biofuel cells incorporating enzymatic cathodes. For instance, a very recent study reported high current density glucose oxidation anodes based on GOx and a ferrocene-modified polymer, which generated limiting current densities of about 2 mA cm^{-2} at 0.3 V vs. SCE and ca. 60 mM glucose [73]. The bioanodes were coupled with Os-mediated laccase cathodes and the resulting biofuel cell generated $56 \mu\text{W cm}^{-2}$ with a stationary cathode and $146 \mu\text{W cm}^{-2}$ under rotation. In respect to operation at low glucose concentrations (5 mM), a notable example is the configuration based on Os redox hydrogels, which generated $280 \mu\text{W cm}^{-2}$ and was reported as the highest power biofuel cell at the lowest concentration [160]. However, this high performance in the latter case was achieved by the use of GOx from another source (*Penicillium pinophilum*) and operation at pH 5. For comparison, when GOx from *Aspergillus niger* was used, the biofuel cell generated only $90 \mu\text{W cm}^{-2}$ under the same conditions. In addition, it should be noted that the respective electrodes were 2 cm long carbon fibers with a diameter of 7 μm , which size and geometry significantly enhance mass transport conditions.

6.3 Influence of the fuel cell architecture

After continuous operation a liquid was detected at the oxygen gas outlet as well as in the graphite flow-field after disassembly of the device. It was assumed that the transport of solution through the membrane will influence the performance of the cathode and different strategies to diminish this effect have been exploited.

The accumulation of liquid water, known as flooding is regarded to be the major cause of oxygen mass transport limitations in PEM fuel cells [161]. Apart from the water generated by oxygen reduction at the cathode, there is a given amount of water transported from the anode to the cathode by an electroosmotic drag and both fluxes are proportional to the current density [162]. If the generation rate exceeds the removal rate, water accumulates and causes blocking of the oxygen transport within the catalyst layer and as a result reduces the cathode performance [161]. The low currents in our system and more important, the aqueous media in the anodic chamber suggest that dominant part of the aqueous solution is being transported through the

membrane by simple diffusion. It is assumed that in the present case the performance of the fuel cell will be influenced not only by the water transported through the membrane but also by the cations from the buffering salts and the dissolved glucose, which are being transported together with the aqueous solution. For instance, the decrease of OCV with an increase of anodic flow rate, shown in Section 6.2 has been ascribed to enhanced crossover of glucose. Having in mind the low current densities that have to be maintained by the cathode, it is unlikely that the accumulation of liquid water and the consequent blocking of gas-phase oxygen transport will influence the fuel cell performance to a great extent. The species dissolved in the anodic solution are expected to have a greater impact on the cathode and fuel cell performance.

6.3.1 Influence of gas-diffusion layer

A common strategy to diminish the flooding rate is hydrophobization of the gas-diffusion layer (GDL) by impregnation with hydrophobic agents such as polytetrafluoroethylene (PTFE) [161] as demonstrated in a recent study by local current distribution and neutron radiography imaging of the cathode in a DMFC [163]. Fig. 6-2 shows polarization curves of the hybrid enzymatic fuel cell with untreated Toray paper, Toray paper impregnated with 50 % PTFE and without any GDL.

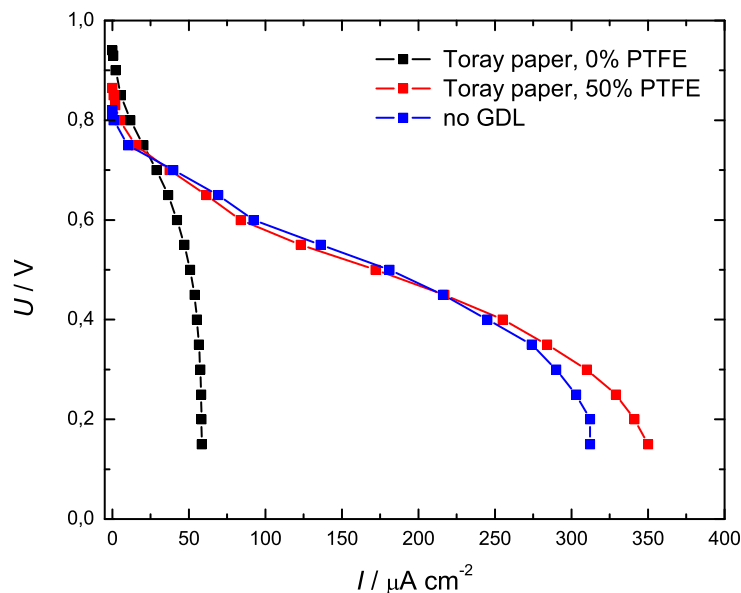


Figure 6-2: Polarization curves of the hybrid fuel cell with different types of GDL and without a GDL. Conditions: Anode: 5 mM glucose in 0.1 M phosphate buffer, 10 ml min⁻¹ flow rate, pH 7.2, 37 °C, N₂ atmosphere; Cathode: 500 ml min⁻¹ dry oxygen flow rate.

Decreasing the wettability of the GDL improves significantly the cell performance. The region of ohmic polarization is notably extended and a small region of mass transport limitation can be observed at ca. $350 \mu\text{A cm}^{-2}$. The maximum power density increases about four times, compared to the case with untreated GDL and reaches $100 \mu\text{W cm}^{-2}$ at 0.4 V. The influence of different Toray paper wetproof levels (10-30 %) on the output of a PEM fuel cell has been studied in [164]. It was observed that the best performance showed GDLs with a PTFE loading of 20 %, suggesting that a careful balance between hydrophilic and hydrophobic properties of the GDL is needed for the precise control of the flooding rate. Similar dependence with an optimum PTFE loading below 50 % might be true in the present system but this was not investigated in detail.

The performance of the fuel cell without any GDL is also improved compared to the case with untreated Toray paper. The absence of a GDL and the hydrophobization of the GDL result in a similar performance (see Fig. 6-2) and the respective polarization curves differ slightly only at the mass transport limited region. In general, the absence of a GDL is expected to reduce the performance in the case of conventional fuel cells due to inefficient gas distribution and bad electrical contact. This would not be the case in the present system due to the high catalyst loading and the low current densities, which are to be maintained by the cathode. In addition to the simplified fuel cell architecture, it is assumed that the absence of GDL will lead to enhanced water removal by the reactant flow as it was shown in [165] by pressure drop measurements.

6.3.2 Influence of separator and cathode hydrophobization

Another possible strategy to diminish the flooding rate is hydrophobization of the catalyst layer. Improvement of the fuel cell performance can be achieved only after careful balance between the hydrophobic properties and the electronic conductivity of the cathode as shown by Liu et al. [166], who studied the effect of PTFE loading on the cathode performance in a DMFC. Another, more straightforward, method is to introduce a physical barrier between the fuel solution and the cathode in order to control the solution supply to the cathode as demonstrated by Sakai et al. [52]. The influence of 10 wt. % PTFE in the catalyst layer and the presence of a cellophane membrane as a separator on the performance of the hybrid fuel cell is shown in Fig. 6-3.

Both, hydrophobization of the catalyst and the utilization of a separator result in an improved performance of the hybrid enzymatic fuel cell, shifting the current densities at 0.2 V to ca. 200 $\mu\text{A cm}^{-2}$ and ca. 240 $\mu\text{A cm}^{-2}$, respectively. As can be seen in Fig. 6-3 the separator has more favorable effect on the performance, in addition to a slight increase of the OCV to 0.99 V, which can be assigned to lower crossover of glucose. The simultaneous utilization of separator and hydrophobized cathode did not show any additive or synergic effect.

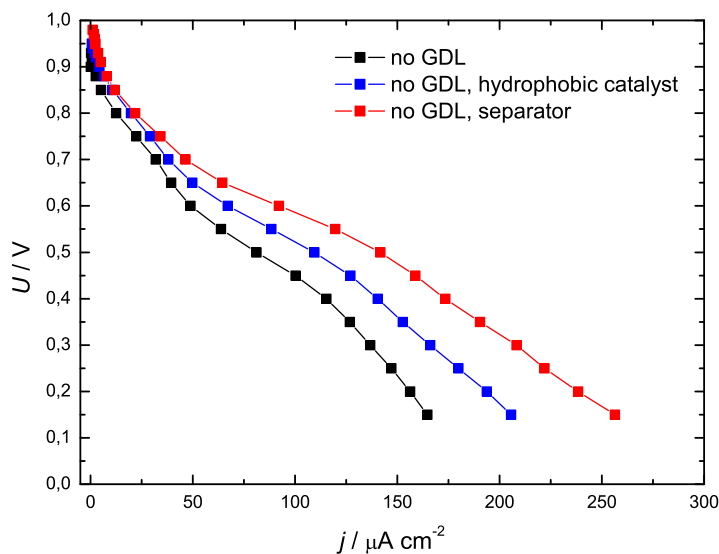


Figure 6-3: Polarization curves of the hybrid fuel cell, showing the influence of a separator and hydrophobization of the catalyst layer. Conditions: Anode: 5 mM glucose in 0.1 M phosphate buffer, 5 ml min⁻¹ flow rate, pH 7.2, 37 °C, N₂ atmosphere; Cathode: 500 ml min⁻¹ dry oxygen flow rate.

6.4 Influence of glucose concentration and oxygen

As shown in Section 6.2 the flow rate of the anodic solution has significant influence on the performance of the hybrid fuel cell. This effect has been ascribed to improved mass transport conditions at the anode. Another operational parameter, which directly influences the glucose oxidation kinetics at the anode, is the concentration of glucose in the bulk. Power curves of the hybrid enzymatic fuel cell with a separator and without a GDL in presence of different glucose concentrations are shown in Fig. 6-4. The maximum power density is shifted from ca. 55 $\mu\text{W cm}^{-2}$ at 5 mM glucose to ca. 90 $\mu\text{W cm}^{-2}$ at 40 mM glucose. The increase is not linear, which fits

well to the observations in single electrode experiments. The OCV values decrease by increasing the glucose concentration from ca. 0.99 V at 5 mM glucose to ca. 0.94 V at 40 mM glucose, which can be ascribed to glucose crossover to the cathode. Similar decrease of OCV by increasing fuel concentration was demonstrated by Chen et al. in the case of a DMFC [159].

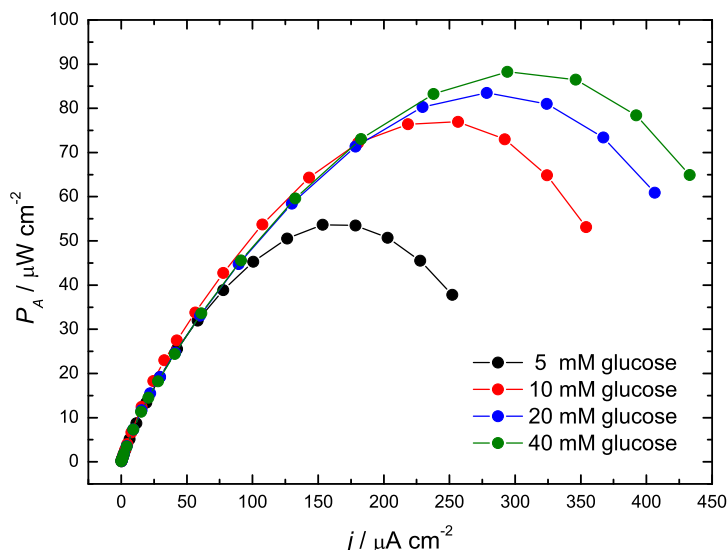


Figure 6-4: Power curves of the hybrid fuel cell with separator in presence of different glucose concentrations. Conditions: Anode: 0.1 M phosphate buffer, 5 ml min⁻¹ flow rate, pH 7.2, 37 °C, N₂ atmosphere; Cathode: 500 ml min⁻¹ dry oxygen flow rate.

As outlined in Section 5.4.3 the oxygen tolerance is a key issue in the case of enzymatic electrodes based on GOx. In order to monitor the effect of oxygen on the anode in a fuel cell configuration, the fuel cell has been fed with nitrogen- and oxygen-saturated glucose solutions. The respective polarization and power curves are shown in Fig. 6-5.

As can be seen from the graph the presence of oxygen in the fuel solution decreases the overall fuel cell performance in the whole investigated range so the shape of the polarization curve remains qualitatively the same. The OCV drops by 120 mV and the maximum power density decreases from ca. 120 μW cm⁻² to ca. 65 μW cm⁻² in presence of oxygen. This observation is in accordance with single electrode experiments, in which a similar rate of performance reduction has been observed.

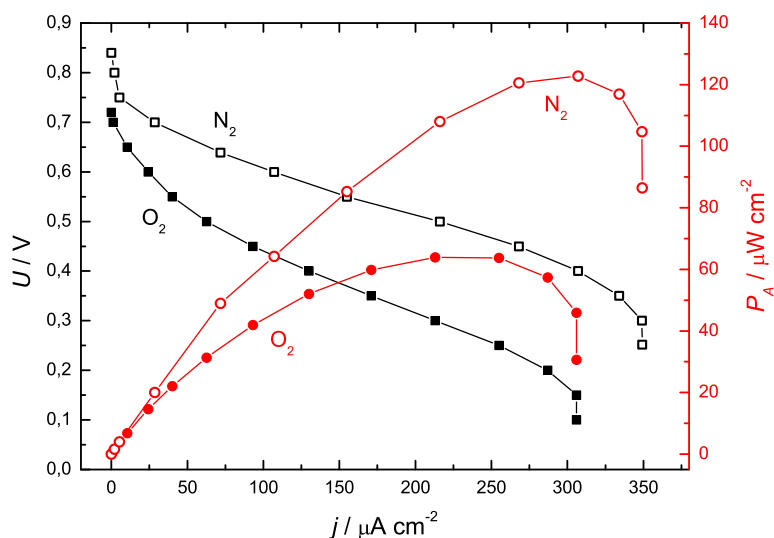


Figure 6-5: Polarization (black squares) and power curves (red circles) of the hybrid fuel cell in presence of nitrogen- (empty symbols) and oxygen-saturated (full symbols) glucose solution. Conditions: Anode: 5 mM glucose in 0.1 M phosphate buffer, 20 ml min⁻¹ flow rate, pH 7.2, 37 °C; Cathode: 500 ml min⁻¹ dry oxygen flow rate.

The decrease in current densities is associated with the reduced number of electrons, which instead of being transported through the mediator to the electrode surface are consumed by oxygen. The OCV drop on the other side could be the consequence of the generation of a mixed potential at the anode in presence of oxygen since TTF is known to exhibit oxygen reduction activity [167].

6.5 Stability of the hybrid fuel cell

The stability of the hybrid fuel cell has been investigated by constant polarization at 0.5 V at two different glucose flow rates. For comparison, the chronoamperometric response of the enzymatic anode, polarized at 0.05 V vs. SCE under forced convection conditions has been also shown. As can be seen in Fig. 6-6, the anode and the fuel cell at lower flow rate exhibit similar, rather stable behavior. Increase in flow rate results in higher currents due to enhanced glucose transport to the enzymatic electrode but with the expense of reduced stability.

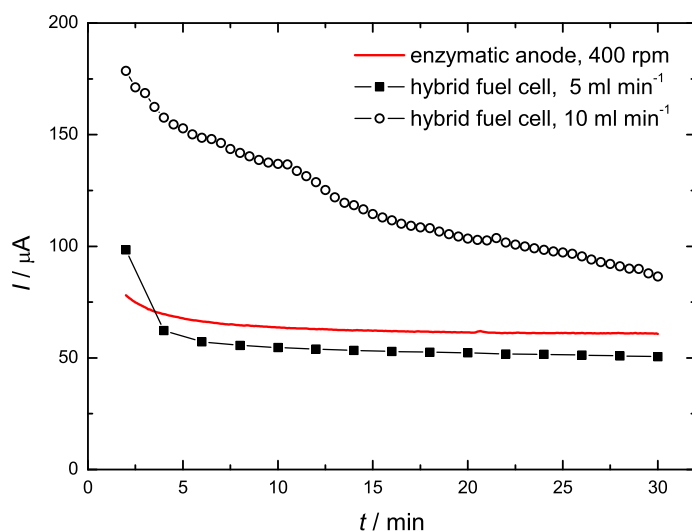


Figure 6-6: Chronoamperometry of the hybrid fuel cell and the enzymatic electrode at different hydrodynamic conditions for 30 min. Conditions: Anode: 5 mM glucose in 0.1 M phosphate buffer, pH 7.2, 37 °C, N₂ atmosphere; Cathode: 500 ml min⁻¹ dry oxygen flow rate.

When the time scale at the higher flow rate was extended to 24 h, the current decayed to 1 $\mu\text{A cm}^{-2}$ as shown in Fig. 6-7. Such a pronounced loss of activity during long-term operation can be due to several reasons, including anode and cathode deactivation or a combination of these as well as some problems with the design of the fuel cell. According to the literature, a similar type of enzymatic anode shows very stable behavior during several days of operation [79], which corresponds to the observations in the present work. This makes anode deactivation, although possible, not likely. On the other hand, similar rate of fuel cell deactivation was reported by Fischback et al. [46], who observed pronounced current decay under constant operation. They were able to regain most of the initial performance by replacement of the MEA, which lead them to the conclusion that the loss of performance was due to poisoning of the membrane by cations from the anodic buffer solution [46]. Similar type of experiment with replacement of MEA was performed in this study and the results were in accordance to the latter work. As can be seen in Fig. 6-7, the fuel cell restores activity almost to the initial level after exchange of the MEA, which is in accordance with the assumption that the enzymatic anode was not deactivated.

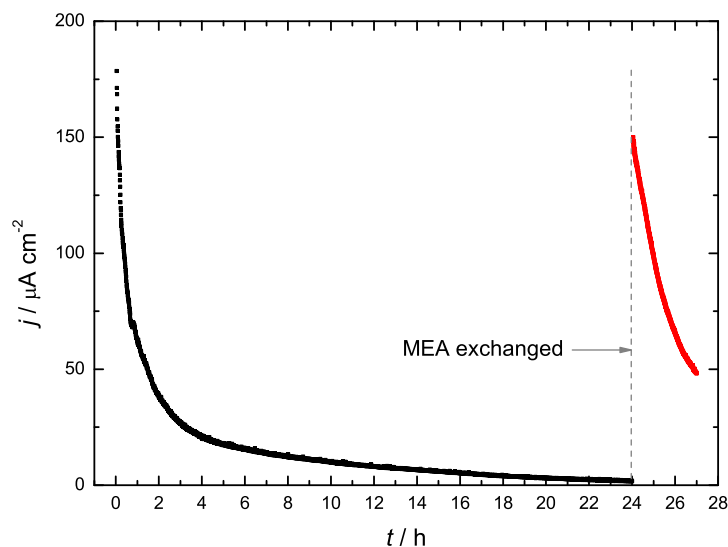


Figure 6-7: Chronoamperometry of the hybrid fuel cell for 24 h (exchange of the MEA denoted by a dashed line. Conditions: Anode: 0.1 M phosphate buffer, 10 ml min⁻¹ flow rate, pH 7.2, 37 °C, N₂ atmosphere; Cathode: 500 ml min⁻¹ dry oxygen flow rate.

As discussed above, Fischback et al. assigned the fuel cell deactivation to impeded proton conductivity through the membrane caused by the competitive affinity of sodium or potassium cations to the anionic sulfonic sites of Nafion [46]. This phenomenon is expected to occur in the present case as well but according to our opinion it cannot explain such a high degree of performance loss. Okada et al. have shown that the ionic conductivity of Nafion decreases from ca. 0.2 to approximately 0.05 S cm⁻¹, when all protons are exchanged with alkali metal cations [168]. This change is not so dramatic and the membrane resistance itself (mΩ range) is expected to increase only about four times, which will lead to a negligible voltage drop, having in mind the low current densities ($\mu\text{A cm}^{-2}$) maintained by the fuel cell.

On the other hand, the exchange of protons with metal cations in the Nafion membrane, in addition to increase of the resistance, will lead to a significant change of pH at the cathode side, which will slow down the cathode kinetics. As discussed in Section 6.2, the pH difference between both electrodes is considered to be accountable for the demonstrated high OCV values. It can be envisaged that during long-term operation the overpotential at the cathode side will increase with pH increase. The stability test shown in Fig. 6-7 has been performed as a chronoamperometric experiment at 0.5 V (voltage, which corresponds to nearly maximum power

in the initial polarization curve). However, with the gradual neutralization of the cathode interface, the OCV of the system decreases and the value of 0.5 V (maintained by the potentiostat) does not correspond to the initial conditions anymore but is rather close to the newly formed OCV and consequently generates very low current densities. In addition, the 24 h test has been performed at higher glucose flow rate, which, as shown in Fig. 6-6, may correspond to higher rate of Nafion neutralization and glucose crossover, respectively.

6.6 Conclusions

After the successful optimization of the electrode modification procedure for anode preparation, the anode has been coupled with Pt based cathode in a hybrid enzymatic fuel cell. The fuel cell device reaches high power density (up to $120 \mu\text{W cm}^{-2}$) at low glucose concentration (5 mM), depending on the anodic flow rate. The dependence of the fuel cell performance on the glucose flow rate and concentration indicates that the fuel cell is limited by the anode in the investigated time scale. The high OCV values demonstrated by the hybrid fuel cell have been tentatively assigned to the different pH at both electrodes. This phenomenon has been also accounted for the lower long-term stability of the fuel cell. However, the stability of the fuel cell at lower flow rates in the time scale, which corresponds to the typical duration of polarization curve recording, is satisfactory, consequently the hybrid device can be used as a platform for testing of enzymatic anodes under fuel cell conditions but at lower glucose flow rates and shorter time scales. Additional studies with a reference electrode can be used to determine more precisely the potentials of the anode and the cathode during fuel cell operation and to clarify the origin of the high OCV value and the loss of activity during long-term polarization.

6.7 Experimental details

6.7.1 Chemicals and materials

The chemicals that have been used for the enzymatic electrodes preparation have been already outlined in Section 5.7.1. Stainless steel discs with a diameter of 24 mm and 2 mm thickness were used as a mechanical and electrical support for the preparation of enzymatic electrodes. The

surface of the discs was masked by adhesive tape in such a way that a square opening with dimensions of 10×10 mm (1 cm^2 working area) was left exposed.

Nafion 117 was used for the preparation of the MEA. The cathode catalyst ink was based on Platinum Black (Alfa Aesar) and aqueous Nafion solution (Pt : Nafion = 9 : 1).

6.7.2 Preparation of the enzymatic anode

The procedure used for the preparation of the enzymatic electrode involves the utilization of an underlying polypyrrole layer and direct growth of the TTF-TCNQ crystals on the electrode surface. Detailed experimental description has been already provided in Section 5.7.2. All electrodes have been prepared with the following loadings, which have been chosen based on the tests for optimization shown in Sections 5.3.1 and 5.3.2: 2 mg cm^{-2} CTC, 0.6 mg cm^{-2} GOx and $40 \mu\text{l cm}^{-2}$ 2.5 % gelatin solution.

6.7.3 Preparation of MEA and fuel cell construction

The MEAs were prepared in-house by spray-painting of the catalyst ink on one of the sides of a Nafion membrane until a loading of approximately 5 mg cm^{-2} was achieved. The projected catalyst area had a square shape with dimensions 10×10 mm (1 cm^2 working area, corresponding to the anode working area). After that the MEAs were sintered at $135 \text{ }^\circ\text{C}$ for 30 min and left to cool down.

A three-dimensional drawing (exploded view) of the hybrid fuel cell device and its components is shown in Fig. 6-8. The cell body was transparent and made out of Makrolon (Bayer). The stainless steel disc covered with anodic catalyst was fixed to the cell body by the anode current collector and sealed by an O-ring. The MEA was placed on the opposite side of the cell body with the bare side of the membrane facing the anodic compartment. A graphite plate with a flow-field was used for gas distribution and a gold-coated copper plate served as a cathode current collector. The cathode components were clamped together and sealed by a PTFE gasket and an end plate, which ensured leak tightness and good electrical contact in the whole assembly. In some cases cellophane P00 (Innovia Films) has been used as a separator between the MEA and the anodic compartment (not shown in Fig. 6-8).

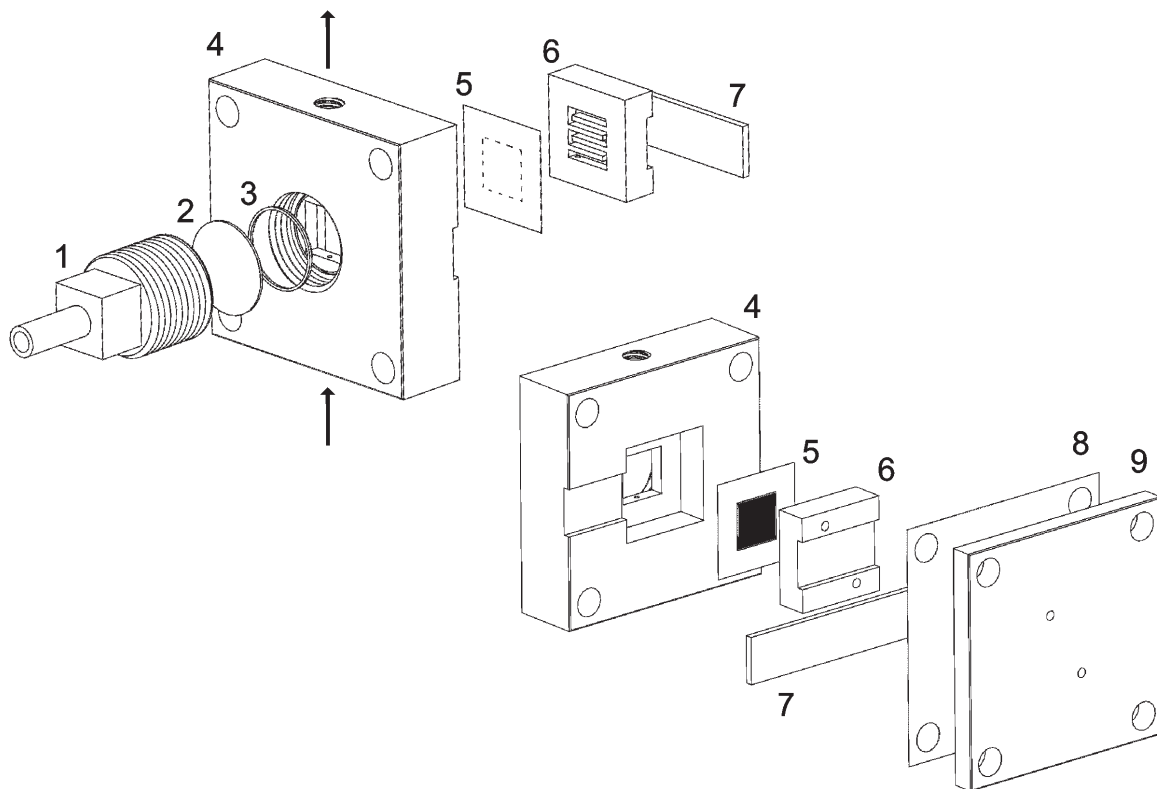


Figure 6-8: An exploded drawing of the fuel cell device with components denoted as follows: 1 - anode current collector, 2 - stainless steel disc with enzymatic catalyst (enzymatic electrode), 3 - O-ring, 4 - cell body, 5 - MEA, 6 - graphite flow-field, 7 - cathode current collector, 8 - PTFE gasket, 9 - end plate.

The fuel cell was mounted vertically in a holder in such a way that the fuel solution was flowing upwards through the cell (see arrows indicating flow direction), whereby the perfusion flow was sustained by a peristaltic pump. The cell was connected to a fuel reservoir, equipped with a temperature control and gas supplies to allow for operation with nitrogen- or oxygen-saturated media. The fuel solution was 0.1 M phosphate buffer with different glucose concentrations. The cathode was fed with dry oxygen at a flow rate of ca. 500 ml min⁻¹.

6.7.4 Electrochemical experiments

Fuel cell experiments were performed by a computer controlled potentiostat PGSTAT302 (Eco Chemie/Autolab). The two-electrode set up has been achieved by connecting the reference and

counter electrodes together. After mounting of the fuel cell in the testing facility the cell was left to equilibrate with constant flow of reactants until a stable OCV value was obtained. This usually took 30 min. Data for polarization curves have been extracted from transient measurements after 2 min at constant voltage. This time was sufficient to obtain a sufficiently stable current signal.

7. Initial studies with an enzymatic cathode

7.1 Concept of the cathode modification procedure

The successful elaboration of the anode modification procedure, involving dispersion of enzyme, mediator and Vulcan nanoparticles in a gelatin matrix has motivated our efforts to adopt such an approach for the development of an enzymatic cathode. As already outlined in Section 2.2.3 laccase and BOD are the typical biocatalysts used for design of oxygen-reducing biocathodes but BOD has an optimum pH at more positive values and is therefore more appropriate for a membraneless configuration, operating around pH 7. BOD is known to exhibit DET in the presence of high surface area carbon nanomaterials such as CNTs [15, 54], Ketjen Black [169] or Vulcan [130]. In addition to DET electrodes, BOD electrodes with a mediator have been also demonstrated in the literature [25, 32, 170] and the utilization of MET approach resulted in higher currents. Our initial studies on the preparation of an enzymatic cathode based on BOD and its combination with a bioanode in an enzymatic fuel cell, which will be shown in the following sections.

7.2 DET and MET performance of the biocathode

The cathode modification procedure that has been employed is identical to the procedure used for preparation of glucose-oxidizing anode. Enzyme and Vulcan particles have been dispersed in gelatin solution and an aliquot of the resulting catalyst ink has been applied on the electrode surface, left to dry and cross-linked with glutaraldehyde. In these first tests the starting values of the ink components have been directly adopted from the optimum anode results, namely 20 mg of Vulcan XC 72R and 2 mg of BOD in 1 ml of 2 % gelatin solution. However, instead of stainless steel electrodes, carbon Toray paper has been used as a mechanical and electrically-conducting support. The use of Toray paper has been motivated by the desire to employ the biocathode directly in the existing fuel cell test set up, which will allow operation with gas-phase oxygen in a three-phase interface.

The voltammograms of the enzymatic cathode in absence and presence of oxygen are shown in Fig. 7-1. As can be seen from that graph the voltammogram in presence of the substrate is

negatively shifted, which indicates activity for oxygen reduction but the associated currents are comparatively low. For comparison, Habrioux et al. have demonstrated around $250 \mu\text{A cm}^{-2}$ at 0.2 V vs. SCE under similar experimental (including hydrodynamic) conditions, using BOD and Vulcan dispersed in a Nafion matrix [130]. The activity in the present case, which has been evaluated after subtraction of the base voltammogram, corresponds to about $80 \mu\text{A cm}^{-2}$. The relatively low performance can be attributed to several reasons, including distribution of oxygen within the electrode architecture, inefficient electrical communication between BOD and Vulcan or inactivation of the enzyme during the electrode modification procedure (e.g. during the drying or cross-linking steps). The possibility of BOD agglomeration as in the case of GOx should be also taken into account.

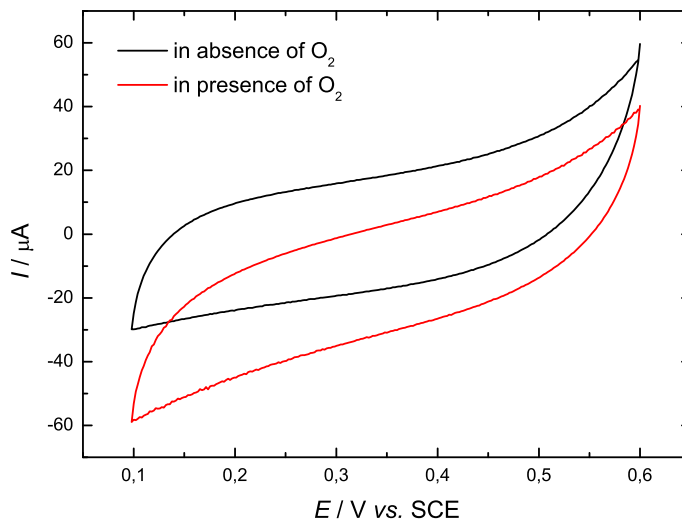


Figure 7-1: Cyclic voltammograms of the enzymatic cathode based on DET, showing oxygen reduction activity. Conditions: 0.1 M phosphate buffer, $\text{pH } 7.2$, $37 \text{ }^\circ\text{C}$, 400 rpm , scan rate 5 mV s^{-1} .

In order to determine whether the enzyme is present at the electrode surface in its active form, ABTS has been added as a diffusional mediator in the experimental solution. The respective voltammograms in absence and presence of oxygen are shown in Fig. 7-2. The voltammetric features of ABTS can be observed at more positive potentials in absence of substrate but the exact position of the redox peak cannot be determined. As can be seen from the graph the biocathode exhibits high activity for oxygen reduction and clearly defined limiting currents. The current density at 0.2 V vs. SCE after correction of the capacitive currents is about $950 \mu\text{A cm}^{-2}$

at 400 rpm. These results indicate that the enzyme activity is preserved during the modification procedure and the reason of the reduced activity in the DET configuration is the inefficient electron transport between the enzyme and the conductive carbon nanoparticles. This implies that the electrode architecture can be optimized by variation of structural parameters in a similar manner as in the case of the bioanode in order to achieve better performance in the DET and MET configurations.

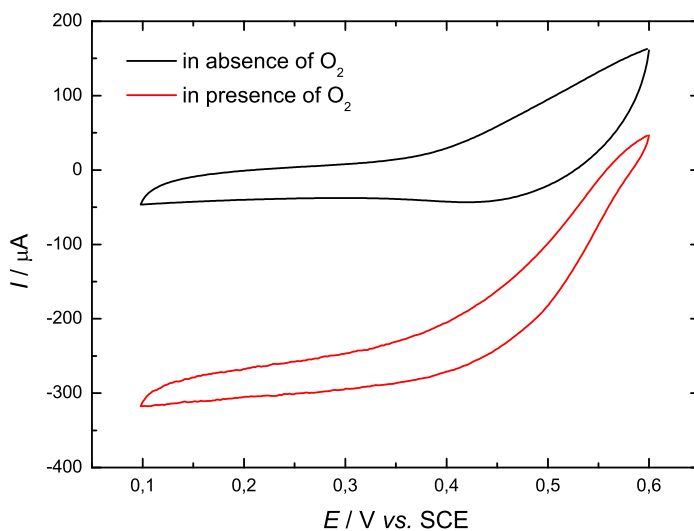


Figure 7-2: Cyclic voltammograms of the enzymatic cathode based on DET, showing oxygen reduction activity in the presence of dissolved ABTS. Conditions: 0.1 M phosphate buffer, pH 7.2, 37 °C, 400 rpm, scan rate 5 mV s⁻¹.

7.3 Enzymatic fuel cell

In the next step the enzymatic cathode has been combined with the enzymatic anode described in Section 5.4 in an enzymatic fuel cell, entirely based on biological catalysts. As already outlined, the existing hybrid fuel cell set up has been used as a technical platform for the fuel cell measurements but in the present case no membrane has been employed. Both DET and MET cathode configurations have been investigated. In the case of MET fuel cell cathodes, ABTS has been co-immobilized with BOD and Vulcan in the gelatin matrix. It should be noted that during the fuel cell operation change of color of the anodic solution due to leaching of ABTS was not observed but it cannot be completely excluded without additional detailed investigations.

Despite of the absence of a membrane, the current design does not represent the classical membraneless configuration, which is expected to find application as an implantable power source. In the case of subcutaneous implantation glucose and oxygen will be dissolved in the interstitial fluid and in this way both fuel and oxidant will be delivered simultaneously to the electrodes in a single feed. However, oxygen has a low solubility and low diffusion coefficient in aqueous solutions, which can limit the performance of the cathode [52]. In addition, the presence of oxygen will deteriorate the performance of the anode as shown in Section 5.4.3. The utilization of the fuel cell set up, which has been used in the case of a hybrid fuel cell configuration allows for a membraneless operation by simultaneous separation of the anodic and cathodic feeds. Such strategy, involving separated feeds of reactants, has been successfully demonstrated in the case of a concentric biofuel cell [171] and an open-air type biofuel cell [52]. In the context of this discussion, it should be mentioned that the concept of semi-implantable applications has been also proposed in the literature [172].

The enzymatic cathode operates in a complex three-phase interface, formed by the current collecting solid phase, a liquid phase for proton transport and proper enzyme hydration and a gas phase for efficient oxygen transport. Common approach in the development of gas-diffusion enzymatic cathodes is the stacking of two layers with different properties [172, 173]. One of the layers has hydrophilic properties and contains the enzyme and the other layer is hydrophobic and ensures effective oxygen diffusion. A similar strategy, involving the combination of untreated Toray paper modified with catalyst ink and Toray paper treated with PTFE, has been used in the present case. A schematic presentation of the respective fuel cell configuration can be found in the experimental section.

The use of a second, hydrophobized GDL has been additionally motivated by the absence of a membrane to limit the flux of liquid to the cathode in the present configuration. In case when no hydrophobic layer was used, water penetrated freely through the Toray support and flooded completely the flow-field channels, which caused blocking of the oxygen supply. On the other side, the positive results in the case of the hybrid fuel cell shown in section 6.3.2 motivated the investigation of architecture with a cellophane separator between the anodic solution and the cathode. However, this approach resulted in negligible performance of the enzymatic fuel cell, which was ascribed to insufficient hydration of the catalyst layer and the enzyme, respectively.

Polarization and power curves of the enzymatic fuel cell employing DET and MET-based cathode in presence of 5 mM glucose are shown in Fig. 7-3. The utilization of MET-based cathode results in an improved fuel cell performance. The addition of ABTS in the cathodic catalyst ink increases the OCV from 0.54 V to 0.64 V and the current density at 0.15 V from nearly 40 $\mu\text{A cm}^{-2}$ to more than 120 $\mu\text{A cm}^{-2}$. The maximum power density increases from 6 $\mu\text{W cm}^{-2}$ to 24 $\mu\text{W cm}^{-2}$, respectively. These results are in good agreement with the behavior of the biocathodes in single electrode experiments. Regarding the different OCV values in both cases, in general it can be anticipated that the introduction of mediator will introduce additional thermodynamic overpotential and will reduce the OCV of the fuel cell. However, the cathode behavior is influenced to a great extent by the respective kinetics, which can explain the better performance of MET-based cathode in terms of potential and voltage. This phenomenon has been demonstrated also in the case of BOD and Vulcan dispersed in a Nafion matrix, where the addition of ABTS resulted in improved kinetics and more positive onset potential for the oxygen reduction [130].

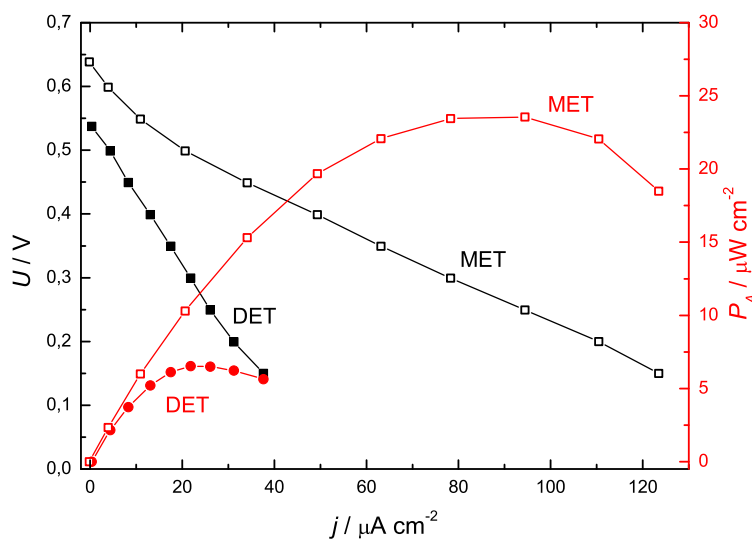


Figure 7-3: Polarization (black squares) and power curves (red circles) of the enzymatic fuel cell with cathode based on MET (empty symbols) and DET (full symbols). Conditions: Anode: 5 mM glucose in 0.1 M phosphate buffer, 5 ml min^{-1} flow rate, pH 7.2, 37 °C, N_2 atmosphere; Cathode: 500 ml min^{-1} dry oxygen flow rate.

The overall performance of the enzymatic fuel cell is significantly lower than the performance of the hybrid fuel cell. At identical glucose concentration and flow rate the hybrid fuel cell generates nearly 200 mV higher OCV and four times higher maximum power density, compared

to the enzymatic fuel cell employing MET-based cathode. Unlike the hybrid fuel cell, in which the hydrodynamic conditions at the anode have pronounced influence on the fuel cell performance, variation of the glucose concentration and flow rate in the case of the enzymatic fuel cell has little influence on the overall output. This indicates that the enzymatic fuel cell is limited by the cathode despite of the efforts to enhance the supply of oxygen through gas-phase operation. Consequently, the lower output of the entirely enzymatic fuel cell can be attributed to the lower cathode performance. However, this is not an intrinsic feature of the catalyst but rather an effect due to the different operating conditions caused by the specific fuel cell design in both cases. The improved behavior of the Pt cathode can be observed only in the present hybrid fuel cell architecture since the cathode is directly adopted from conventional fuel cells and allows for operation at highly acidic conditions at the Nafion interface. As already discussed in Section 6.2, if the Pt catalyst operates under similar (neutral) conditions as the biocathode it exhibits lower activity in terms of overpotential. This observation is also in accordance with the performance of Os-mediated BOD [25].

The initial tests with the enzymatic cathode, which employs BOD as an oxygen-reducing catalyst, indicate that the cathode can be successfully combined with an anode based on GOx and TTF-TCNQ in a fuel cell device. However, the lower output demonstrated by the cell implies that further optimization of the cathode modification procedure, as well as on the overall fuel cell architecture, is needed. The cathode design has to be optimized in respect to implantable and semi-implantable applications and employed in the respective fuel cell configurations.

7.4 Experimental details

7.4.1 *Preparation of the enzymatic anodes*

The chemicals that have been used for the enzymatic electrodes preparation have been already outlined in Section 5.7.1. Stainless steel discs with a diameter of 24 mm and 2 mm thickness were used as a mechanical and electrical support for the preparation of enzymatic anodes. A square profile with dimensions of 10 × 10 mm (1 cm² working area) was cut on the surface of the discs. The procedure used for the preparation of the enzymatic electrode involves the dispersion of GOx, TTF-TCNQ and Vulcan XC 72R in a gelatin matrix. Detailed experimental

description has been already provided in Section 5.7.3. 150 μl of the anodic catalyst ink was applied on the stainless steel electrode. All electrodes have been prepared with a catalyst ink with the following composition, which has been chosen based on the tests for optimization shown in Sections 5.4.1 and 5.4.2: 10 mg ml^{-1} CTC, 2 mg ml^{-1} GOx and 20 mg ml^{-1} Vulcan in 2 % gelatin solution.

7.4.2 Preparation of the enzymatic cathodes

The procedure used in the case of the enzymatic anodes was adopted for the preparation of enzymatic cathodes. Toray paper was used as a mechanical and electrical support. The surface of the Toray paper was masked in such a way that a square opening with dimensions of 10×10 mm (1 cm^2 working area, corresponding to the anode surface area) was left exposed. The catalyst ink had the following composition: 20 mg ml^{-1} Vulcan and 2 mg ml^{-1} BOD dispersed in 2 % gelatin solution. In case of MET fuel cell tests the catalyst ink contained additionally 10 mg ml^{-1} ABTS. The Toray paper was polished shortly with emery paper and 150 μl of the anodic catalyst ink was applied on the exposed surface and left to dry. After that the electrode was cross-linked by dipping for 60 s in 5 % glutaraldehyde solution, washed and left to dry again. In case of single electrode measurements, discs with a diameter of 6 mm were cut from the 10×10 mm square profiles and mounted in the sample holder.

7.4.3 Enzymatic fuel cell construction

The experimental set-up for the hybrid fuel cell, described in Section 6.7.3 (Fig. 6-8) was used for testing of the enzymatic fuel cell. However, in the present case no membrane was employed. The anode was mounted in a similar way as in the hybrid fuel cell. The Toray paper, modified with cathodic catalyst was placed on the opposite side of the cell body with the covered side facing the anodic compartment. Another piece of Toray paper, hydrophobized with 50 % PTFE was placed over the supporting Toray paper. Schematic presentation of the enzymatic fuel cell set-up is shown in Fig. 7-4.

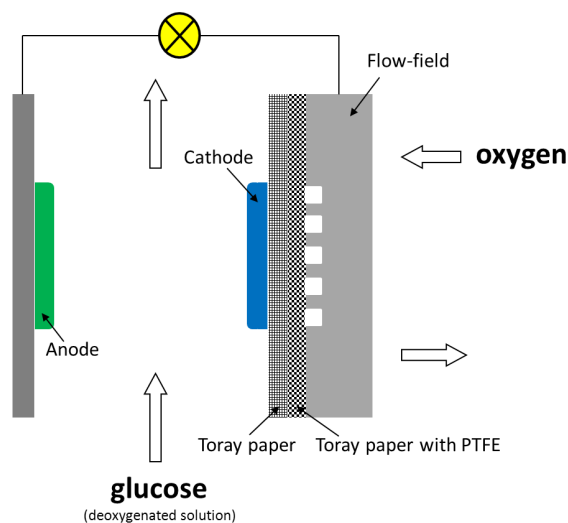


Figure 7-4: Schematic presentation of the enzymatic fuel cell set-up.

Finally, the cathode compartment was sealed by the graphite flow-field, the cathode current collector and the PTFE gasket as in the case of the hybrid fuel cell. The enzymatic fuel cell was mounted vertically in the existing testing set-up and was fed with deoxygenated 0.1 M phosphate buffer containing 5 mM glucose at the anode and dry oxygen at the cathode. The anodic flow rate was 5 ml min^{-1} and the cathodic flow rate was ca. 500 ml min^{-1} .

7.4.4 Electrochemical experiments

Electrochemical experiments have been performed by a computer controlled potentiostat PGSTAT302 (Eco Chemie/Autolab). In case of MET single electrode measurements the electrolyte contained 1 mg ml^{-1} ABTS. After mounting of the enzymatic fuel cell in the testing facility the cell was left to equilibrate with constant flow of reactants until a stable OCV value was obtained, which usually took about 30 min. Data for polarization curves have been extracted from transient measurements after 2 min at constant voltage.

8. Concluding remarks

The development of enzymatic fuel cells is associated with various problems such as enzyme immobilization, communication between the enzyme and the electrode surface, design of optimal enzymatic electrode architecture, coupling of the electrodes in a fuel cell and design of the overall system. The first two points have been extensively studied in the past, mainly regarding the application in amperometric biosensors, which resulted in numerous preparation methods for enzymatic electrodes. However, little emphasis has been put on the optimization of electrode modification procedures with respect to energy production and the construction of the respective fuel cell devices. More attention has been focused on the bioelectrochemistry of the electrodes and often the studies have been performed in an inappropriate manner, in respect to the fuel cell investigation.

In this work the development of a glucose-oxygen enzymatic biofuel cell has been presented from the point of view of chemical engineering and practical applications with focus on the anode process. The main attention has been put on the performance of the respective electrodes and the resulting fuel cell output. From the numerous approaches for construction of enzymatic anodes for glucose oxidation, two procedures have been identified as potential candidates for fuel cell studies. The first procedure employs the chemical modification of gold electrode with mediator and a modified co-factor and the subsequent reconstitution of the apo-enzyme over the resulting assembly. The procedure has been successfully reproduced and the respective electrodes exhibited reasonable activity. However, the present results indicated that major part of the activity does not have biological but inorganic origin due to the pronounced electrocatalytic activity of gold. This compromises to some extent the results published in the literature and emphasizes the importance of the underlying substrate used in the preparation of enzymatic electrodes.

The second procedure employs the electrical contacting of glucose oxidase to electrodes through a charge-transfer complex based on TTF-TCNQ. In this case the enzyme has been simply adsorbed on the surface of the TTF-TCNQ crystals and the whole electrode assembly has been protected by a gelatin layer. In the first steps of the study the modification procedure has been adopted from the literature and reproduced successfully. However, some new insights on

the structure of the electrode and the influence of the structural parameters have been brought and the importance of the optimization of the electrode architecture has been identified. Another important aspect that has been studied is the electron transfer mechanism in the bioelectrochemical system, which has been a subject of controversy for long time. The results in the present study indicate that the electron transfer pathway involves a mediator, which is generated *in situ* from the surface of the charge-transfer complex and that several mediators can be involved. This mechanism summarizes several hypotheses, which have been proposed so far and is supported by further experimental evidences.

In addition to these findings, a new immobilization procedure based on different architecture and high surface area carbon materials with enhanced performance has been elaborated. The influence of structural parameters has been also investigated and the procedure has been optimized.

The high performance of the enzymatic anodes employing glucose oxidase and charge-transfer complex has motivated the construction of a fuel cell device with a Pt cathode. The architecture of the resulting hybrid fuel cell has been adopted from the conventional fuel cell design. The device exhibits high OCV and high current densities at low glucose concentrations but insufficient long-term stability. The high OCV and the limited stability have been ascribed to effects associated with the pH difference at the electrodes. The hybrid fuel cell device can be used as a platform for the investigation of enzymatic anodes but only under certain conditions, namely low anodic flow rates and polarization experiments at a shorter time scale.

The successful elaboration of the anode modification procedure and the hybrid fuel cell test set-up have motivated the adoption of the immobilization approach for the cathode and the construction of a biofuel cell entirely based on enzymatic catalysts. The initial tests indicated that both DET and MET pathways are possible but higher performance can be achieved with the help of a mediator. The first results imply that the architecture of the cathode and the fuel cell have to be optimized in a similar way to the anode and the hybrid fuel cell. Also, the architecture of the existing fuel cell test set-up may be improved and additional components such as a reference electrode can be introduced.

Literature

1. Grove, W.R., *On voltaic series and the combination of gases by platinum*, Philosophical Magazine and Journal of Science, 1839. **14**: p. 127-130.
2. Bard, A.J., Stratmann, M., Wilson, G.S., ed., *Encyclopedia of Electrochemistry Volume 9: Bioelectrochemistry*, 2002. Wiley VCH: Weinheim.
3. Bartlett, P.N., ed. *Bioelectrochemistry, Fundamentals, Experimental Techniques and Applications*, 2008. Wiley: Chichester.
4. Yahiro, A.T., Lee, S.M., and Kimble, D.O., *Bioelectrochemistry I. Enzyme utilizing bio-fuel cell studies*. Biochimica et Biophysica Acta, 1964. **88**(2): p. 375-383.
5. Davis, J.B. and Yarbrough, H.F., *Preliminary experiments on a microbial fuel cell*, Science, 1962. **137**(3530): p. 615-616.
6. Barton, S.C., Gallaway, J., Atanassov, P., *Enzymatic biofuel cells for Implantable and microscale devices*, Chemical Reviews, 2004. **104**(10): p. 4867-4886.
7. Ramanavicius, A., Ramanaviciene, A., *Hemoproteins in Design of Biofuel Cells*, Fuel Cells, 2009. **9**(1): p. 25-36.
8. Habermuller, L., Mosbach, M., Schuhmann, W., *Electron-transfer mechanisms in amperometric biosensors*, Fresenius Journal of Analytical Chemistry, 2000. **366**(6-7): p. 560-568.
9. Cooney, M.J., Svoboda, V. Lau, C. Martin, G., Minteer, S.D., *Enzyme catalysed biofuel cells*, Energy & Environmental Science, 2008. **1**(3): p. 320-337.
10. Ivanov, I., Vidakovic-Koch, T., Sundmacher, K., *Recent advances in enzymatic fuel cells: Experiments and modeling*, Energies, 2010. **3**(4): p. 803-846.
11. Ramirez, P., Mano, N., Andreu, R., Ruzgas, T., Heller, A., Gorton, L., Shleev, S., *Direct electron transfer from graphite and functionalized gold electrodes to T1 and T2/T3 copper centers of bilirubin oxidase*, Biochimica et Biophysica Acta-Bioenergetics, 2008. **1777**(10): p. 1364-1369.
12. Shleev, S., Jarosz-Wilkolazka, A., Khalunina, A., Morozova, O., Yaropolov, A., Ruzgas, T., Gorton, L., *Direct electron transfer reactions of laccases from different origins on carbon electrodes*, Bioelectrochemistry, 2005. **67**(1): p. 115-124.
13. Zhao, H.Y., Zhou, H.M., Zhang, J.X., Zheng, W., Zheng, Y.F., *Carbon nanotube-hydroxyapatite nanocomposite: A novel platform for glucose/O-2 biofuel cell*, Biosensors & Bioelectronics, 2009. **25**(2): p. 463-468.
14. Wang, S.C., Yang, F., Silva, M., Zarow, A., Wang, Y. B., Iqbal, Z., *Membrane-less and mediator-free enzymatic biofuel cell using carbon nanotube/porous silicon electrodes*, Electrochemistry Communications, 2009. **11**(1): p. 34-37.
15. Wu, X., Zhao, F., Varcoe, J.R., Thumser, A.E., Avignone-Rossa, C., Slade, R.C.T., *A one-compartment fructose/air biological fuel cell based on direct electron transfer*, Biosensors & Bioelectronics, 2009. **25**(2): p. 326-331.
16. Tan, Y.M., Deng, W.F., Ge, B., Xie, Q.J., Huang, J.H., Yao, S.Z., *Biofuel cell and phenolic biosensor based on acid-resistant laccase-glutaraldehyde functionalized chitosan-multiwalled carbon nanotubes nanocomposite film*, Biosensors & Bioelectronics, 2009. **24**(7): p. 2225-2231.
17. Kuwahara, T., Oshima, K., Shimomura, M., Miyauchi, S., *Properties of the enzyme electrode fabricated with a film of polythiophene derivative and its application to a glucose fuel cell*, Journal of Applied Polymer Science, 2007. **104**(5): p. 2947-2953.

18. Liu, Y., Wang, M.K., Zhao, F., Liu, B.F., Dong, S.J., *A low-cost biofuel cell with pH-dependent power output based on porous carbon as matrix*, Chemistry - a European Journal, 2005. **11**(17): p. 4970-4974.
19. Heller, A., *Electron-conducting redox hydrogels: design, characteristics and synthesis*, Current Opinion in Chemical Biology, 2006. **10**(6): p. 664-672.
20. Mano, N., Mao, F., Heller, A., *On the parameters affecting the characteristics of the "wired" glucose oxidase anode*, Journal of Electroanalytical Chemistry, 2005. **574**(2): p. 347-357.
21. Soukharev, V., Mano, N., Heller, A., *A four-electron O₂-electroreduction biocatalyst superior to platinum and a biofuel cell operating at 0.88 V*, Journal of the American Chemical Society, 2004. **126**(27): p. 8368-8369.
22. Mao, F., Mano, N., Heller, A., *Long tethers binding redox centers to polymer backbones enhance electron transport in enzyme "wiring" hydrogels*, Journal of the American Chemical Society, 2003. **125**(16): p. 4951-4957.
23. Mano, N., Mao, F., Shin, W., Chen, T., Heller, A., *A miniature biofuel cell operating at 0.78 V*, Chemical Communications, 2003(4): p. 518-519.
24. Mano, N., Mao, F., Heller, A., *Characteristics of a miniature compartment-less glucose-O₂ biofuel cell and its operation in a living plant*, Journal of the American Chemical Society, 2003. **125**(21): p. 6588-6594.
25. Mano, N., Fernandez, J.L., Kim, Y., Shin, W., Bard, A.J., Heller, A., *Oxygen is electroreduced to water on a "wired" enzyme electrode at a lesser overpotential than on platinum*, Journal of the American Chemical Society, 2003. **125**(50): p. 15290-15291.
26. Kim, H.H., Mano, N., Zhang, X.C., Heller, A., *A miniature membrane-less biofuel cell operating under physiological conditions at 0.5 V*, Journal of the Electrochemical Society, 2003. **150**(2): p. A209-A213.
27. Barriere, F., Kavanagh, P., Leech, D., *A laccase-glucose oxidase biofuel cell prototype operating in a physiological buffer*, Electrochimica Acta, 2006. **51**(24): p. 5187-5192.
28. Barriere, F., Ferry, Y., Rochefort, D., Leech, D., *Targetting redox polymers as mediators for laccase oxygen reduction in a membrane-less biofuel cell*, Electrochemistry Communications, 2004. **6**(3): p. 237-241.
29. Zafar, M.N., Tasca, F., Gorton, L., Patridge, E. V., Ferry, J.G., Noll, G., *Tryptophan repressor-binding proteins from Escherichia coli and Archaeoglobus fulgidus as new catalysts for 1,4-dihydronicotinamide adenine dinucleotide-dependent amperometric biosensors and biofuel Cells*, Analytical Chemistry, 2009. **81**(10): p. 4082-4088.
30. Tasca, F., Gorton, L., Harreither, W., Haltrich, D., Ludwig, R., Noll, G., *Highly efficient and versatile anodes for biofuel cells based on cellobiose dehydrogenase from Myriococcum thermophilum*, Journal of Physical Chemistry C, 2008. **112**(35): p. 13668-13673.
31. Sakai, M., Vonderheit, A., Wei, X., Kuttel, C., Stemmer, A., *A novel biofuel cell harvesting energy from activated human macrophages*, Biosensors & Bioelectronics, 2009. **25**(1): p. 68-75.
32. Habrioux, A., Servat, K., Tingry, S., Kokoh, K.B., *Enhancement of the performances of a single concentric glucose/O₂ biofuel cell by combination of bilirubin oxidase/Nafion cathode and Au-Pt anode*, Electrochemistry Communications, 2009. **11**(1): p. 111-113.

33. Zheng, W., Zho, H.M., Zheng, Y.F., Wang, N., *A comparative study on electrochemistry of laccase at two kinds of carbon nanotubes and its application for biofuel cell*, Chemical Physics Letters, 2008. **457**(4-6): p. 381-385.
34. Smolander, M., Boer, H., Valkiainen, M., Roozeman, R., Bergelin, M., Eriksson, J.E., Zhang, X.C., Koivula, A., Viikari, L., *Development of a printable laccase-based biocathode for fuel cell applications*, Enzyme and Microbial Technology, 2008. **43**(2): p. 93-102.
35. Habrioux, A., Sibert, E., Servat, K., Vogel, W., Kokoh, K.B., Alonso-Vante, N., *Activity of platinum-gold alloys for glucose electrooxidation in biofuel cells*, Journal of Physical Chemistry B, 2007. **111**(34): p. 10329-10333.
36. Colmati, F., Yoshioka, S.A., Silva, V.L.V.B., Varela, H., Gonzalez, E.R., *Enzymatic based biocathode in a polymer electrolyte membrane fuel cell*, International Journal of Electrochemical Science, 2007. **2**(2): p. 195-202.
37. Hudak, N.S., Barton, S.C., *Mediated biocatalytic cathode for direct methanol membrane-electrode assemblies*, Journal of the Electrochemical Society, 2005. **152**(5): p. A876-A881.
38. Palmore, G.T.R., Kim, H.H., *Electro-enzymatic reduction of dioxygen to water in the cathode compartment of a biofuel cell*, Journal of Electroanalytical Chemistry, 1999. **464**(1): p. 110-117.
39. Muguruma, H., *Biofuel cell based on a complex between glucose oxidase and a plasma-polymerized film containing a redox site*, IEICE Transactions on Electronics, 2008. **E91C**(11): p. 1811-1815.
40. Togo, M., Takamura, A., Asai, T., Kaji, H., Nishizawa, M., *An enzyme-based microfluidic biofuel cell using vitamin K-3-mediated glucose oxidation*, Electrochimica Acta, 2007. **52**(14): p. 4669-4674.
41. Okuda, J., Yamazaki, T., Fukasawa, M., Kakehi, N., Sode, K., *The application of engineered glucose dehydrogenase to a direct electron-transfer-type continuous glucose monitoring system and a compartmentless biofuel cell*, Analytical Letters, 2007. **40**(3): p. 431-440.
42. Arechederra, R.L., Treu, B.L., Minter, S.D., *Development of glycerol/O-2 biofuel cell*, Journal of Power Sources, 2007. **173**(1): p. 156-161.
43. Zhang, X.C., Ranta, A., Halme, A., *Direct methanol biocatalytic fuel cell - Considerations of restraints on electron transfer*, Biosensors & Bioelectronics, 2006. **21**(11): p. 2052-2057.
44. Tamaki, T., Yamaguchi, T., *High-surface-area three-dimensional biofuel cell electrode using redox-polymer-grafted carbon*, Industrial & Engineering Chemistry Research, 2006. **45**(9): p. 3050-3058.
45. Kakehi, N., Yamazaki, T., Tsugawa, W., Sode, K., *A novel wireless glucose sensor employing direct electron transfer principle based enzyme fuel cell*, Biosensors & Bioelectronics, 2007. **22**(9-10): p. 2250-2255.
46. Fischback, M.B., Youn, J.K., Zhao, X.Y., Wang, P., Park, H.G., Chang, H.N., Kim, J., Ha, S., *Miniature biofuel cells with improved stability under continuous operation*, Electroanalysis, 2006. **18**(19-20): p. 2016-2022.
47. Sato, F., Togo, M., Islam, M. K., Matsue, T., Kosuge, J., Fukasaku, N., Kurosawa, S., Nishizawa, M., *Enzyme-based glucose fuel cell using Vitamin K-3-immobilized polymer as an electron mediator*, Electrochemistry Communications, 2005. **7**(7): p. 643-647.

48. Akers, N.L., Moore, C.M., Minteer, S.D., *Development of alcohol/O₂ biofuel cells using salt-extracted tetrabutylammonium bromide/Nafion membranes to immobilize dehydrogenase enzymes*, *Electrochimica Acta*, 2005. **50**(12): p. 2521-2525.
49. Palmore, G.T.R., Bertschy, H., Bergens, S.H., Whitesides, G.M., *A methanol/dioxygen biofuel cell that uses NAD(+)-dependent dehydrogenases as catalysts: application of an electro-enzymatic method to regenerate nicotinamide adenine dinucleotide at low overpotentials*, *Journal of Electroanalytical Chemistry*, 1998. **443**(1): p. 155-161.
50. Choi, Y.K., Wang, G., Nayfeh, M.H., Yau, S.T., *A hybrid biofuel cell based on electrooxidation of glucose using ultra-small silicon nanoparticles*, *Biosensors & Bioelectronics*, 2009. **24**(10): p. 3103-3107.
51. Wilson, R., Turner, A.P.F., *Glucose oxidase - an ideal enzyme*, *Biosensors & Bioelectronics*, 1992. **7**(3): p. 165-185.
52. Sakai, H., Nakagawa, T., Tokita, Y., Hatazawa, T., Ikeda, T., Tsujimura, S., Kano, K., *A high-power glucose/oxygen biofuel cell operating under quiescent conditions*, *Energy & Environmental Science*, 2009. **2**(1): p. 133-138.
53. Li, X., Zhang, L., Su, L., Ohsaka, T., Mao, L., *A miniature glucose/O₂ biofuel cell with a high tolerance against ascorbic acid*, *Fuel Cells*, 2009. **9**(1): p. 85-91.
54. Gao, F., Yan, Y.M., Su, L., Wang, L., Mao, L.Q., *An enzymatic glucose/O₂ biofuel cell: Preparation, characterization and performance in serum*, *Electrochemistry Communications*, 2007. **9**(5): p. 989-996.
55. Coman, V., Vaz-Dominguez, C., Ludwig, R., Herreither, W., Haltrich, D., De Lacey, A.L., Ruzgas, T., Gorton, L., Shleev, S., *A membrane-, mediator-, cofactor-less glucose/oxygen biofuel cell*, *Physical Chemistry Chemical Physics*, 2008. **10**(40): p. 6093-6096.
56. Tsujimura, S., Kano, K., Ikeda, T., *Glucose/O₂ biofuel cell operating at physiological conditions*, *Electrochemistry*, 2002. **70**(12): p. 940-942.
57. Kamitaka, Y., Tsujimura, S., Setoyama, N., Kajino, T., Kano, K., *Fructose/dioxygen biofuel cell based on direct electron transfer-type bioelectrocatalysis*, *Physical Chemistry Chemical Physics*, 2007. **9**(15): p. 1793-1801.
58. Sokic-Lazic, D., Minteer, S.D., *Citric acid cycle biomimic on a carbon electrode*, *Biosensors & Bioelectronics*, 2008. **24**(4): p. 939-944.
59. Ramanavicius, A., Kausaite, A., Ramanaviciene, A., *Enzymatic biofuel cell based on anode and cathode powered by ethanol*, *Biosensors & Bioelectronics*, 2008. **24**(4): p. 761-766.
60. Arechederra, R.L., Minteer, S.D., *Complete oxidation of glycerol in an enzymatic biofuel cell*, *Fuel Cells*, 2009. **9**(1): p. 63-69.
61. Vincent, K.A., Cracknell, J.A., Lenz, O., Zebger, I., Friedrich, B., Armstrong, F.A., *Electrocatalytic hydrogen oxidation by an enzyme at high carbon monoxide or oxygen levels*, *Proceedings of the National Academy of Sciences of the United States of America*, 2005. **102**(47): p. 16951-16954.
62. Katz, E., Willner, I., Kotlyar, A.B., *A non-compartmentalized glucose vertical bar O₂ biofuel cell by bioengineered electrode surfaces*, *Journal of Electroanalytical Chemistry*, 1999. **479**(1): p. 64-68.
63. Willner, I., Katz, E., Patolsky, F., Buckmann, A.F., *Biofuel cell based on glucose oxidase and microperoxidase-11 monolayer-functionalized electrodes*, *Journal of the Chemical Society - Perkin Transactions 2*, 1998(8): p. 1817-1822.

64. Pizzariello, A., Stred'ansky, M., Miertus, S., *A glucose/hydrogen peroxide biofuel cell that uses oxidase and peroxidase as catalysts by composite bulk-modified bioelectrodes based on a solid binding matrix*, *Bioelectrochemistry*, 2002. **56**(1-2): p. 99-105.
65. Katz, E., Filanovsky, B., Willner, I., *A biofuel cell based on two immiscible solvents and glucose oxidase and microperoxidase-11 monolayer-functionalized electrodes*, *New Journal of Chemistry*, 1999. **23**(5): p. 481-487.
66. Heller, A., *Miniature biofuel cells*, *Physical Chemistry Chemical Physics*, 2004. **6**(2): p. 209-216.
67. Bullen, R.A., Arnot, T.C., Lakeman, J.B., Walsh, F.C., *Biofuel cells and their development*, *Biosensors & Bioelectronics*, 2006. **21**(11): p. 2015-2045.
68. Heller, A. *Potentially implantable miniature batteries*, *Analytical and Bioanalytical Chemistry*, 2005. **385**(3): p. 469-473.
69. Heller, A. *Integrated medical feedback systems for drug delivery*, *AIChE Journal*, 2005. **51**(4): p. 1054-1066.
70. Cinquin, P., Gondran, C., Giroud, F., Mazabrard, S., Pellissier, A., Boucher, F., Alcaraz, J.P., Gorgy, K., Lenouvel, F., Mathe, S., Porcu, P., Cosnier, S., *A glucose biofuel cell implanted in rats*, *PLOS One*, 2010. **5**(5).
71. Alberty, R.A., *Calculating apparent equilibrium constants of enzyme-catalyzed reactions at pH 7*, *Biochemical Education*, 2000. **28**(1): p. 12-17.
72. Cosnier, S., Shan, D., Ding, S.N., *An easy compartment-less biofuel cell construction based on the physical co-inclusion of enzyme and mediator redox within pressed graphite discs*, *Electrochemistry Communications*, 2010. **12**(2): p. 266-269.
73. Meredith, M.T., Kao, D.Y., Hickey, D., Schmidtke, D.W., Glatzhofer, D.T., *High current density ferrocene-modified linear poly(ethylenimine) bioanodes and their use in biofuel cells*, *Journal of the Electrochemical Society*, 2011. **158**(2): p. B166-B174.
74. Nazaruk, E., Smolinski, S., Swatko-Ossor, M., Ginalska, G., Fiedurek, J., Rogalski, J., Bilewicz, R., *Enzymatic biofuel cell based on electrodes modified with lipid liquid-crystalline cubic phases*, *Journal of Power Sources*, 2008. **183**(2): p. 533-538.
75. Kowalewska, B., Kulesza, P.J., *Application of tetrathiafulvalene-modified carbon nanotubes to preparation of integrated mediating system for bioelectrocatalytic oxidation of glucose*, *Electroanalysis*, 2009. **21**(3-5): p. 351-359.
76. Merle, G., Habrioux, A., Servat, K., Rolland, M., Innocent, C., Kokoh, K.B., Tingry, S., *Long-term activity of covalent grafted biocatalysts during intermittent use of a glucose/O₂ biofuel cell*, *Electrochimica Acta*, 2009. **54**(11): p. 2998-3003.
77. Katz, E., Riklin, A., Heleg-Shabtai, V., Willner, I., Buckmann, A.F., *Glucose oxidase electrodes via reconstitution of the apo-enzyme: tailoring of novel glucose biosensors*, *Analytica Chimica Acta*, 1999. **385**(1-3): p. 45-58.
78. Willner, I., Heleg-Shabtai, V., Blonder, R., Katz, E., Tao, G.L., Buckmann, A.F., Heller, A., *Electrical wiring of glucose oxidase by reconstitution of FAD-modified monolayers assembled onto Au-electrodes*, *Journal of the American Chemical Society*, 1996. **118**(42): p. 10321-10322.
79. Khan, G.F., Ohwa, M., Wernet, W., *Design of a stable charge transfer complex electrode for a third-generation amperometric glucose sensor*, *Analytical Chemistry*, 1996. **68**(17): p. 2939-2945.

80. Zayats, M., Katz, E., Willner, I., *Electrical contacting of glucose oxidase by surface-reconstitution of the apo-protein on a relay-boronic acid-FAD cofactor monolayer*, Journal of the American Chemical Society, 2002. **124**(10): p. 2120-2121.
81. Xiao, Y., Patolsky, F., Katz, E., Hainfeld, J.F., Willner, I., *"Plugging into enzymes": Nanowiring of redox enzymes by a gold nanoparticle*, Science, 2003. **299**(5614): p. 1877-1881.
82. Patolsky, F., Weizmann, Y., Willner, I., *Long-range electrical contacting of redox enzymes by SWCNT connectors*, Angewandte Chemie - International Edition, 2004. **43**(16): p. 2113-2117.
83. Swoboda, B.E.P., *Relationship between molecular conformation and binding of flavin-adenine dinucleotide in glucose oxidase*, Biochimica et Biophysica Acta, 1969. **175**(2): p. 365-&.
84. Sehgal, D., Vijay, I.K., *A method for the high-efficiency of water-soluble carbodiimide-mediated amidation*, Analytical Biochemistry, 1994. **218**(1): p. 87-91.
85. Staros, J.V., Wright, R.W., Swingle, D.M., *Enhancement by N-hydroxysulfosuccinimide of water-soluble carbodiimide-mediated coupling reactions*, Analytical Biochemistry, 1986. **156**(1): p. 220-222.
86. Katz, E., Schlereth, D.D., Schmidt, H.L., *Electrochemical study of pyrroloquinoline quinone covalently immobilized as a monolayer onto a cystamine-modified gold electrode*, Journal of Electroanalytical Chemistry, 1994. **367**(1-2): p. 59-70.
87. Cho, S., Shin, H., Kang, C., *Catalytic glucose oxidation on a polycrystalline gold electrode with an amalgamation treatment (TM 05092)*, Electrochimica Acta, 2006. **51**(18): p. 3781-3786.
88. Trasatti, S., Petrii, O.A., *Real surface area measurements in electrochemistry*, Pure and Applied Chemistry, 1991. **63**(5): p. 711-734.
89. Ivanov, I., Vidakovic, T.R., Sundmacher, K., *The influence of a self-assembled monolayer on the activity of rough gold for glucose oxidation*, Electrochemistry Communications, 2008. **10**(9): p. 1307-1310.
90. Gooding, J.J., Mearns, F., Yang, W.R., Liu, J.Q., *Self-assembled monolayers into the 21(st) century: Recent advances and applications*, Electroanalysis, 2003. **15**(2): p. 81-96.
91. Chaki, N.K., Vijayamohanam, K., *Self-assembled monolayers as a tunable platform for biosensor applications*, Biosensors & Bioelectronics, 2002. **17**(1-2): p. 1-12.
92. Gooding, J.J., Jingquan, L., Paddon-Row, M.N., *Surface reconstitution of glucose oxidase onto a norbornylogous bridge self-assembled monolayer*, Chemical Physics, 2006. **324**(1): p. 226-35.
93. Vincent, K.A., Belsey, N.A., Lubitz, W., Armstrong, F.A., *Rapid and reversible reactions of NiFe -hydrogenases with sulfide*, Journal of the American Chemical Society, 2006. **128**(23): p. 7448-7449.
94. Hsiao, M.W., Adzic, R.R., Yeager, E.B., *Electrochemical oxidation of glucose on single crystal and polycrystalline gold surfaces in phosphate buffer*, Journal of the Electrochemical Society, 1996. **143**(3): p. 759-767.
95. Rooryck, V., Reniers, F., Buess-Herman, C., Attard, G. A., Yang, X., *The silver upd on gold(111) revisited*, Journal of Electroanalytical Chemistry, 2000. **482**(2): p. 93-101.
96. Cho, S., Kang, C., *Nonenzymatic glucose detection with good selectivity against ascorbic acid on a highly porous gold electrode subjected to amalgamation treatment*, Electroanalysis, 2007. **19**: p. 2315-2320.

97. Arvia, A.J., Canullo, J.C., Custidiano, E., Perdriel, C.L., Triaca, W.E., *Electrochemical faceting of metal-electrodes*, *Electrochimica Acta*, 1986. **31**(11): p. 1359-1368.
98. Chialvo, A.C., Triaca, W.E., Arvia, A.J., *Changes in the polycrystalline gold electrode surface produced by square-wave potential perturbations*, *Journal of Electroanalytical Chemistry*, 1984. **171**(1-2): p. 303-316.
99. Angerstein-Kozłowska, H., Conway, B.E., Barnett, B., Mozota, J., *Role of ion adsorption in surface oxide formation and reduction at noble-metals – general features of the surface process*, *Journal of Electroanalytical Chemistry*, 1979. **100**(1-2): p. 417-446.
100. Luna, A.M.C., Demele, M.F.L., Arvia, A.J., *The electrooxidation of glucose on microcolumnar gold electrodes in different neutral solutions*, *Journal of Electroanalytical Chemistry*, 1992. **323**(1-2): p. 149-162.
101. Hsiao, M.W., Adzic, R.R., Yeager, E.B., *The effects of adsorbed anions on the oxidation of deuterium-glucose on gold single-crystal electrodes*, *Electrochimica Acta*, 1992. **37**(2): p. 357-363.
102. El-Deab, M.S., Arihara, K., Ohsaka, T., *Fabrication of Au(111)-like polycrystalline gold electrodes and their applications to oxygen reduction*, *Journal of the Electrochemical Society*, 2004. **151**(6): p. E213-E218.
103. Ivanov, I., Vidakovic, T.R., Sundmacher, K., *Glucose electrooxidation for biofuel cell applications*, *Chemical and Biochemical Engineering Quarterly*, 2009. **23**(1): p. 77-86.
104. Engelsmann, K., Lorenz, W.J., Schmidt, E., *Underpotential deposition of lead on polycrystalline and single-crystal gold surfaces. 1 Thermodynamics*, *Journal of Electroanalytical Chemistry*, 1980. **114**(1): p. 1-10.
105. Buckmann, A.F., Wray, V., Stocker, A., *Synthesis of N-6-(2-aminoethyl)-FAD, N-6-(6-carboxyhexyl)-FAD, and related compounds*, *Vitamins and Coenzymes, Pt J*, 1997. Academic Press Inc: San Diego. p. 360-374.
106. Bryce, M.R., Murphy, L.C., *Organic metals*, *Nature*, 1984. **309**(5964): p. 119-126.
107. Akamatu, H., Inokuchi, H., Matsunaga, Y., *Electrical conductivity of the perylene-bromine complex*, *Nature*, 1954. **173**(4395): p. 168-169.
108. Jerome, D., Schulz, H.J., *Organic conductors and superconductors*, *Advances in Physics*, 1982. **31**(4): p. 299-490.
109. Ferraris, J., Walatka, Jr., V., Perlstein, J.H., Cowan, D.O., *Electron-transfer in a new highly conducting donor-acceptor complex*, *Journal of the American Chemical Society*, 1973. **95**(3): p. 948-949.
110. Jerome, D., *Organic conductors: From charge density wave TTF-TCNQ to superconducting (TMTSF)(2)PF₆*, *Chemical Reviews*, 2004. **104**(11): p. 5565-5591.
111. Jaeger, C.D., Bard, A.J., *Electrochemical behavior of tetrathiafulvalene-tetracyanoquinodimethane electrodes in aqueous-media*, *Journal of the American Chemical Society*, 1979. **101**(7): p. 1690-1699.
112. Cenas, N.K., Kulys, J.J., *Biocatalytic oxidation of glucose on the conductive charge-transfer complexes*, *Bioelectrochemistry and Bioenergetics*, 1981. **8**(1): p. 103-113.
113. Kulys, J.J., Samalius, A.S., Svirnickas, G.J.S., *Electron exchange between the enzyme active-center and organic metal*, *FEBS Letters*, 1980. **114**(1): p. 7-10.
114. Albery, W.J., Bartlett, P.N., Craston, D.H., *Amperometric enzyme electrodes. 2. Conducting salts as electrode materials for the oxidation of glucose-oxidase*, *Journal of Electroanalytical Chemistry*, 1985. **194**(2): p. 223-235.

115. Albery, W.J., Bartlett, P.N., Bycroft, M., Craston, D.H., Driscoll, B.J., *Amperometric enzyme electrodes. 3. A conducting salt electrode for the oxidation of 4 different flavoenzymes*, Journal of Electroanalytical Chemistry, 1987. **218**(1-2): p. 119-126.
116. Pauliukaite, R., Malinauskas, A., Zhylyak, G., Spichiger-Keller, U.E., *Conductive organic complex salt TTF-TCNQ as a mediator for biosensors. An overview*, Electroanalysis, 2007. **19**(24): p. 2491-2498.
117. Palmisano, F., Zambonin, P.G., Centonze, D., Quinto, M., *A disposable, reagentless, third-generation glucose biosensor based on overoxidized poly(pyrrole)/tetrathiafulvalene-tetracyanoquinodimethane composite*, Analytical Chemistry, 2002. **74**(23): p. 5913-5918.
118. Pauliukaite, R., Zhylyak, G., Citterio, D., Spichiger-Keller, U.E., *L-glutamate biosensor for estimation of the taste of tomato specimens*, Analytical and Bioanalytical Chemistry, 2006. **386**(2): p. 220-227.
119. Liu, H.B., Li, J.B., Lao, C.S., Huang, C.S., Li, Y.L., Wang, Z.L., Zhu, D.B., *Morphological tuning and conductivity of organic conductor nanowires*, Nanotechnology, 2007. **18**(49): p. 7.
120. De Caro, D., Jacob, K., Faulmann, C., Legros, J.P., Senocq, F., Fraxedas, J., Valade, L., *Ionic liquid-stabilized nanoparticles of charge transfer-based conductors*, Synthetic Metals, 2010. **160**(11-12): p. 1223-1227.
121. Kulys, J., Simkeviciene, V., Higgins, I.J., *Concerning the toxicity of 2 compounds used as mediators in biosensor devices – 7,7,8,8-tetracyanoquinodimethane (TCNQ) and tetrathiafulvalene (TTF)*, Biosensors & Bioelectronics, 1992. **7**(7): p. 495-501.
122. Wang, H.J., Shi, J., Fang, M., Li, Z., Guo, Q.X., *Design of new neutral organic super-electron donors: a theoretical study*, Journal of Physical Organic Chemistry, 2010. **23**(1): p. 75-83.
123. Warren, L.F., Anderson, D.P., *Polypyrrole films from aqueous-electrolytes - the effect of anions upon order*, Journal of the Electrochemical Society, 1987. **134**(1): p. 101-105.
124. Inganas, O., Erlandsson, R., Nylander, C., Lundstrom, I., *Proton modification of conducting polypyrrole*, Journal of Physics and Chemistry of Solids, 1984. **45**(4): p. 427-432.
125. Dirksen, J.A., Ring, T.A., *Fundamentals of crystallization - kinetic effects on particle-size distributions and morphology*, Chemical Engineering Science, 1991. **46**(10): p. 2389-2427.
126. Myler, S., Collyer, S.D., Bridge, K.A., Higson, S.P.J., *Ultra-thin-polysiloxane-film-composite membranes for the optimisation of amperometric oxidase enzyme electrodes*, Biosensors & Bioelectronics, 2002. **17**(1-2): p. 35-43.
127. Moehlenbrock, M.J. Minteer, S.D., *Extended lifetime biofuel cells*, Chemical Society Reviews, 2008. **37**(6): p. 1188-1196.
128. Bigi, A., Cojazzi, G., Panzavolta, S., Rubini, K., Roveri, N., *Mechanical and thermal properties of gelatin films at different degrees of glutaraldehyde crosslinking*, Biomaterials, 2001. **22**(8): p. 763-768.
129. Cano, M., Avila, J.L., Mayen, M., Mena, M.L., Pingarron, J., Rodriguez-Amaro, R., *A new, third generation, PVC/TTF-TCNQ composite amperometric biosensor for glucose determination*, Journal of Electroanalytical Chemistry, 2008. **615**(1): p. 69-74.
130. Habrioux, A., Napporn, T., Servat, K., Tingry, S., Kokoh, K.B., *Electrochemical characterization of adsorbed bilirubin oxidase on Vulcan XC 72R for the biocathode*

- preparation in a glucose/O₂ biofuel cell*, *Electrochimica Acta*, 2010. **55**(26): p. 7701-7705.
131. De Wael, K., De Belder, S., Van Vlierberghe, S., Van Steenberge, G., Dubruel, P., Adriaens, A., *Electrochemical study of gelatin as a matrix for the immobilization of horse heart cytochrome C*, *Talanta*, 2010. **82**(5): p. 1980-1985.
 132. Sheldon, R.A., *Cross-Linked Enzyme Aggregates as Industrial Biocatalysts*, *Organic Process Research & Development*, 2011. **15**(1): p. 213-223.
 133. Ispirli, Y., Ayhan, H., *Proteic Feeder Effect on Glucose Oxidase Aggregates Formation*, *Hacettepe Journal of Biology and Chemistry*, 2008. **36**(4): p. 313-318.
 134. Minter, S.D., Liaw, B.Y., Cooney, M.J., *Enzyme-based biofuel cells*, *Current Opinion in Biotechnology*, 2007. **18**(3): p. 228-234.
 135. Courjean, O., Gao, F., Mano, N., *Deglycosylation of Glucose Oxidase for Direct and Efficient Glucose Electrooxidation on a Glassy Carbon Electrode*, *Angewandte Chemie - International Edition*, 2009. **48**(32): p. 5897-5899.
 136. Liu, H.Y., Deng, J.Q., *An amperometric glucose sensor based on Eastman-AQ-tetrathiafulvalene modified electrode*, *Biosensors & Bioelectronics*, 1996. **11**(1-2): p. 103-110.
 137. Atanasov, P., Kaisheva, A., Iliev, I., Razumas, V., Kulys, J., *Glucose biosensor based on carbon-black strips*, *Biosensors & Bioelectronics*, 1992. **7**(5): p. 361-365.
 138. Albery, W.J., Bartlett, P.N., Cass, A.E.G., Eisenthal, R., Higgins, I.J., *Amperometric enzyme electrodes*, *Philosophical Transactions of the Royal Society of London Series B - Biological Sciences*, 1987. **316**(1176): p. 107-119.
 139. Freund, M.S., Brajter-Toth, A., Ward, M.D., *Electrochemical and quartz crystal microbalance evidence for mediation and direct electrochemical reactions of small molecules at tetrathiafulvalene-tetracyanoquinodimethane (TTF-TCNQ) electrodes*, *Journal of Electroanalytical Chemistry*, 1990. **289**(1-2): p. 127-141.
 140. Hill, B.S., Scolari, C.A., Wilson, G.S., *Enzyme electrocatalysis at the TTF-TCNQ electrode*, *Philosophical Transactions of the Royal Society of London Series A - Mathematical Physical and Engineering Sciences*, 1990. **333**(1628): p. 63-69.
 141. Bartlett, P.N., *Some studies of electrodes made from single-crystals TTF-TCNQ*, *Journal of Electroanalytical Chemistry*, 1991. **300**(1-2): p. 175-189.
 142. Bartlett, P.N., Bradford, V.Q., *Modification of glucose-oxidase by tetrathiafulvalene*, *Journal of the Chemical Society - Chemical Communications*, 1990(16): p. 1135-1136.
 143. Albery, W.J., Bartlett, P.N., Driscoll, B.J., Lennox, R.B., *Amperometric enzyme electrodes. 5. The homogeneous mediated mechanism*, *Journal of Electroanalytical Chemistry*, 1992. **323**(1-2): p. 77-102.
 144. Bond, A.M., Fletcher, S., Symons, P.G., *The relationship between the electrochemistry and the crystallography of microcrystals. The case of TCNQ (7,7,8,8-tetracyanoquinodimethane)*, *Analyst*, 1998. **123**(10): p. 1891-1904.
 145. Vogt, M.R., Lachenwitzer, A., Magnussen, O.M., Behm, R.J., *In-situ STM study of the initial stages of corrosion of Cu(100) electrodes in sulfuric and hydrochloric acid solution*, *Surface Science*, 1998. **399**(1): p. 49-69.
 146. Wilde, C.P., Hu, A., Rondeau, C.M., Wood, M., *Cyclic voltammetry and charge accumulation at conducting organic salt enzyme electrodes*, *Journal of Electroanalytical Chemistry*, 1993. **353**(1-2): p. 19-31.

147. Zhao, S., Korell, U., Cuccia, L., Lennox, R.B., *Electrochemistry of organic conducting salt electrodes – a unified mechanistic description*, Journal of Physical Chemistry, 1992. **96**(13): p. 5641-5652.
148. Bartlett, P.N., Tong, X.Q., *Dissolution processes at TTF-TCNQ single-crystal electrodes: A dynamic in situ electrochemical scanning tunneling microscopy study*, Journal of Physical Chemistry B, 1997. **101**(42): p. 8540-8549.
149. Robles-Martinez, J.G., Salmeron-Valverde, A., Zehe, A., Toscano, R.A., *Determination of the degree of charge-transfer in the complex HNAFIN-TCNQ*, Crystal Research and Technology, 1995. **30**(2): p. K21-K25.
150. Chappell, J.S., Bloch, A.N., Bryden, W.A., Maxfield, M., Poehler, T.O., Cowan, D.O., *Degree of charge-transfer in organic conductors by infrared-absorbtion spectroscopy*, Journal of the American Chemical Society, 1981. **103**(9): p. 2442-2443.
151. Bellec, V., De Backer, M.G., Levillain, E., Sauvage, F.X., Sombret, B., Wartelle, C., *In situ time-resolved FTIR spectroelectrochemistry: study of the reduction of TCNQ*, Electrochemistry Communications, 2001. **3**(9): p. 483-488.
152. Hudak, N.S., Gallaway, J.W., Barton, S.C., *Mediated Biocatalytic Cathodes Operating on Gas-Phase Air and Oxygen in Fuel Cells*, Journal of the Electrochemical Society, 2009. **156**(1): p. B9-B15.
153. Reshetenko, T., Kim, H., Lee, H., Jang, M., Kweon, H., *Performance of a direct methanol fuel cell (DMFC) at low temperature: Cathode optimization*, Journal of Power Sources, 2006. **160**(2): p. 925-932.
154. Apblett, C.A., Ingersoll, D., Sarangapani, S., Kelly, M., Atanassov, P., *Direct glucose fuel cell: Noble metal catalyst anode polymer electrolyte membrane fuel cell with glucose fuel*, Journal of the Electrochemical Society, 2010. **157**(1): p. B86-B89.
155. Cui, H.F., Ye, J.S., Zhang, W.D., Wang, J., Sheu, F.S., *Electrocatalytic reduction of oxygen by a platinum nanoparticle/carbon nanotube composite electrode*, Journal of Electroanalytical Chemistry, 2005. **577**(2): p. 295-302.
156. Kongkanand, A., Kuwabata, S., Girishkumar, G., Kamat, P., *Single-wall carbon nanotubes supported platinum nanoparticles with improved electrocatalytic activity for oxygen reduction reaction*, Langmuir, 2006. **22**(5): p. 2392-2396.
157. Parthasarthy, A., Srinivasan, S., Appleby, A.J., Martin, C.R., *Electrode-kinetics of oxygen reduction at carbon-supported and unsupported platinum microcrystallite Nafion interfaces*, Journal of Electroanalytical Chemistry, 1992. **339**(1-2): p. 101-121.
158. Ernst, S., Heitbaum, J., Hamann, C.H., *Electrooxidation of glucose in phosphate buffer solutions. 1. Reactivity and kinetics below 350 mV-RHE*, Journal of Electroanalytical Chemistry, 1979. **100**(1-2): p. 173-183.
159. Chen, S.Z., Ye, F., Lin, W.M., *Effect of operating conditions on the performance of a direct methanol fuel cell with PtRuMo/CNTs as anode catalyst*, International Journal of Hydrogen Energy, 2010. **35**(15): p. 8225-8233.
160. Mano, N., *A 280 muW cm(-2) biofuel cell operating at low glucose concentration*, Chemical Communications, 2008(19): p. 2221-2223.
161. Li, H., Tang, Y., Wang, Z., Shi, Z., Wu, S., Song, D., Zhang, J., Fatih, K., Wang, H., *A review of water flooding issues in the proton exchange membrane fuel cell*, Journal of Power Sources, 2008. **178**(1): p. 103-117.
162. Xu, C., Zhao, T.S., *In situ measurements of water crossover through the membrane for direct methanol fuel cells*, Journal of Power Sources, 2007. **168**(1): p. 143-153.

163. Schroder, A., Wippermann, K., Lehnert, W., Stolten, D., Sanders, T., Baumhofer, T., Kardjilov, N., Hilger, A., Banhart, J., Manke, I., *The influence of gas diffusion layer wettability on direct methanol fuel cell performance: A combined local current distribution and high resolution neutron radiography study*, Journal of Power Sources, 2010. **195**(15): p. 4765-4771.
164. Lin, G.Y., Van Nguyen, T., *Effect of thickness and hydrophobic polymer content of the gas diffusion layer on electrode flooding level in a PEMFC*, Journal of the Electrochemical Society, 2005. **152**(10): p. A1942-A1948.
165. Jiao, K., Park, J., Li, X., *Experimental investigations on liquid water removal from the gas diffusion layer by reactant flow in a PEM fuel cell*, Applied Energy, 2010. **87**(9): p. 2770-2777.
166. Liu, J.H., Jeon, M.K., Choi, W.C., Woo, S.I., *Highly-optimized membrane electrode assembly for direct methanol fuel cell prepared by sedimentation method*, Journal of Power Sources, 2004. **137**(2): p. 222-227.
167. Ndamanisha, J.C., Bo, X.J., Guo, L.P., *Electrocatalytic reduction of oxygen at ordered mesoporous carbon functionalized with tetrathiafulvalene*, Analyst, 2010. **135**(3): p. 621-629.
168. Okada, T., Satou, H., Okuno, M., Yuasa, M., *Ion and water transport characteristics of perfluorosulfonated ionomer membranes with H⁺ and alkali metal cations*, Journal of Physical Chemistry B, 2002. **106**(6): p. 1267-1273.
169. Togo, M., Takamura, A., Asai, T., Kaji, H., Nishizawa, M., *Structural studies of enzyme-based microfluidic biofuel cells*, Journal of Power Sources, 2008. **178**(1): p. 53-58.
170. Topcagic, S., Minter, S.D., *Development of a membraneless ethanol/oxygen biofuel cell*, Electrochimica Acta, 2006. **51**(11): p. 2168-2172.
171. Habrioux, A., Merle, G., Servat, K., Kokoh, K.B., Innocent, C., Cretin, M., Tingry, S., *Concentric glucose/O₂ biofuel cell*, Journal of Electroanalytical Chemistry, 2008. **622**(1): p. 97-102.
172. Shleev, S., Shumakovich, G., Morozova, O., Yaropolov, A., *Stable 'floating' air diffusion biocathode based on direct electron transfer reactions between carbon particles and high redox potential laccase*, Fuel Cells, 2010. **10**(4): p. 726-733.
173. Gupta, G., Lau, C., Rajendran, V., Colon, F., Branch, B., Ivnitski, D., Atanassov, P., *Direct electron transfer catalyzed by bilirubin oxidase for air breathing gas-diffusion electrodes*, Electrochemistry Communications, 2011. **13**(3): p. 247-249.

CURRICULUM VITAE

PERSONAL INFORMATION

Name **IVAN IVANOV**
Address **411 Waupelani Dr., State College, PA, USA**
Telephone **+1 814 777 5310**
E-Mail **ivanov.ivan.uctm@gmail.com**
Nationality Bulgarian
Date of birth 30 MARCH 1983

WORK EXPERIENCE

June 2011 – January 2012 Max Planck Institute Magdeburg (Scientific co-worker)
October 2010 – June 2011 Otto von Guericke University Magdeburg (Scientific co-worker)
July 2010 – September 2010 Max Planck Institute Magdeburg (Scientific co-worker)
June 2001 – September 2001 Overseas Environmental Contractors Bulgaria (Technical assistant)
July 2000 – September 2000 Overseas Environmental Contractors Bulgaria (Technical assistant)

EDUCATION AND TRAINING

January 2010 – Juni 2010 Otto von Guericke University Magdeburg (Scholarship holder)
2007 – 2009 Max Planck Institute Magdeburg (Scholarship holder)
2005 - 2006 UCTM Sofia, Fine Organic Synthesis (Master's degree)
2001 – 2005 UCTM Sofia, Organic Chemical Technologies, Organic Synthesis (Bachelor's degree)
1997 – 2000 High school "Sava Savov" Pirdop, Profile "Chemistry and Biology"

PERSONAL SKILLS

MOTHER TONGUE BULGARIAN

OTHER LANGUAGES

ENGLISH
Fluent written and spoken
GERMAN
Good written and spoken